

# **Functional analysis of cytoskeletal signalling in the defence response of grapevine**

Zur Erlangung des akademischen Grades eines

**DOKTORS DER NATURWISSENSCHAFTEN**

(Dr. rer. Nat.)

Fakultät für Chemie und Biowissenschaften  
Karlsruher Institut für Technologie (KIT) – Universitätsbereich  
genehmigte

**DISSERTATION**

von

Xin Guan

aus Jinan, China

Dekan: Prof. Dr. M. Bastmeyer

Referent: Prof. Dr. P. Nick

Korreferent: Prof. Dr. U. Schepers

Tag der mündlichen Prüfung: 19.07.2013



This thesis was conducted in the Department of Molecular Cell Biology, Botanical Institute, Karlsruhe Institute of Technology. My Ph.D. study started from September 2010.

I want to show my great appreciation to my supervisor Prof. Dr. Peter Nick for the assignment of the topic and the possibility to work in his lab. One of the new words I learnt in Germany was “Doktorvater”. Peter meets the criteria of the proper sense of this word thoroughly! His patience, his encouragement, his brilliant ideas, lead me to come across obstacles one by one; light me the road how to be a good scientist, how to design one’s life.

Many thanks to Dr. Günther Buchholz. Sometimes it is hard to tell whether he is a skillful supervisor, a trustworthy co-operator, or an old friend. His in-time trouble shooting, his selfless offers always give me a feeling that I am at home.

My special thanks to Dr. Michael Riemann for his countless advices and supervising me throughout my whole Ph.D. studies; as well as his beautiful wife Maren, thanks for their constantly considerations to my daily-life.

Many thanks to Prof. Tilman Lamparter, Dr. Jan Maisch, Dr. Gregor Rottwinkel, Dr. Kai Eggenberger, Xiaoli, Katha, Jan, Steffen, Fan, Thomas and Rui for the constructive advices during the running of my experiments. Ahmed, Sebastian, Qiong, Ningning, Rita, Viki, Natalie, Bea and Dong cheers for our delight cooperations and I thank you sincerely for your warm offers. Maren, Jochen and Xiaoli, the joyfulness in our office will be always so impressive for me.

I would like to warmly thank Joachim, Dr. Yubin Kashef, Sybille, Sabine, Max, Ernst, and our lovely “Azubi”s, Thorsten and Mario at RLP AgroScience in Neustadt/W, for your excellent and experienced technical assistance in the garden and laboratory.

I would also like to thank the students I supervised since they were a constant drive for me with their questions and impressions.

All the staff in Molecular and Cell Biology of the Botanical Institute, I thank you all, for many constructive discussions within and beyond the research.

My parents, thank you for your coming to Germany to visit me; my boyfriend Heqing, thank you for your constant supports in the past three years.



## Zusammenfassung

Das pflanzliche Zellskelett, bestehend aus Microtubuli (MT) und Actinmikrofilamenten (AF), vermittelt die pflanzliche Antwort auf zahlreiche biotische oder abiotische Stressfaktoren. Die vorliegende Arbeit befasste sich mit der Rolle des Zellskeletts für die zelluläre Antwort auf einen dieser Faktoren, nämlich biotischen Stress durch Pathogene. Die pflanzliche angeborene Immunität besteht aus zwei Schichten. Eine basale Immunität wird durch sogenannte *pathogen-associated molecular patterns* (PAMPs), wie z.B. das Flagellinpeptid flg22, ausgelöst und wird als *PAMP-triggered immunity* (PTI) bezeichnet. Dies wird durch eine zweite Ebene, die sogenannte *effector-triggered immunity* (ETI) überlagert. Die ETI geht mit programmiertem Zelltod und einer Umorganisation des Zellskeletts einher und kann durch Faktoren aus dem Pathogen, wie den aus pflanzenpathogenen Bakterien stammenden HrpZ-Proteinen, ausgelöst werden.

Um den Zusammenhang zwischen Zellskelett und PTI oder ETI besser verstehen zu können, wurde in dieser Arbeit zunächst die Antwort von Actinfilamenten und Mikrotubuli auf flg22 und HrpZ *in vivo* mithilfe hochauflösender *spinning-disc confocal microscopy* in Markerlinien von Tabak BY-2 verfolgt, wo das Zellskelett durch Fusion mit dem Grün Fluoreszenten Protein (GFP) markiert. Selbst bei einer Konzentration, die deutlich antimotisch wirkt, konnte flg22 nur sehr subtile Antworten des Zellskeletts hervorrufen. Im Gegensatz dazu, verursachte HrpZ eine schnelle und massive Bündelung der AF (binnen ~20 min, also fast gleichzeitig mit der extrazellulären Alkalinisierung), gefolgt von einem fortschreitenden Zerfall der Actinkabel und cytoplasmatischen MT, einem Verlust der cytoplasmatischen Struktur und einer Auflösung der Vacuole. Der Zerfall des Zellskeletts ist vermutlich ein früher Schritt, der HrpZ-induzierte ETI-artige Abwehr von der flg22-induzierten PTI unterscheidet.

Die Resistenz gegen Stress ist zu einem zentralen Thema nachhaltiger Landwirtschaft geworden, gerade auch bei der Weinrebe, der Feldfrucht mit dem höchsten ökonomischen Ertrag pro Fläche. Wir haben daher transgene Winreben-Linien in der *Vitis vinifera* Sorte 'Chardonnay' hergestellt, die eine Proteinfusion zwischen GFP und der zweiten Actinbinde-Domäne von Arabidopsis (*Arabidopsis thaliana*) Fimbrin, AtFIM1 (pK7WGF2-FABD2) exprimiert. Ebenso wurde eine Suspensions-Zell-Linie in der amerikanischen Felsenrebe, *Vitis rupestris*, erzeugt, die Arabidopsis  $\beta$ -Tubulin-6 in einer N-terminalen Fusion mit GFP (pCambia1300(CAA)<sub>n</sub> 2XT-gfp-Tub6) hergestellt. Dies sind die ersten Zellskelett-Markerlinien für diese wichtige Nutzpflanze und stellen wertvolle Werkzeuge dar, mit denen die Rolle des Zellskeletts für pflanzliche Abwehr und Stresstoleranz untersucht werden kann. *Plasmopara viticola*, der Verursacher des Falschen Mehltaus der Weinrebe, ist der gefährlichste Krankheitserreger im mitteleuropäischen Weinbau.

In der vorliegenden Arbeit untersuchten wir daher, mithilfe unserer transgenen Linie, die Antwort der AF auf Infektion mit *P. viticola*, aber auch mit über dTomato fluoreszent markierten transgenen Stämmen der pflanzenpathogenen Bakterien *Erwinia amylovora*, *Agrobacterium tumefaciens* Stamm EHA105, und *A. vitis*. Die Befunde aus der ersten Zellskelett-Marker Linie in der Weinrebe zeigen, dass die AF in den Schließzellen nach Kontakt mit Zoosporen von *P. viticola* zerfallen. Interessanterweise zeigen auch in den Zellen der unteren Epidermis, die selbst keinen direkten Kontakt mit den Zoosporen hatten, eine starke Antwort des Actins – hier bildet sich ein Actinkorb um den Zellkern herum. Unsere Ergebnisse stützen eine Hypothese, wonach die Schließzellen als Schrittmacher der pflanzlichen Abwehr fungieren und die Reaktion der umliegenden Zellen steuern. Mithilfe der MT-Marker-Zell-Linie konnten wir erstmals *in vivo* die Antwort der MT auf verschiedene abiotische und biotische Stressfaktoren verfolgen. Beispielsweise gelang es uns, die Bildung von MT-Bündeln (sogenannter Makrotubuli) in Antwort auf Trocken- und Salzstress zeigen. Diese Makrotubuli bilden sich innerhalb von 30 min, und diese Antwort ist nach Gabe des natürlichen Auxins IES reversibel. Weiterhin konnten wir spezifische Antworten der MT auf verschiedene Bakterien nachweisen, was neue Erkenntnisse über die zelluläre Antwort auf Wirt- und Nichtwirt-Pathogene zulässt.

Zusammenfassend lässt sich sagen, dass es im Laufe der vorliegenden Arbeit gelungen ist, *in-vivo* Bildgebung des Zellskeletts in die für die Anwendung wichtige Modellpflanze Weinrebe zu integrieren und so die Funktion von Actinfilamenten und Mikrotubuli in einem für die landwirtschaftliche Anwendung zentralen Zusammenhang zu studieren.

# Table of Contents

<b>1 Introduction .....</b>	<b>1</b>
<b>1.1 Plant innate immunity .....</b>	<b>1</b>
1.1.1 Six obstacles of plant resistance.....	1
1.1.2 Zig-Zag model of PAMP-triggered immunity and effector-triggered immunity.....	3
1.1.3 Elicitors to mimic PAMP-triggered immunity and effector-triggered immunity .....	4
<b>1.2 Cytoskeleton and defence: structural events.....</b>	<b>5</b>
1.2.1 Towards understanding the role of actin in defence.....	6
1.2.2 Towards understanding the role of microtubule in defence .....	8
1.2.3 Macrotubules as stress-specific MT-array.....	10
<b>1.3 Cytoskeleton and defence: signalling events.....</b>	<b>10</b>
1.3.1 Time course of events triggered by pattern recognition receptors .....	10
1.3.2 Reactive oxygen species .....	11
1.3.3 Nitric oxide .....	11
1.3.4 Hormonal transduction.....	12
1.3.5 Ion channels .....	15
1.3.6 Phytoalexins .....	15
1.3.7 Programmed cell death.....	16
<b>1.4 Case studies for cytoskeletal functions in the response to biotic/abiotic stress .....</b>	<b>17</b>
1.4.1 Bacterial, fungal, oomycete and viral infection .....	17
1.4.2 Salt stress.....	19
1.4.3 Cold stress .....	20
<b>1.5 Scope of this study.....</b>	<b>21</b>
<b>2 Materials and methods.....</b>	<b>24</b>
<b>2.1 Plasmid construction .....</b>	<b>24</b>
<b>2.2 <i>Agrobacterium</i> mediated transformation of grapevine.....</b>	<b>24</b>
2.2.1 Leaves of <i>V. vinifera</i> ‘Chardonnay’ expressing <i>GFP-AtFABD2</i> .....	24
2.2.2 <i>Ex vitro</i> acclimation of transgenic plant.....	26
2.2.3 Cells of <i>V. rupestris</i> expressing <i>GFP-AtTUB6</i> .....	27
<b>2.3 PCR detection and southern blot of genomic DNA. ....</b>	<b>27</b>
<b>2.4 Quantitative phenotyping of transformed <i>Vitis</i> leaves.....</b>	<b>28</b>
<b>2.5 Tobacco BY-2 cell lines and cultivation.....</b>	<b>29</b>
<b>2.6 Elicitors .....</b>	<b>29</b>
<b>2.7 Inoculation with dTomato tagged Gram-negative bacteria: <i>Agrobacterium tumefaciens</i> EHA105, <i>Ewinia amylovora</i>, <i>Agrobacterium vitis</i> S4 and <i>Escherichia coli</i> ..</b>	<b>30</b>
2.7.1 Leaves of <i>V. vinifera</i> ‘Chardonnay’ expressing <i>GFP-AtFABD2</i> .....	30
2.7.2 Cells of <i>V. rupestris</i> expressing <i>GFP-AtTUB6</i> .....	30

## Table of Contents

---

2.8 Inoculation and staining of <i>Plasmopara viticola</i> .....	30
2.9 Life-cell microtubule imaging in <i>V. rupestris</i> cells during stress .....	31
2.9.1 Biotic stress treatment.....	31
2.9.2 Abiotic stress treatment.....	31
2.10 Microscopy .....	32
2.11 Quantitative image analysis of actin filaments and microtubules.....	33
2.12 Measurement of extracellular alkalinisation.....	34
2.13 Phenotyping of cellular responses .....	34
<b>3 Results .....</b>	<b>36</b>
3.1 Actin responses to flg22 are subtle, those to HrpZ are drastic .....	36
3.2 Microtubules respond to HrpZ, but not to flg22 .....	38
3.3 Apoplastic alkalinisation as rapid defence readout is more sensitive to flg22 as compared to HrpZ.....	40
3.4 Cell division and cellular morphogenesis are altered by HrpZ.....	41
3.5 HrpZ, but not flg22 can induce cell death.....	43
3.6 Phenotypic analysis of transformed plants .....	44
3.7 PCR detection and southern blot of genomic DNA .....	47
3.8 Response of actin filaments to <i>P. viticola</i> .....	48
3.9 Response of actin filaments to different Gram-negative bacteria.....	49
3.10 Formation of <i>V. rupestris</i> calli and suspension cells expressing <i>GFP-AtTUB6</i> .....	50
3.11 Morphogenetic response to biotic and abiotic stresses .....	51
3.12 Sustained microtubule response to biotic and abiotic stresses .....	52
3.13 Rapid microtubule responses to biotic and abiotic stresses.....	53
3.14 IAA effects on MTs in <i>V. rupestris</i> suspension cells expressing <i>GFP-AtTUB6</i> .....	55
3.15 IAA effects on cell division, morphogenesis and mortality in <i>V. rupestris</i> suspension cells expressing <i>GFP-AtTUB6</i> .....	55
3.16 IAA is antagonistic to JA, but not to HrpZ, with respect to the microtubular response .....	58
3.17 Response of microtubules to different Gram-negative bacteria.....	60
3.18 Summary .....	63
<b>4 Discussion.....</b>	<b>65</b>
4.1 Temporal signature of AFs and MTs in decoding elicitor signals of PTI and ETI ...	65
4.2 A new tool to understand the role of cytoskeleton in biotic/abiotic defence.....	69
4.3 The Actin Guard Cell Gatekeeper model .....	71
4.4 Formation of macro-tubules in response to osmotic stress .....	76
4.5 Conclusion.....	79
4.6 Outlook.....	80
<b>Acknowledgements .....</b>	<b>81</b>



<b>References .....</b>	<b>82</b>
<b>Appendix .....</b>	<b>103</b>
<b>Curriculum Vitae.....</b>	<b>110</b>



---

## List of Abbreviations

ABP	Actin-binding protein
AFs	Actin filaments
<i>AtFABD2</i>	Second actin-binding domain of <i>Arabidopsis thaliana</i> fimbrin
<i>AtTUB6</i>	<i>Arabidopsis</i> $\beta$ -Tubulin6
BY-2	<i>Nicotiana tabacum</i> L. cv Bright Yellow 2
ETI	Effector-triggered immunity
EtOH	Ethanol
flg22	A synthetic 22-amino-acid peptide from a conserved flagellin domain
GFP	Green fluorescent protein
HrpZPspH	Harpin protein originating from <i>Pseudomonas syringae</i> pv. <i>phaseolicola</i>
IAA	Indolyl-3-acetic acid
JA	Jasmonate
MAPK	Mitogen-activated protein kinases
MAPs	Microtubule-associated proteins
MTs	Microtubules
NaCl	Sodium chloride
NB-LRR	Nucleotide-binding leucine rich repeat
PAMPs	Pathogen-associated molecular patterns
PCD	Programmed cell death
PCV	Packed cell volume
PEG 6000	Polyethylene glycol 6000
PFD	Perfluorodecalin
PLD	Phospholipase D
PTI	PAMP-triggered immunity
RFP	Red fluorescent protein
ROS	Reactive oxygen species



# 1 Introduction

## 1.1 Plant innate immunity

Plants lack the somatic adaptive immune system based on mobile defence cells characteristic for animal immunity. Plant defence, in contrast, is based upon an innate immunity of each individual cell (Jones & Dangl, 2006).

### 1.1.1 Six obstacles of plant resistance

Thordal-Christensen (2003) demonstrated that there are six obstacles of resistance that must be overcome during pathogen infection. Progression through these obstacles not only promotes pathogen virulence, but also initiates the activation of innate immune signalling. As shown in **Fig. 1.1**, first, some pathogens use plant cues to trigger pathogen differentiation; second, the pathogen has to pass through preformed barriers of the plant host - such barriers can be chemical, enzymatic or structural; third, pathogens need to overcome “ancient” inducible barriers in the plant; fourth, in case of fungal biotrophs, they interact with the plant in order to acquire nutrients; fifth, robust surveillance by the host which is based on several independent *R-/Avr-* gene recognition events, and sixth, breakable surveillance based on a single *R-/Avr-* gene recognition event impede infection.

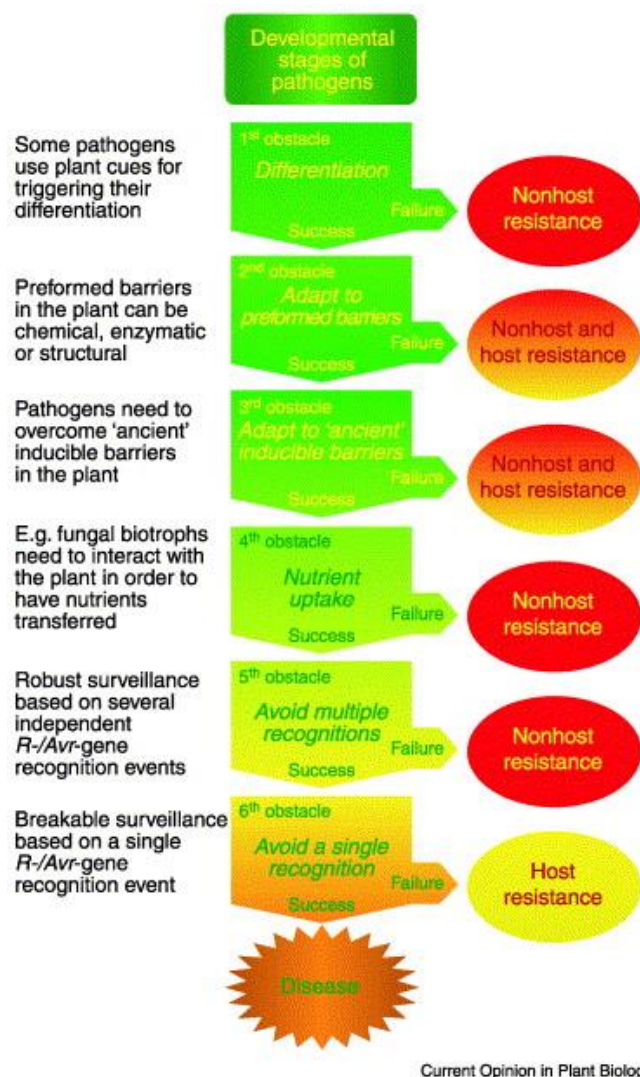


**Fig 1.1** A simplified view of the challenges met by a pathogen as it attempts to cause disease. Stages at which nonhost and host resistance are manifested are indicated (from Thordal-Christensen, 2003).

Based on the model described above, innate immune signalling could evolve towards the following targets: first, abrogation of pathogen growth; second, genetic adaptation; third, biochemical defence; and fourth, structural changes of the host cells (Day *et al.*, 2011). It seems that plants employ more than one strategy: 25% of the genes in a given cell can display altered expression pattern after pathogen inoculation (Ascencio-Ibanez *et al.*, 2008).

### 1.1.2 Zig-Zag model of PAMP-triggered immunity and effector-triggered immunity

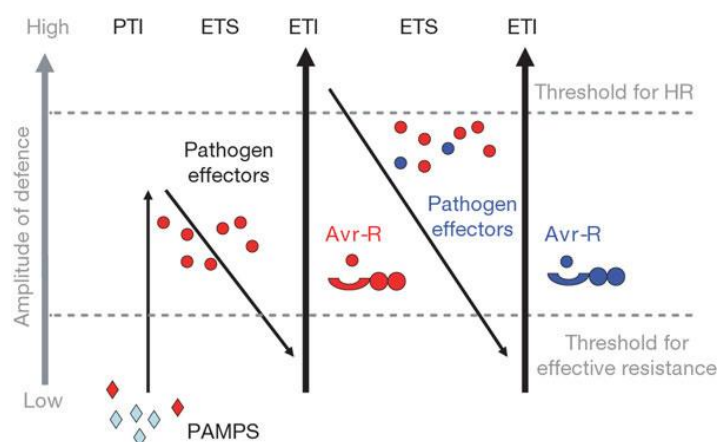


**Fig 1.2** A zigzag model illustrates the quantitative output of the plant immune system (from Jones & Dangl, 2006).

The complexity of plant-pathogen interaction has been conceptually advanced by the widely accepted notion that plant cells produce different immune responses depending on the nature of the pathogen and depending on the coevolutionary history of host and pathogen. Plant innate immunity comprises two distinct layers: the basal layer is evolutionarily ancient and triggered by conserved pathogen structures termed pathogen-associated molecular patterns (PAMPs). These PAMPs, e.g. flagellin, the subunit building the filament of bacterial flagellum, bind to specific receptors in the plasma membrane triggering so-called PAMP-triggered immunity (PTI) acting against a whole group of pathogens (e.g. all flagellate bacteria harbouring flagellin). This basal layer of broad immunity is often accompanied by a more advanced and strain-specific immunity termed effector-triggered immunity (ETI), which is triggered by pathogen effectors that have to enter the cytoplasm of the host cell (**Fig. 1.2**). The reason for this complexity is linked to coevolution between host and pathogen: PTI would be expected to select for pathogens, where the eliciting PAMPs are lost. However, since PAMPs are essential for the lifecycle of the pathogen, this evolutionary strategy does not work – a bacterial intruder lacking the PAMP flagellin would not elicit a PTI response, but it would also not be able to move. This dilemma stimulated, during a second round of host–pathogen warfare, the development of microbial effector proteins. These effectors are secreted into the cytoplasm of the host and suppress PTI (for review, see Tsuda & Katagiri, 2010). In response to these pathogen effectors, the host plant has evolved additional pathogen-specific receptors (encoded by so-called R genes) that specifically recognize the effectors in the cytoplasm and trigger the second layer of immunity, ETI (Boller & He, 2009). In many cases, ETI culminates in a plant-specific version of programmed cell death, the hypersensitive response, often followed by systemic acquired resistance of the host. The conceptual dichotomy between PTI and ETI has been very valuable to interpret and classify the

huge variety of plant defence responses, but this concept is presently on the move again. Recent studies show that the difference between PAMPs and effectors is more gradual than previously conceived (Thomma *et al.*, 2011). Moreover, PTI and ETI share numerous common events (Tsuda & Katagiri, 2010). Thus, the apparent dichotomy might be a question of signal quantity rather than quality. In addition, plants can discriminate different pathogens and activate different responses that are appropriate for the respective pathogen. Therefore, at present, the PTI-ETI concept is extended towards a signature based model (for review, see Aslam *et al.*, 2009).

### **1.1.3 Elicitors to mimic PAMP-triggered immunity and effector-triggered immunity**

Plant-immune receptors of the nucleotide-binding leucine-rich repeat (NB-LRR) protein family can be activated either by direct binding of elicitors or, alternatively, by elicitor action on an associated target protein that generates a “modified-self” molecule (Dodds & Rathjen, 2010). The archetypal elicitor of PTI is bacterial flagellin, which triggers defence responses in various plants (Gómez-Gómez & Boller, 2002). A synthetic 22-amino-acid peptide from a conserved flagellin domain (flg22) is sufficient to induce most of the cellular responses (Felix *et al.*, 1999). A genetic screen in *Arabidopsis thaliana* using flg22 identified the *Arabidopsis* leucine-rich repeat receptor kinase FLS2, which binds flg22 (for review, see Chinchilla *et al.*, 2006). Upon binding of the ligand, FLS2 is internalized by a receptor-mediated endocytic process that presumably has regulatory functions (Jones & Dangl, 2006; Bonardi *et al.*, 2011). A second example is the ADR1 family of *Arabidopsis* NB-LRR receptors, which in addition to its canonical functions such as phosphate-binding loop (P-loop) dependent activation by specific virulence effectors, can complete additional tasks, such as regulating the accumulation of the defence hormone salicylic acid, transducing signals down-stream of the activated NB-LRR, or mediating basal defence against virulent pathogens (Bonardi *et al.*, 2011). The *Arabidopsis* NB-LRR protein RPS5 as third example has recently been shown to function as fine-tuned sensor of alteration in the structures of effector targets (DeYoung *et al.*, 2012).

To trigger ETI-like programmed cell death experimentally, Harpin proteins can be used. These bacterial proteins, first discovered in *Erwinia amylovora*, a phytopathogenic bacterium causing the fire-blight disease of apple and pears (Wei *et al.*, 1992), have acquired considerable interest as triggers for hypersensitive response-like cell death and systemic acquired resistance. They act as components of a bacterial type-III secretion system and can induce host events characteristic for ETI, including production of reactive oxygen species (ROS), accumulation of defence-related transcripts, and cell death (for review, see Tampakaki *et al.*, 2010). Harpin proteins comprise different types that fulfil different functions during type-III secretion: HrpN is translocated into



the host cytoplasm, and a commercial elicitor based on HrpN was used in previous work from my group to mimic various aspects of ETI in grapevine suspension cells (Chang & Nick, 2012). In contrast, HrpZ, originating from the bean halo-blight pathogen, *Pseudomonas syringae* pv. *phaseolicola* (HrpZPsph), is localized in the apoplast and acts as helper protein supporting type-III secretion. Functional proof for a role in type-III secretion comes from experiments, where HrpZ could be successfully integrated into the type-III secretion model system of the mammalian pathogen *Yersinia enterocolitica* (Lee *et al.*, 2001). Furthermore, HrpZ was found to associate stably with liposomes and synthetic bilayer membranes and to form an ion-conducting pore *in vitro*. Whether HrpZ can trigger ETI in the strict sense, is not clear. The finding of pathovar-specific activities in *A. thaliana* (Haapalainen *et al.*, 2012) indicates the existence of cognate R-gene products. Due to this conceptual uncertainty, the term ‘ETI-like’ response will be used throughout the current work. In animal cells, the host cytoskeleton, in particular actin microfilaments (AFs), is a major target of type-III effectors (Cossart & Sansonetti, 2004). Although various type-III effectors of plant pathogenic bacteria can suppress plant defence responses such as hypersensitive cell death and expression of defence genes (for review, see Takemoto & Hardham, 2004), it is unclear whether they target to the cytoskeleton as observed in animal cells. So far, AvrBs3, an effector from *Xanthomonas campestris*, was reported to induce swelling of mesophyll cells, a response indicative of disrupted plant microtubules, and HopZ1a, a type-III secreted effector from *P. syringae* was claimed to interact with both tubulin heterodimers and polymerized microtubules (Marois *et al.*, 2002; Lee *et al.*, 2012).

## 1.2 Cytoskeleton and defence: structural events

Since several plant pathogens produce anticytoskeletal compounds during invasion (reviewed by Kobayashi & Kobayashi, 2008), the cytoskeleton seems to be an important player in plant defence. In fact, actin filaments appear to act cooperatively with PEN2 and PEN3 in penetration resistance against a broad range of pathogenic fungi (Stein *et al.*, 2006). The role of the cytoskeleton has been mainly discussed in the context of barrier responses to pathogen penetration, for example, by cell-wall papillae that can be observed at sites of penetration attempts. The formation of these papillae is preceded by a reorganization of the cytoskeleton, causing redistribution of vesicle traffic and cytoplasmic aggregation towards the penetration site (for reviews, see Takemoto & Hardham, 2004; Kobayashi & Kobayashi, 2008), and a somewhat slower migration of the nucleus (for review, see Schmelzer, 2002). In addition, the cytoskeleton participates in the execution of hypersensitive cell death that involves and requires massive remodelling of AFs and MTs (for review, see Smertenko & Franklin-Tong, 2011).

Outside a defence context, these cytoskeletal networks perform numerous functions that are essential for cell division, the integrity of cytoplasm, intracellular transport and cell shape. They play a central role in development, reproduction, and the cellular responses to biotic and abiotic stimuli. To study functions of MTs and AFs, pharmacological compounds are useful: colchicine (Green, 1962) and oryzalin (Wasteneys, 1992) have been used as MTs-depolymerizing agents; whereas taxol, stabilizes the MTs by inhibition of disassembly (Dhonukshe *et al.*, 2003); several cytochalasins (MacLean-Fletcher & Pollard, 1980) as well as latrunculin B sequester actin monomers and thus eliminate AFs due to their innate turnover (Wakatsuki, *et al.*, 2001); phalloidin and jasplakinolide instead stabilize AFs by inhibiting the disassembly of F-actin (Holzinger, 2009). Together with advances in life-cell imaging of cytoskeletal dynamics these tools have markedly altered our view of this network in plants (Guan *et al.*, 2013; for review, see Schmelzer, 2002; Kobayashi & Kobayashi, 2008).

### 1.2.1 Towards understanding the role of actin in defence

AFs are a dynamic, filamentous network of polymers constructed from a large pool of cytoplasmic actin monomers. This network of 5 to 7 nm diameter filaments (F-actin) as well as higher-order structures termed AF bundles, is generated from a cytoplasmic pool of monomers or G-actin. In plant cells, less than 5% of the G-actin pool are polymerized into filamentous actin (in contrast to some 50% in animal cells), which means that a large fraction of actin is kept in a stand-by mode with potential for explosive polymerization (Day *et al.*, 2011). In plants, this large G-actin pool is likely bound by profilin, adenylate cyclase-associated protein (CAP), and several actin-depolymerizing factors (ADF) (Chaudhry *et al.*, 2007).

The rate-limiting step of actin nucleation is the creation of a so called plus end (by nucleation factors like formin and the Arp2/3 complex), from where subsequently polymerization will proceed. This polymerization polarity is conferred by the endogenous asymmetry of subunits that assemble in a head-to-tail fashion, generating two intertwined, helical strands. Polarity is perpetuated as well by a lag between assembly, nucleotide hydrolysis, and phosphate release from subunits along the filament (Cecchini *et al.*, 2010). Besides the classical treadmill mechanism with assembly at the plus and disassembly at the minus end of the filaments, in plant cells a second mechanism contributes to actin reorganization that is termed stochastic dynamics (Konopka & Bednarek, 2008). Hereby, filament fragments anneal onto existing uncapped ends, resulting in rapid elongation (Smertenko *et al.*, 2010). By this mechanism, the growth speed of individual filaments could reach up nearly  $2 \mu\text{m s}^{-1}$ , allowing filaments to span the width of a cell in about 10 s. Most lifespans of AFs are less than 30 s; they do not disappear through loss of subunits from the minus end, but by prolific severing activity.

The complex and extensive organization of AFs conveys a multitude of important cellular functions, including cell division and development (Burgos-Rivera *et al.*, 2008; Deeks *et al.*, 2007), pattern formation and positioning (Klwine-Vehn *et al.*, 2006; Schellmann & Hülskamp, 2005), vesicle and organelle movements (Lee *et al.*, 2008, Pollard & Cooper, 2009), signalling (Samaj *et al.*, 2006), as well as responses to biotic (Opalski *et al.*, 2005), and abiotic stresses (Kadota *et al.*, 2009).

**Roles of AFs in PTI.** Binding of PAMPs activates mitogen-activated protein kinases (MAPK) signalling, a tightly regulated process that governs developmental, reproductive, and stress processes of host (Rodriguez & Mundy, 2010). In mammalian cells, AF assembly is regulated by both p38 MAPK and phosphatidylinositol-3-kinase (Khurana & Dey, 2003). In plant cells, there is no direct evidence for a link between activation of MAPK signalling and the regulation of AFs. However, there is evidence for AF responses linked with basal defence (Samaj *et al.*, 2003). For instance, the pathogen-derived toxin coronatine stimulates the rapid opening of stomata by chemical mimicry of the general plant stress signal jasmonate, facilitating pathogen entry. Since stomatal aperture is linked with reorganisation of AFs, this example indicates a link between general defence and AFs. AFs participate in callose deposition and organelle clustering around fungal penetration sites, as an important element of basal defence (Bestwick *et al.*, 1995; Opalski *et al.*, 2005; for review, see Schmelzer, 2002). In addition, the endocytotic recycling of plant PAMP receptors depends on AFs, as first discovered for the FLS2 receptor of Arabidopsis. This actin-mediated endocytosis of receptors is often necessary for signalling from intracellular compartments (Robatzek *et al.*, 2006). Thus, AFs are implicated in vesicle trafficking, organelle movements, cell wall deposition, and receptor recycling in the context of PTI.

**Roles of AFs in ETI.** Over the past several decades, the gene-for-gene concept of plant defence, originally confined to pathogen-derived avirulence (*Avr*) genes and their corresponding host-resistance (*R*) genes (Flor, 1956) has been extended by other cellular processes including development, gene expression, and reorganization of AFs into a more synthetic model referred to as the guard hypothesis (Chisholm *et al.*, 2006). The basic idea behind this guard hypothesis is the concept that plant cells are by default in the alert state and that defence has to be actively suppressed in the absence of pathogen challenge.

In animal cells, pathogens usurp the actin-based motility of the host to invade their victim and to propagate within the host tissue. This strategy includes inhibition of phagocytosis, induction of internalization by nonphagocytic cells, hijacking actin polymerization for bacterial motility, and alteration of actin homeostasis (for review, see Day *et al.*, 2011). Since actin-based motility does not play a role in walled plant cells, the role of actin must be fundamentally different. Here, it is mainly the role of actin in signalling that matters. In plant defence signalling, AFs are modified

through the activation of a coordinated network involving Rho-GTPase family members and their respective target proteins (Yang & Fu, 2007). As worked out for the R-protein RPS5 (RESISTANCE TO *PSEUDOMONAS SYRINGAE*-5) and its cognate pathogen effector molecule AvrPphB (cysteine protease delivered via the Type III secretion system (T3SS) of *P. syringae*), AFs participate in the perception of the effector and thus are essential for ETI. Interestingly, despite the different mechanism (actin-dependent signalling in plants, actin-dependent motility in mammalian cells), there seems to exist an evolutionary link: The effector AvrPphB shares homology with the effector YopT of *Yersinia pestis* (the pathogen causing the human Plague). YopT is a cysteine protease that, upon activation, can shut down the function of AFs.

Although the role of plant AFs as site of action for bacterial effectors is clearly different from the situation in mammalian cells, it is evident that they represent important targets. Whether pathogens directly manipulate AFs via the action of secreted effector molecules, or if the activity of these molecules disrupts the regulatory (i.e., GTPase) or structural (i.e., actin-binding protein, ABP) processes required for actin organization, needs further studies.

### **1.2.2 Towards understanding the role of microtubule in defence**

MTs are dynamic tubular structures composed of 13 protofilaments, each of which is formed by a linear polymerization of  $\alpha$ - and  $\beta$ -tubulin heterodimers. Microtubules are 25 nm in diameter and range up to 20  $\mu$ m in length (Nogales, 2000). Cortical MTs are important in the control of plant morphogenesis, because they control the direction of cell expansion by orienting microfibril deposition in the cell wall (Giddings & Staehelin, 1991). Cortical MTs in elongating cells often align transversely reinforcing a transverse alignment of cellulose microfibril deposition (Wymer & Lloyd, 1996). MTs reorient from transverse to longitudinal or oblique in response to various signals or developmental conditions (Giddings & Staehelin, 1991). In addition, MTs form a pre-prophase band guiding division symmetry (Gunning, 1982). In the mitotic spindle, MTs separate the duplicated chromosomes (Baskin & Cande, 1990). Specific for plants, microtubules deposit an endosomic belt prior to mitosis that later will guide the localisation of the phragmoplast, in concert with highly dynamic exploratory MTs nucleated at the spindle poles (for review, see Nick, 2008). The phragmoplast MTs form tracks for vesicles that provide the material for the new cell wall that physically separates the daughter cells (Verma, 2001; for review, see Collings, 1999; Dhonukshe *et al.*, 2003).

The dynamic polymerization and depolymerization of MTs is essential for their cellular function. These dynamics include two events dependent on GTP hydrolysis: during dynamic instability polymer assembly at the (+) ends is suddenly switched to disassembly, whereas treadmilling is based on a net growth of MTs at their (+) ends and shrinkage at their (-) ends (Wang *et al.*, 2011).

These dynamic events depend on MT-associated proteins (MAPs) and, in particular, a subclass of MAPs called (+)-end-tracking proteins (+TIPs) (Lloyd & Hussey, 2001). This scintillating behaviour allows MTs to decode temporal signatures of signals (for review, see Nick, 2013)

Recent evidence suggests a role of MTs upstream in signalling. For instance, in carrot protoplasts pharmacological elimination of MTs increased the time that voltage-gated calcium channels stayed open suggesting that they control the gating of these channels (Thion *et al.*, 1996). In response to salt stress MTs disintegrate rapidly depending on the MT-associated protein SPIRAL1 (SPR1) (Wang *et al.*, 2011). This disintegration is necessary for efficient adaptation to salt and involves the reformation of a more stable network of MTs, so called macrotubules (Komis *et al.* 2006). MTs are preadapted for a function as mechanosensors due to their relative rigidity in combination with their innate nonlinear dynamics, and were proposed to act as elements of a sensory hub that decodes stress-related signal signatures with phospholipase D (for review, see Nick, 2013). According to this model, MTs function in the decoding of stress signatures (**Fig. 1.3**).

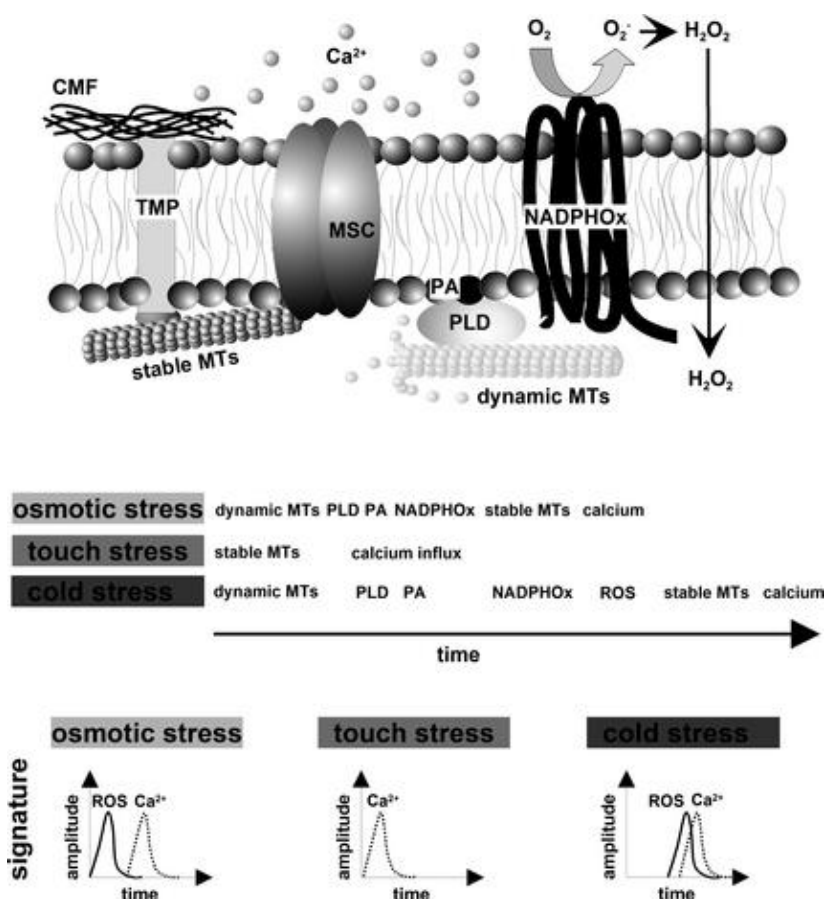


**Fig 1.3** Working model for microtubular function in the decoding of stress signatures. Microtubules with elevated stability, and microtubules with elevated dynamics interact in a different way, depending on the stress quality. This will yield different temporal readouts for osmotic stress, touch or wounding stress and cold stress (from Nick, 2013).

### 1.2.3 Macrotubules as stress-specific MT-array

Warfield & Bouck (1974) demonstrated *in vitro* that MTs can form so called macrotubules, consisting of tightly coiled helices formed by longitudinal compaction of loosely coiled protofilament pair intermediates. Such bifilar rings (which in some cases can even reorganize into highly organized paracrystals (Marantz & Shelanski, 1970)) and bifilar helices were produced by addition of the antimitotic drug vinblastine to either assembled MTs or soluble tubulin heterodimers *in vitro* within 10 min. The diameter of such macrotubules is in average 48 nm (Hinkley, 1978).

However, in plant cells, macrotubules have been observed *in vivo* in response to osmotic stress. These macrotubules are not a byproduct of the stress response, but actually necessary for osmoadaptation. The formation of macrotubules requires the initial disassembly of cortical MTs (Komis *et al.*, 2002). Inhibitors of PLD such as *n*-butanol can suppress both macrotubule formation and osmotic adaptation (Komis *et al.*, 2006), suggesting that membrane linkage of cortical MTs to PLD via phosphatidic acid, the product of this enzyme, is modulated by osmotic stress giving evidence for the PLD-MT-based signalling hub described above.

## 1.3 Cytoskeleton and defence: signalling events

### 1.3.1 Time course of events triggered by pattern recognition receptors

In order to study the sequential steps of the activation process and the precise timing of the cellular events, suspension-cultured plant cells have been used, because, here, the elicitors reach all cells and thereby trigger their receptors simultaneously (Boller & Felix, 2009). It should be clear that cell suspensions provide a typical reductionist approach focussed on the cellular responses – the study of systemic responses of defence, or the interaction with real pathogen interaction requires whole-plant systems.

**Initial responses (1-5 min).** Alkalinisation of the growth medium is considered to be the fastest cellular event to PAMPs and reports on changes of ion fluxes across the plasma membrane. These changes include increased influx of H<sup>+</sup>, Ca<sup>2+</sup>, and a concomitant efflux of K<sup>+</sup> and anions such as nitrate (Wendehenne *et al.*, 2002). These ion fluxes are accompanied by an apoplastic oxidative burst. These ROS might act as antibiotic agents, as originally shown for macrophages. In plant cells, however, they also contribute indirectly to defence by causing cell wall crosslinking, or acting as secondary stress signals to induce various defence responses (for review, see Boller & Felix, 2009). As third rapid response, calcium channels open which triggers MAPK cascades (Cheong *et al.*, 2003). For example, the PAMP flg22 triggered a transient increase in AtMPK6

activity in Arabidopsis, starting with a lag phase of ~1-2 min and peaking after 5-10 min (Nühse *et al.*, 2000).

**Early responses (5-30 min).** Following the initial responses, a panel of early responses is activated including ethylene biosynthesis, receptor endocytosis, and gene activation. For instance, an increased activity of 1-aminocyclopropane-1-carboxylate (ACC) synthase, a key enzyme in ethylene production, can be detected within 10 min. The flagellin receptor, FLS2 undergoes ligands-induced endocytosis leading to sensory adaptation safe guarding against over stimulation of defence (Robatzek *et al.*, 2006).

**Late Responses (hours).** Deposition of callose around the penetration site, and growth inhibition fall into this phase. Seedling growth inhibition might be a simple byproduct of defence, because a considerable portion of energy is channelled towards defence and thus is not available for growth. However, there might be also specific signals as indicated from a defence-induced miRNA in Arabidopsis that negatively regulates the F-box auxin receptors transport inhibitor response 1 and auxin signalling F-box proteins (Navarro *et al.*, 2006).

### 1.3.2 Reactive oxygen species

Both biotic (pathogen induced) and abiotic stress (injury, cold, ozone, hypo-osmotic, salinity desiccation, metals, etc.) can cause both intracellular and apoplastic production of ROS by oxidative burst. The different sources of ROS probably depend on the stress triggering ROS generation as well as on the plant organ that produces it (Garrido *et al.*, 2012). Intracellular sources of ROS are enzymes localized in mitochondria, chloroplasts and peroxisomes, such as xanthine oxidases and oxalate oxidases (Bolwell, 1999); apoplastic sources of ROS (mainly  $O_2^-$  and  $H_2O_2$ ) are enzymatic systems, such as the trans-plasmamembrane NADPH-oxidases (NOX), the NOX-respiratory burst oxidase (Torres *et al.*, 2006), and as third enzyme system the apoplastic peroxidases (cell-wall or plasma membrane localized extracellular peroxidases, ECPOX) (Minibayeva *et al.*, 2001).

### 1.3.3 Nitric oxide

Nitric oxide (NO) participates in multiple reactions: root branching, defence response, tropisms, flowering, stomatal aperture, xylem formation, stress response and stress adaptation (for review, see Hancock 2012). Besides, NO can also modify various proteins including tubulin (Salzano *et al.*, 2008). The sources for NO in plants are still under debate and experimentally hard to determine (Hancock, 2012). NO generation in chloroplasts (Jasid *et al.*, 2006) and mitochondria (Gupta *et al.*, 2010; Kasprowicz *et al.*, 2009) has been demonstrated, but the subsequent

metabolism seems to take place in other cellular domains. Unlike animals, there is no evidence that a nitric oxide synthase (NOS) enzyme exists in higher plants. However, the recent discovery of an algal NOS-like sequence (Foresi *et al.*, 2010; Del R ó, 2011) led to speculations that the peroxisomes might harbour a NOS activity. Alternative sources of NO in plants might be the nitrate reductase (NR) central for the reduction of inorganic nitrogen to ammonium to be integrated into the amino-acid metabolism (Rockel *et al.*, 2002).

The NO signal transduction pathway is mediated by the activation of cGMP synthesis, changes in cytosolic Ca<sup>2+</sup> concentrations, and activation of various protein kinases. NO modulates dynamic AFs and vesicle trafficking in root apices of maize, and recycling of wall polysaccharides in plants via the endocytic pathway (Kasproicz *et al.*, 2009). It has been speculated that NO might therefore directly affect actin or actin-binding proteins. Alternatively, it might primarily affect molecules of the vesicle trafficking apparatus, through *S*-nitrosylation of cysteine residues (Hess *et al.*, 2005), or nitration of aromatic amino acids, usually tyrosines that are essential for the function of these proteins (Monteiro, 2002).

### 1.3.4 Hormonal transduction

The chemical natures of plant hormones are diverse. Some are related to adenine (cytokinins), others are terpenoids (gibberellins, GA; abscisic acid, ABA), or small organic molecules synthesized from amino acids (auxin, ethylene). “New hormones” (in addition to the classical five classes listed above) have been identified including strigolactones (involved in rhizosphere signalling, control of dormancy, and branching), polyhydroxysteroids (brassinosteroids), phenol derivatives (salicylic acid, SA) or derivatives from oxidised fatty acid (jasmonate, JA), as well as peptide hormones (systemin). This chemical complexity is complemented by numerous cross-talks among the respective signalling pathways, for instance, between JA and ethylene, JA and auxins, ROS and oxylipins (for review, see Zhao *et al.*, 2005; Hoffmann *et al.*, 2011). The canonical view is that this crosstalk occurs mainly at the level of gene regulation. However, in the meantime, a number of good examples demonstrate that hormonal crosstalk already happens during signal transduction as well, e.g. the early signalling for auxin (Tan *et al.*, 2007), GA (Ueguchi-Tanaka *et al.*, 2005), JA (Sheard *et al.*, 2010), and ABA (Melcher *et al.*, 2010) shows numerous overlaps and cross-influences.

**Crosstalk between IAA and JA.** The antagonistic interaction between growth and defence seems to be brought about by antagonistic cross talk between IAA and JA signalling. The genes responding to these two hormones are, in the default state, inactivated by repressors. As repressors the Auxin/Indole 3-acetic acid (Aux/IAA), and Jasmonate ZIM-domain (JAZ) proteins have been identified, respectively. In response to the respective hormonal signal specific ubiquitin



protein ligase (E3) complexes are formed (for auxin signalling, the Transport Inhibitor Response, for JA signalling, the Coronatine Insensitive 1, COI1). As consequence of these events, the corresponding repressor protein is then degraded by the 26S proteasome, and the respective genes are released from repression. Since several components of these complexes are shared by auxin and JA signalling, mutations in these core components will affect IAA and JA signalling at the same time (Moon *et al.*, 2007). One of these components is AXR1 required for the activation of the E3 ubiquitin ligases SCF<sub>TIR1</sub> and SCF<sub>COI1</sub>, respectively (for review, see, Nick, 2006). Thus, activation of the JA pathway (during defence) will recruit AXR1 such that AXR1 is not available for auxin signalling, providing a simple mechanism to inhibit growth upon activation of defence.

**Phospholipid signalling.** Phospholipid signalling is a major player in several stress-related transduction pathways including osmotic stress or salicylic acid transduction. Distinct members of the phospholipase/phospholipid signalling system are involved in defence responses (**Fig. 1.4**). One of the most important signalling lipids is phosphatidic acid. It can modulate protein kinase and/or protein phosphatases involved in hormonal signalling; as well as activate the NADPH oxidase leading to the production of ROS; it can also integrate G protein and calcium signaling (Janda *et al.*, 2013).

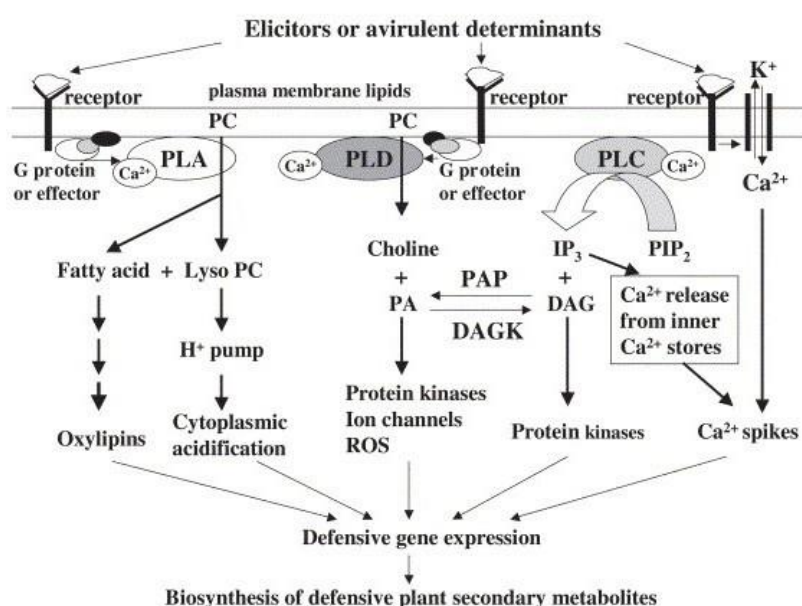


**Fig 1.4** Lipid messengers derived from hydrolysis of the plasma membrane. Proteins in the plasma membrane and the plasma membrane itself can perceive various stresses at first. Phospholipase A (PLA), phospholipase C (PLC), and phospholipase D (PLD), upon activation are by various environmental and hormonal stresses, hydrolyze membrane phospholipids, such as phosphatidylcholine (PC) and PIP<sub>2</sub>, to produce various lipid signal molecules. Free fatty acid products from PLA-catalyzed cleavage can be used for oxylin signalling pathway. A further PLA-generated hydrolysis product of PC, lysophosphatidylcholine (lyso PC), has multiple cellular functions, including activation of proton pumping from endomembrane systems to the cytosol resulting in cytoplasmic acidification and activation of the

## Introduction

biosynthesis of secondary metabolites. PLC hydrolyzes  $\text{PIP}_2$  into DAG and  $\text{IP}_3$ , which can activate protein kinases and mobilize  $\text{Ca}^{2+}$  from intracellular Ca stores. The central messenger, PA, can be produced either by PLD hydrolyzing phospholipids or through DAG phosphorylation by DAG kinase (DAGK). On the other hand, PA can also be converted into DAG by PA phosphatase (PAP). PA may directly or indirectly affect plant secondary metabolism (from Zhao *et al.*, 2005).

Recently it has become evident, that phospholipases interact with the cytoskeleton, which is relevant for both fundamental physiological processes and plant defence.

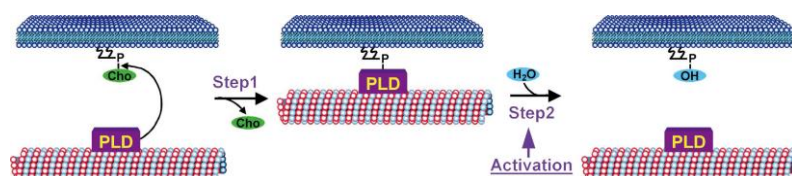


**Fig 1.5** Model for PLD-activated reorganization of plant microtubules (from Dhonukshe *et al.*, 2003).

PLD was purified originally as microtubule-associated protein from tobacco (Marc *et al.*, 1996) and subsequently shown to mediate the effect of a couple of environmental signals on the organization of cortical microtubules (for review, see Dhonukshe *et al.*, 2003; **Fig. 1.5**). The model is based on a two-step transphosphatidylation catalyzed by PLD. PLD forms a covalent intermediate with the phosphatidyl moiety through a His residue in the catalytic site of the enzyme. In the first step, the choline group is removed, leaving PLD and its associated microtubule covalently attached to the phosphatidyl moiety. Both PLD and MTs remain anchored to the membrane until transphosphatidylation occurs in the second step. At that moment, the PLD-microtubule complex detaches from the membrane, but the neighbouring PLDs remains attached, maintaining the membrane link of the MT.

Upon the interaction with activators of PLD, such as *n*-butanol (but not *sec*- and *tert*- butanol, that cannot act as targets for the second step, the “transphosphatidylation”), mastoparan, xylanase, NaCl, and hypoosmotic stress, cortical MTs are released from the plasma membrane and partially depolymerized. This effect can be reversible. Activation by *n*-butanol allows to monitor the formation of phosphatidylbutanol *in vivo* using fluorescent dyes and was therefore in the center of interest. This agent not only influences the interphase cortical MTs, but also those of other membrane-associated MT arrays, such as the preprophase band (PPB) and the phragmoplast, however, not those in the (not membrane-associated) spindle apparatus (Dhonukshe *et al.*, 2003). The treatments used to activate PLD will activate other signalling pathways as well. For instance, most of them have been shown to activate  $\text{Ca}^{2+}$  signalling (Knight, 2000) with implications for membrane biogenesis and trafficking (for review, see Wang, 2001).

**Feedback loop between auxin and AFs.** The cytoskeleton, this time through actin, also provides a link between auxin signalling and defence. The directional flux of auxin depends on the effect of actomyosin-driven cycling of auxin-efflux carriers (Friml, 2003). Therefore, elimination of AFs can block auxin-dependent growth significantly (Thimann & Biradivolu, 1994). Cells that undergo rapid elongation are endowed with fine strands of AFs (correlated with a cytosolic fraction of actin), but they are bundled (correlated with vesicle-bound actin) in response to conditions that inhibit growth. These bundles can be rescued, when auxin is added (Waller *et al.*, 2002). As discussed above, AFs participate either in basal defence (regulation of stomatal aperture, implication in vesicle trafficking, organelle movements, cell wall deposition, and receptor recycling) or in ETI (participation in the perception of the effector). Hereby, the auxin and AFs are involved in the feedback loop to keep the balance of plant growth and defence.

### 1.3.5 Ion channels

AFs dynamics regulates  $\text{Ca}^{2+}$  and  $\text{K}^{+}$  fluxes across the membrane of guard cells, which is of importance for guard cell function (Liu & Luan, 1998; Hwang & Lee, 2001; MacRobbie & Kurup, 2007; Kim *et al.*, 2010). However, little is known about the molecular nature of the corresponding ion channels or transporters (Ranf *et al.*, 2008). Two genes encoding putative calcium channels have been cloned in *Nicotiana tabacum* and are discussed as possible candidates: *NtTPC1A* and *B* encode putative voltage-gated calcium channel located at the tonoplast, whereas *NtMCA1* and *2* code for putative mechanosensitive calcium channel located at the plasma membrane. Microbial elicitors of PTI stimulate an influx of  $\text{Ca}^{2+}$  from the apoplast and cause a rapid increase in cytoplasmic  $\text{Ca}^{2+}$  concentration, which might serve as second messenger to promote the opening of other membrane channels (Lecourieux *et al.*, 2002), or to activate calcium-dependent protein kinases (Ludwig *et al.*, 2005).

### 1.3.6 Phytoalexins

Plant secondary metabolites are unique resources for pharmaceuticals, food additives, and fine chemicals. Some products are successfully industrialized for commercial application, e.g. shikonin from *Lithospermum erythrorhizon* cell cultures, taxol from *Taxus* cell cultures; moreover, numerous compounds were purified and intensively studied, e.g. sanguinarine, ajmalicine,  $\beta$ -Thujaplicin and resveratrol. Phytoalexins, a functionally defined class of secondary metabolites, are generated *de novo* in response to stress factors, such as pathogen attack, on grapevine in particular, e.g. the induction of stilbenes and resveratrol. Resveratrol, in addition to its classical role as antimicrobial phytoalexin, was considered as an important regulator for initiation of HR-related cell death, and could cause the AFs bundling, but not the MTs disruption (that can be triggered by Hrp) (Chang *et al.*, 2011). The synthesis of specific secondary

metabolites with antibiotic activities will be helpful not only to dissect the chemical processing, signal transduction networks, molecular regulatory mechanisms, engineering metabolic fluxes, but also to administer the chain of the events interacting with cytoskeletal.

### 1.3.7 Programmed cell death

Programmed cell death (PCD), a genetically controlled process leading to the selective elimination of unwanted or damaged cells in all eukaryotes, is also essential for the development and maintenance of immune system and its responses to exogenous and endogenous stimuli. The mechanisms leading to PCD differ between plants and animals, and the nomenclature is still on the move. For the animal field, at least two mutually exclusive pathways, termed apoptosis and necroptosis, have been identified (for review, see Han *et al.*, 2011). Apoptosis involves the activation of caspases, DNA fragmentation and membrane blebbing. In contrast, features of necroptosis are swelling of cellular organelles and cytoplasm with subsequent rupture of the plasma membrane and cell lysis. Programmed cell death in plants differs fundamentally (for a conceptual review see Jones, 2001) – neither caspases, nor NF- $\kappa$ B, nor membrane blebbing, central players or events in mammalian programmed cell death could be detected in plant cells. But also in plants, it becomes progressively clear that there exist several forms of programmed cell death. In addition to the defence-related hypersensitive response often observed as final outcome of successful ETI, there exist more general types that are currently designated as autophagy (Lai *et al.*, 2011).

This brief summary of the cellular events to pathogen attack pinpoint the following key elements: activation of the membrane-located receptors, modulation of (mechanosensitive) ion channels, oxidative burst in the apoplast, reorganization of the cytoskeleton, activation of MAPK cascades and JA signalling, and induction of phytoalexin metabolism as elements of basal immunity (PTI). In case of ETI, pathogen effectors silence different targets of this basal defence signalling, but are then sensed by intracellular receptors that can then induce a strong oxidative burst, vacuolar disintegration (**Fig. 1.6**), and PCD (Qiao *et al.*, 2010; Zhao *et al.*, 2005).

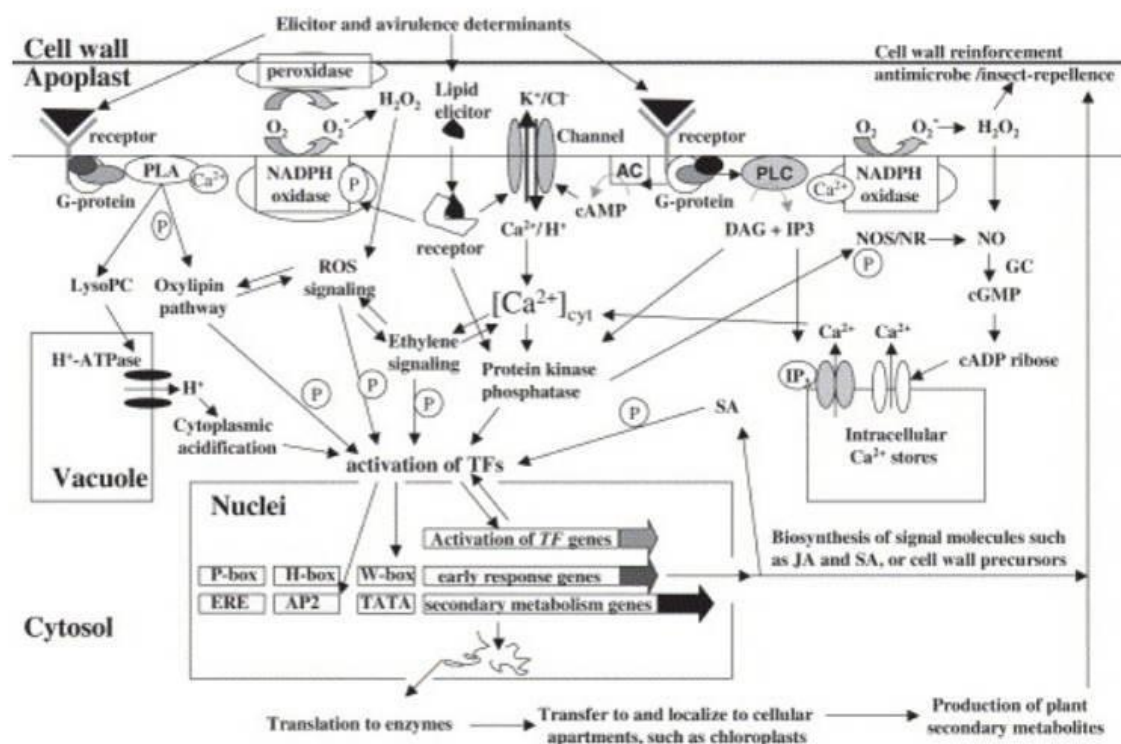


**Fig 1.6** A comprehensive schematic illustration of elicitor signal transduction network for PTI. Proteinaceous or carbohydrate elicitor molecules are recognized by specific receptors on the plasma membrane. G-proteins may be coupled to receptors and mediate elicitor-induced ion channel activation. Ion fluxes, especially  $\text{Ca}^{2+}$  influx, cause cytosolic free  $\text{Ca}^{2+}$  spiking which causes activation of protein kinases, peroxidases, NADPH oxidases, and phospholipases, which further generate other signalling messengers, such as reactive oxygen species, DAG,  $\text{IP}_3$ , cAMP, lysoPC, JA, ethylene, NO, cADP ribose, and SA. These messengers trigger parallel, but mutually interactive signal pathways that integrate these signals onto regulation of transcription factors (TFs) to activate gene expression by transcriptional regulation. The phenylpropanoid is central for cell-wall reinforcement (lignin precursors), but also for flavonoid and stilbenoid phytoalexins. The circled “P” shows protein phosphorylation and dephosphorylation-dependent regulation while the circled “Ca” shows  $\text{Ca}^{2+}$ -dependent regulation. Lipid elicitor such as syringolide or cerebroside could be perceived by receptors localized to the cytoplasm as well as bacterial effectors activating ETI. NOS: nitric oxide synthase; NR: nitrate reductase; AC: AMP cyclase; GC: GMP cyclase. It must be noted that a plant can use and combine also parts of this signalling network (from Zhao *et al.*, 2005).

## 1.4 Case studies for cytoskeletal functions in the response to biotic/abiotic stress

### 1.4.1 Bacterial, fungal, oomycete and viral infection

Takemoto & Hardham (2004) demonstrated before pathogen attachment, MTs and AFs within the cell display an overall axial or helical alignment. MTs maintain the nucleus in a subapical position about 30-40  $\mu\text{m}$  behind the apex. AFs remain thick bundles in vacuolated regions, and merge into finer bundles in the subapical cytoplasm. Within minutes of infection, reorganization of both MTs

and AFs happened. These various reorganizations depend on pathogen (bacteria, fungi, oomycetes) and host (**Fig. 1.7**).

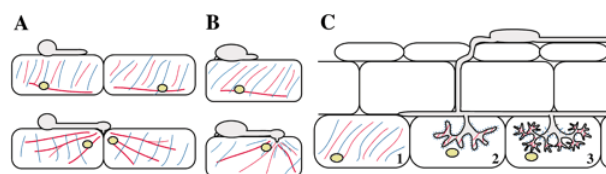


**Fig 1.7** Diagrammatic representation of the organization of the plant cytoskeleton during different plant-microbe interactions. **A** Interaction between a plant and a filamentous pathogen, such as that between *Arabidopsis* and *P. parasitica*. Top, Microtubules (blue), actin microfilaments (red), and nuclei (green) before appressorium formation or attempted penetration. Bottom, Actin microfilaments become focused on the penetration site and the nucleus is moved close to the invading pathogen. **B** Interaction between a plant and a filamentous pathogen, such as that between barley and *Erysiphe*. Top, Cytoskeleton and nucleus before appressorium formation. Bottom, Microtubules and actin microfilaments become focused below the infection site and the nucleus also moves to this site. **C** Cytoskeletal rearrangements during colonization by an arbuscular endomycorrhizal fungus. Before colonization, microtubules and actin microfilaments are aligned in ordered cortical arrays in cortex cells (**C**, subsection 1). During arbuscule development (**C**, subsection 2), actin microfilaments and apparently unpolymerized tubulin occur next to the perifungal membrane around the arbuscule. As the arbuscule matures (**C**, subsection 3), dense arrays of short microtubules and actin microfilaments line the perifungal membrane. The plant nucleus becomes positioned adjacent to the arbuscule (from Takemoto & Hardham, 2004).

Whereas the cytoskeleton participates in early sensing or defence responses in the interaction of oomycetes, bacteria or fungi, viruses usurp the plant cytoskeleton for disease spread such that the plant cannot use it to mediate its own defence responses (for review, see Takemoto & Hardham, 2004). To combat viral infections, plants attempt to silence viral gene expression by microRNA, and small interfering RNAs accompanied by salicylic-acid mediated signalling to the still uninfected parts of the plant (Singh *et al.*, 2004; Chen, 2010; Vance & Vaucheret, 2001). Plant viral nucleic acids and virions far exceed the size exclusion limit of plasmodesmata, the intercellular contacts of plant cells. As discovered first for the Tobacco Mosaic Virus (TMV), plant viruses utilise microtubules of the host cells to spread through the plant (Heinlein *et al.*, 1995), making use of molecular mimicry. A viral movement protein mimicks tubulin and can bind to plant microtubules. The exact mechanism of movement is still far from clear. Since viral movement is slowed down in tobacco mutants with reduced microtubular dynamics, a simple motor-driven transport can be ruled out (Ouko *et al.*, 2010). A current model assumes that complexes of viral RNA and movement protein assemble near the endoplasmic reticulum and move towards the plasmodesmata by an ER-mediated mechanism that depends also on MTs (reviewed in Heinlein, 2008); MTs are not actin isolated, however, on the contrary, there is evidence for a supporting role of AFs in the intracellular and intercellular movement of TMV replication complexes (Kawakami *et al.*, 2004).

### 1.4.2 Salt stress

The salt stress response includes a rapid depolymerisation of MTs followed by the formation of a new MT network that is very stable. Wang *et al.* (2011) showed that the MT-associated protein SPR1 plays a key role in salt stress-induced MT disassembly. Salt stress accelerates the 26S proteasome-dependent degradation of SPR1 which facilitates and promotes MT disassembly (**Fig. 1.8**). This MT decay is an active process and can be suppressed by inhibitors of the proteasome or, genetically, in mutants of the proteasome. Suppression of the MT decay results in elevated sensitivity to salt stress. Thus, MTs have to yield first in order to activate efficient salt adaptation. In tobacco (*Nicotiana tabacum*) BY-2 cells cortical MTs change from a structured to a random organization within 15 min (Dhonukshe *et al.*, 2003). Also in Arabidopsis, sustained salt stress affects cortical MT organization and impairs growth, especially pronounced in *spr1* mutants (Shoji *et al.*, 2006). Thus, the microtubular response to salt stress is biphasic, starting with a massive MT depolymerization followed by the formation of new, stable MT networks (Wang & Yuan, 2007).

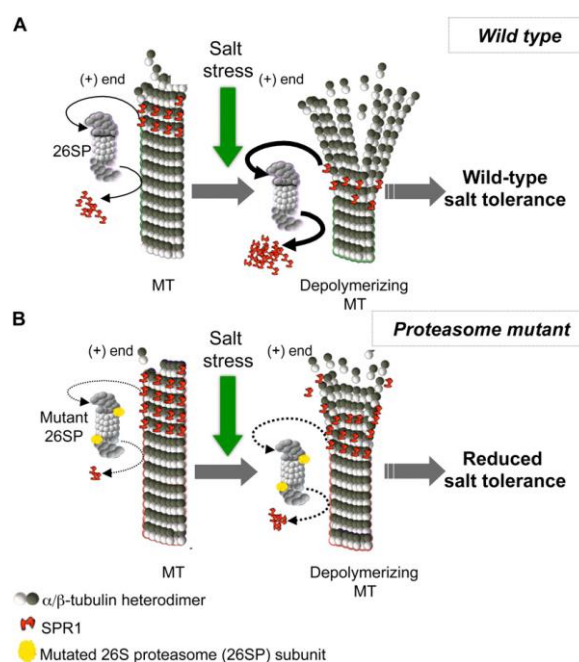


**Fig 1.8** Model summarizing the role of SPR1 proteolysis in the salt stress tolerance of wild-type and proteasome mutant cells. SPR1, a (+)-end MAP, is degraded by the 26S proteasome (26SP). In 26S proteasome mutants, the degradation rate is reduced and the MTs are more stable due to SPR1 accumulation. Upon perception of salt stress, a still unknown mechanism leads to the increased proteasome-dependent degradation of SPR1 that facilitates MT depolymerization. In proteasome mutants, salt stress-induced degradation of SPR1 is reduced, which slows down MT depolymerization and causes salt stress hypersensitivity. This schematic is simplified for the purpose of clarity: no other (+)-end MAPs but SPR1 are depicted, and all (-)-end components are omitted (from Wang *et al.*, 2011).

Not only MTs, but also AFs are affected by salt stress. The underlying mechanism has been partially elucidated by a recent study on the Arabidopsis mutant *salt overly sensitive 3* (*sos3*). The SOS3 protein plays an important role in plant salt tolerance by mediating the effect of salt-stress induced calcium influx on transporters that restore  $\text{Na}^+/\text{K}^+$  homeostasis. Under salt stress AFs assemble abnormally, which is more pronounced in the *sos3* mutant. The mutant phenotype can be partially rescued by addition of external calcium (Ye *et al.*, 2013).

### 1.4.3 Cold stress

The adaptation of plants to cold stress requires low temperature that can be sensed. As “thermometer” plants use changes of membrane fluidity and MT disassembly that are transduced into calcium influx) (for review, see Nick, 2013). Traditionally, chilling tolerance to cool, but non-freezing temperatures is distinguished from freezing tolerance. The cytoskeleton seems to be one of the primary targets during chilling damage. Cytoplasmic streaming, conveyed by actomyosin, is blocked within a few minutes when temperature falls to 10 °C in cucumber or tomato (Wood *et al.*, 1984), whereas it can proceed down to 0 °C in chilling-resistant species (Lyons, 1973). A cold-induced rapid, but transient partial disassembly of microtubules preceded the formation of cold-stable MTs and the recovery of growth rate in freezing tolerant cultivars of winter wheat (Abdrakhamanova *et al.*, 2003). Similar to the MT response in salt stress, this early disassembly was followed by reformation of a stable MT network and was found to be necessary and sufficient to induce cold acclimation. This cold acclimation has been considered traditionally to be linked with increases in the content of abscisic acid. However, the cold hardening of MTs could be shown to occur independently of abscisic acid in winter wheat (Wang & Nick, 1998), consistent with evidence that a certain part of cold-induced gene expression is independent of abscisic acid. This second pathway involves a calcium-influx triggered kinase cascade (thus showing signal overlap with basal defence), which will culminate in the expression of freezing protectants (Medina *et al.*, 1999).

The cold-induced microtubule disassembly was found in tobacco BY-2 to be followed by accumulation of tubulin in the nucleus (Schwarzerová *et al.*, 2006). Upon rewarming, new MTs rapidly emerged from the nuclear periphery and reconstituted new cortical arrays. This reversible permeabilization of the nuclear envelope for tubulin is probably linked with the identification of nuclear-export sequences in plant tubulin that meanwhile were shown to be functional (Schwarzerová *et al.*, manuscript in preparation). According to the textbooks, tubulin is strictly excluded from the karyoplasm by the nuclear envelope, and the disintegration of the nuclear envelope during mitosis is a prerequisite that microtubules can link with chromatin during the establishment of the division spindle. However, tubulin has a long intranuclear history as evident from so-called closed mitosis in protists and algae, where nuclear division takes place within an



intact nuclear envelope (reviewed in Schmit & Nick, 2008). Apparently, this evolutionary ancient mechanism is activated in response to cold stress.

## 1.5 Scope of this study

Microtubules and actin filaments are central players for the plant response to various stress factors and therefore have great potential for novel approaches to increase the stress tolerance of crop plants. However, this potential has not been exploited so far. Grapevine has emerged as model for applied plant biology since it is well studied on the level of functional genomics (with several genome projects completed) and the crop with the highest cash yield per area. In my Ph.D. work, I therefore studied the responses of the cytoskeleton to abiotic and biotic stress factors in grapevine.

Grapevine harbours some 30000 predicted genes (Velasco *et al.*, 2007). Some of these genes are implicated in traits relevant to grapevine resistance, secondary metabolites, and wine quality. Jaillon *et al.* (2007) reported a high-quality draft of the genome sequence of grapevine PN40024 genotype that was derived from *Vitis vinifera* 'Pinot Noir' being bred close to fully homozygosity by successive selfings. Soon after, a physical map was constructed for *Vitis vinifera* 'Cabernet Sauvignon', contributing to studies of candidate genes for disease resistance and signalling (Moroldo *et al.*, 2008). Grapevine was the second sequenced woody species after poplar, and the first sequenced fruit crop. Compared to Arabidopsis, the potential for agronomy is overwhelming, and meanwhile, grapevine is considered as “the” model for perennial plants, especially with respect to defence. The use of grapevine as model for plant defence is not only linked to agronomy, however, but based on the fact that there exist disease-resistant wild species of grapevine, whereas cultivated grapes are disease-susceptible, which allows to link genetics with resistance. The background for this peculiar phenomenon is linked with evolution and globalization:

Prior to the glacial period, the genus *Vitis* was widely distributed over the entire Northern hemisphere with numerous species in Europe (Kirchheimer, 1938). By the end of the Pleistocene, it had declined in Europe with only one fossile record for *Vitis vinifera ssp. sylvestris* reported for Southern France (de Lumley, 1988). The cultivated grapevine *Vitis vinifera ssp. vinifera* was derived from this founder population. In contrast, North America and East Asia have preserved numerous species of the genus *Vitis*. Nowadays, the world has approximately 7.4 million hectares of vineyards, which means that 0.5% of the total world arable land is mainly dedicated to wine production (Canada's Michael Smith Genome Sciences Centre). In addition to its enormous agronomic merits, the phytoalexins produced by grapevine in response to abiotic and biotic stress have attracted considerable interest for medical reasons. For instance, resveratrol, a stilbene

phytoalexin from grapevine produced in response to pathogen elicitors (Chang *et al.*, 2011) is well-known for its health benefits to human including prevention of cardiovascular disease, protection against cancers, obesity, diabetes and neurodegenerative diseases, and extension of lifespan by mimicking the effects of caloric restriction.

Among the numerous diseases of grapevine, Downy Mildew of Grapevine, caused by the oomycete *Plasmopara viticola*, is the most serious problem for viticulture in Central Europe. *Plasmopara viticola* was introduced to Europe in 1860 with contaminated rootstocks of wild grapes from North America (in order to combat *Phylloxera*, a noxious insect that had been brought to Europe a few decades earlier). Since then, Downy Mildew causes substantial losses in viticulture. In the Upper Rhine Region in average 25% of the harvest are destroyed by this disease. Since the economic value of grapevines is very high (about 40-50 T€ per ha), the losses amount to some 10 T€ per ha and year, in some cases even total loss of harvests are reported. The traditional German cultivars are all highly susceptible to this disease. Without chemical plant protection profitable production of quality wine is almost impossible. About 8-10 treatments per season are required, which amounts on the about 100000 ha vineyards in Germany to some 175 t of fungicides (making up for the vast majority of fungicide use). The biology of this pathogen is only partially understood, because it can only be maintained and propagated on the host plant, not on host-free media rendering many molecular approaches cumbersome or even impossible.

Consumers and society are progressively asking for sustainable forms of agriculture. In viticulture, there is strong demand for so called “ecological wine”, which has been produced without the massive use of fungicides. Thus, the key aspect for sustainable viticulture is grapevine defence. The cytoskeleton with its relevance for stress adaptation in general, and its role in defence in particular, would provide interesting targets to achieve this goal. What are the roles that cytoskeleton plays in defence in grapevine? To answer this question, GFP-tagged cytoskeleton marker lines are required for *in vivo* observation, since the traditional methodology for cytoskeleton visualization, by either immunofluorescence (MTs) or by fluorescent phalloidin (AFs), both required fixation of the cells, such that only the bulk changes of the cytoskeleton occurring at the late stages of the response are detectable. In this study, first, the tobacco BY-2 system was investigated, where GFP-tagged cytoskeleton marker lines for the cytoskeleton have been already established, which allowed to follow the cytoskeletal response over time in living cells and thus also detection of the earlier stages of cytoskeletal remodelling. The cellular responses of BY-2 to flg22 (PTI) and HrpZ (ETI-like response) were compared with focus on the cytoskeleton. Then, transgenic grapevine plants and suspension cells were generated that express GFP-tagged markers for AFs and MTs, respectively. Making use of these fluorescent tags, it became possible, for the first time, to study the role of cytoskeleton in biotic/abiotic stress factors

relevant to “real life” in viticulture *in vivo* using state-of-the-art spinning-disc confocal microscopy. This approach allowed to observe the formation of macrotubules in response to osmotic stress, JA, and Hrp, the emergence of tubulin in interphase nuclei, and the formation of perinuclear actin baskets in response to inoculation with *P. viticola*. These observations are consistent with the published record from other plants and show that these cytoskeletal marker lines of grapevine allow to monitor the responses of microtubules and actin in a non-invasive manner, preserving the physiology of the cells. In addition to numerous details of these cellular responses that could be observed for the first time, this technology also allowed novel insights into the interaction between host and pathogen during infection with *P. viticola* and various phytopathogenic bacteria. Based on these observation, we arrive at a model, where the stomata act as gatekeeper signaling the presence of *P. viticola* zoospores to the surrounding epidermal cells that then trigger defence-related AF responses prior to direct contact with the pathogen.

## 2 Materials and methods

### 2.1 Plasmid construction

To generate a fluorescent actin marker, the GATEWAY vector pK7WGF2-GFP-*AtFABD2* (Durst *et al.*, 2013) was transformed into the *Agrobacterium tumefaciens* strain EHA105 by means of an improved freeze-thaw transformation protocol (Chen *et al.*, 1994): After thawing cells at room temperature for 10 min, 700 ng of plasmid DNA were added to competent cells, and mixed gently. The cells were then frozen in liquid nitrogen for 1 min, and thawed again for 5 min in a water bath at 37 °C. 500 µl of LB medium (Bertani, *et al.*, 1951). Duchefa, Haarlem, The Netherlands) were added and incubated shaking at 28 °C for 2 h, before plating aliquots of 100-200 µl on solidified LB medium with 50 µg/ml spectinomycin, 15 µg/ml rifampicin and 300 µg/ml streptomycin. Colonies appeared after 2-3 days.

To generate a fluorescent microtubule marker, the GFP-*AtTUB6* (GFP was fused to the N-terminus of Arabidopsis  $\beta$ -tubulin 6 (At5g12250), Nakamura *et al.*, 2004) was used. The insert was amplified by PCR from pBI121-GFP-*AtTUB6*, and then two constructs were conducted (since none transformed plants were obtained from the first construct, so a second one was conducted). The first one was introduced into the binary vector pCambia1300\_(CAA)<sub>n</sub>2×T (Francesca *et al.*, 2007; Luo & Chen, 2007). The first construct is based on GATEWAY vector pH7WGF2-GFP- *AtTUB6* (Durst *et al.*, 2013); the second construct, GFP-*AtTUB6* was under control of the constitutive CaMV35S promoter, and two terminators, one of nopaline synthase (NOS), and one of CaMV35S. The construct was introduced into *Agrobacterium tumefaciens* strain EHA105 by means of the improved freeze-thaw transformation protocol described above (Chen *et al.*, 1994). With respect to the antibiotics, 50 µg/ml kanamycin (for vector pCambia1300\_(CAA)<sub>n</sub>2×T) 50 µg/ml spectinomycin (for vector pH7WGF2-GFP- *AtTUB6*), 15 µg/ml rifampicin and 300 µg/ml streptomycin were utilized.

### 2.2 *Agrobacterium* mediated transformation of grapevine

#### 2.2.1 Leaves of *V. vinifera* ‘Chardonnay’ expressing GFP-*AtFABD2*

**Preparation of suspension embryos and *Agrobacterium*:** Suspension embryo cultures of *V. vinifera* ‘Chardonnay’ generated from anther, maintained as suspension cell line were used in this experiment (**Fig. 2.1A**). The embryos were cultivated in liquid NN<sub>69</sub> medium [2.2 g L<sup>-1</sup>, maltose 20 g L<sup>-1</sup>, glycerol 4.6 g L<sup>-1</sup>, MES 0.5 g L<sup>-1</sup>, 6-benzylaminopurine (BA) 0.25 mg L<sup>-1</sup>, 2, 4-dichlorophenoxyacetic acid (2,4-D), adjusted to a pH of 5.8]. Embryos were subcultured weekly,

inoculating 10 ml of stationary culture into 200 ml of fresh medium in 500-ml Erlenmeyer flasks. The cell suspensions were incubated at 25 °C in the dark on an orbital shaker (KS250 basic, IKA Labortechnik, Staufen, Germany) at 150 rpm.

**Agro-infiltration:** A single colony of *Agrobacterium tumefaciens* strain EHA105 growing on selective agar plates was inoculated into 20 ml of LB medium supplemented with the appropriate antibiotics, incubated at 28 °C at 200 rpm on an orbital shaker for 48 h.

**Pre-culture:** 30 µl *Agrobacterium* (cultivated in LB medium to an optical density at 600 nm 0.6-2.0) were inoculated into 25 ml infiltration medium [50 ml 20X AB salt solution ( $\text{NH}_4\text{Cl}$  20 g L<sup>-1</sup>,  $\text{MgSO}_4 \cdot 7\text{H}_2\text{O}$  6 g L<sup>-1</sup>,  $\text{KCl}$  3 g L<sup>-1</sup>,  $\text{CaCl}_2$  0.2 g L<sup>-1</sup>,  $\text{FeSO}_4 \cdot 7\text{H}_2\text{O}$  15 mg L<sup>-1</sup>), 2.4 ml 500 mM phosphate solution ( $\text{K}_2\text{HPO}_4$  60 g L<sup>-1</sup>,  $\text{NaH}_2\text{PO}_4$  20 g L<sup>-1</sup>, pH 7.5), 100 ml 20% (w/v) Sucrose, 848 ml MES solution (3.9 g L<sup>-1</sup>, pH 5.8) per liter] with the appropriate antibiotics were cultivated in a 250 ml flask for one day. The next day, the *Agrobacterium* culture was centrifuged at 5,500 for 15 min, and re-suspended in 25 ml induction medium [50 ml 20X AB salt solution ( $\text{NH}_4\text{Cl}$  20 g L<sup>-1</sup>,  $\text{MgSO}_4 \cdot 7\text{H}_2\text{O}$  6 g L<sup>-1</sup>,  $\text{KCl}$  3 g L<sup>-1</sup>,  $\text{CaCl}_2$  0.2 g L<sup>-1</sup>,  $\text{FeSO}_4 \cdot 7\text{H}_2\text{O}$  15 mg L<sup>-1</sup>), 2.4 ml 500 mM phosphate solution ( $\text{K}_2\text{HPO}_4$  60 g L<sup>-1</sup>,  $\text{NaH}_2\text{PO}_4$  20 g L<sup>-1</sup>, pH 7.5), 100 ml 20% (w/v) Glucose, 848 ml MES solution (3.9 g L<sup>-1</sup>, pH 5.8) per liter] with the given antibiotics in a 250 ml flask. The next day, *Agrobacterium* was sedimented by centrifugation for 15 min at 5,500 rpm, re-suspended in 25 ml S-medium [NN<sub>69</sub> medium 2.2 g L<sup>-1</sup>, maltose 20 g L<sup>-1</sup>, glycerol 4.6 g L<sup>-1</sup>, 2-ethanesulfonic acid (MES) 0.5 g L<sup>-1</sup>, to final pH of 5.8] supplemented with 1 mg L<sup>-1</sup> of 1-naphthoxyacetic acid (NOA), in a 250-ml flask incubating at 28 °C, 200 rpm on an orbital shaker for 2 h.

At the same day, 5 ml packed cell volume (PCV) of 3 day old *V. vinifera* ‘Chardonnay’ embryo suspension cells suspended with co-medium [NN<sub>69</sub> medium 2.2 g L<sup>-1</sup>, maltose 20 g L<sup>-1</sup>, glycerol 4.6 g L<sup>-1</sup>, MES 0.5 g L<sup>-1</sup>, PVPP 2.5 g L<sup>-1</sup>, gelrite 3 g L<sup>-1</sup>, to final pH of 5.8] supplemented with acetosyringone (100 µM), were placed on filter paper, and briefly drained by a mild vacuum for 3-5 s. Together with the filter paper, the embryo cells were transferred into a petri dish with solid co-medium, sealed with parafilm, keep at 22 °C for two days.

**Co-cultivation:** Drops of *Agrobacterium* were spread onto the pre-cultured *V. vinifera* ‘Chardonnay’ embryo cells and co-cultivated at 22 °C for 3 days.

**Elimination of *Agrobacterium*:** From then on, the cultivation were incubated in phytotrons (Käte Kamrath, Germany), under a light regime of 16 h light / 8 h darkness using mixed light of Sylvania GRO-LUX F38W/GRO T8 and OSRAM L38W/840 LUMILUX cool white. After 3 days of cocultivation, the filter papers were transferred into selective medium [NN<sub>69</sub>-medium saccharose 30 g L<sup>-1</sup>, gelrite 3 g L<sup>-1</sup>, kanamycin 50 mg L<sup>-1</sup>, and carbenicillin 500 mg L<sup>-1</sup>, to final

## Materials and Methods

pH of 5.8]. 1 week later, the filter papers were transferred into fresh selective medium (**Fig. 2.1B**), from then on subcultured every 4 weeks (**Fig. 2.1C** shows the situation 4 weeks after the onset of selection). Transformed embryos form callus on selective medium were observed from 8 weeks after the onset of selection. Representative stages of embryo regeneration are shown in **Fig. 2.1D, E** some of them generated stem-like structure indicated by red arrows. At the same time early globular embryos (**Fig. 2.1H**) were the same stages of **Fig. 2.1D**, heart-stage embryo (**Fig. 2.1I**) torpedo-stage embryos (**Fig. 2.1J**), and first embryos with cotyledon could be observed (**Fig. 2.1K**). Embryogenesis lasted for another 6-12 months, still plantlets were formed and could be transferred into tubes (**Fig. 2.1F**). After a further month of growth in a test-tube, plantlets were propagated to a plastic box (**Fig. 2.1G**). From 10 months later, the plants had reached a size that the structure of AFs could be examined. A screen of different lines for a physiological actin organisation yielded two lines named as 5a and 10a, respectively. The whole process from transformation till transfer of the transgenic plants to the greenhouse required more than a year.

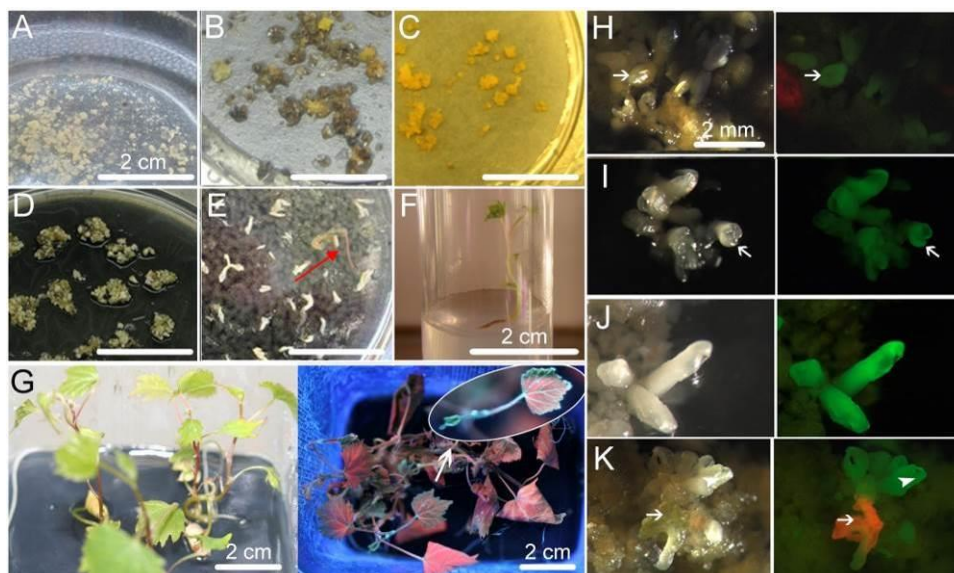


**Fig 2.1** Generation of transgenic *V. vinifera* 'Chardonnay' expressing the fluorescent actin marker GFP-AtFABD2 visualized by fluorescence stereo microscopy. **A** embryos generated from anther. **B, C** Transformed embryos to form callus on selection medium 1 week (**B**) and 4 weeks (**C**) later. Regeneration of embryos (**D** and **E**), around 8 weeks after transformation, stem-like structures indicated by red arrows. Plantlet formation from month 6 after transformation, developing plantlets after transfer into a Magenta box (**F**). **G** in the light and under the UV-lamp - to show the GFP signal. The inset image in **Fig.G** shows the green fluorescence best in the chlorophyll free leaf veins. **H** globular embryo. **I** heart embryo. **J** torpedo embryo. **K** cotyledonary embryo (arrow heads), and later stage with synthesis of chlorophyll (white arrows). Left, differential interference contrast, dic; right, GFP-filterset.

### 2.2.2 *Ex vitro* acclimation of transgenic plant

After 3 months of culture on selection medium ( $12 \text{ mg L}^{-1}$  Hyg B), the transgenic plantlets were acclimated. At first the transgenic plantlets *in vitro* (still in flasks) were placed in greenhouse for

1 week under a light regime of 16 h light / 8 h darkness with a temperature setting of 26 °C/22 °C (day/night), using sodium vapour lamps Philips SON-T AGRO 400 (Luxlight, Germany), 220  $\mu\text{mol m}^{-2} \text{s}^{-1}$ ). After washing out the agar attached to the roots, shoots and roots were cut back, keeping 4-5 nodes and 3-4 cm in length, respectively. Plantlets were cultivated in *Floradur* potting mix (Floraguard, Germany). In order to prevent direct sunshine, the plantlets were covered with a plastic lid and gauze. After two days, plantlets were sprayed with Ronilan DF (BASF, Germany). The plastic lids were removed after one week.

### 2.2.3 Cells of *V. rupestris* expressing *GFP-AtTUB6*

Suspension cell cultures of *V. rupestris* generated from leaves (Seibicke *et al.*, 2002) were used in this experiment. They were cultivated in liquid medium containing 4.3 g l<sup>-1</sup> Murashige and Skoog salts (Duchefa, Haarlem, The Netherlands), 30 g l<sup>-1</sup> sucrose, 200 mg l<sup>-1</sup> KH<sub>2</sub>PO<sub>4</sub>, 100 mg l<sup>-1</sup> inositol, 1 mg l<sup>-1</sup> thiamine, and 0.2 mg l<sup>-1</sup> 2, 4-dichlorophenoxyacetic acid (2, 4-D), pH was adjusted to 5.8. Cells were subcultured weekly, inoculating 8-10 ml of stationary cells into 30 ml of fresh medium in 100 ml Erlenmeyer flasks. The cell suspensions were incubated at 25 °C in the dark on an orbital shaker (KS250 basic, IKA Labortechnik, Staufen, Germany) at 150 rpm.

For the details of agro-infiltration, cocultivation and elimination of Agrobacteria refer to the previous section.

For preculture suspension cells of *V. rupestris* at day 3 after subcultivation (using aliquots corresponding to 7 ml packed cells) were used.

Subculture every 4 weeks till the stable transformed callus established and enough amount were gained for suspension culture induction (~ 6-8 weeks the first formed callus could be detected). Then the callus were collected and transferred into a 500 mL Erlenmeyer flask with 25 ml S-medium with NOA 1 mg/L with final pH of 5.8. Two weeks after, the callus were transferred into new medium (the same gradients as above) but with 150 ml volume of medium. Till homologous suspension cell could be gain (~ 6 weeks).

## 2.3 PCR detection and southern blot of genomic DNA.

Genomic DNA of transformants was extracted using a cetyl trimethyl ammonium bromide (CTAB) based protocol (Doyle and Doyle, 1987). The purified DNA was analysed by genomic PCR reactions. For the tested actin marker lines, insertion of probing for *eGFP* (using primers 5'-TGTCGGCCATGATATAGACG-3' and 5'-GTAAACGGCCACAAGTTCAG-3'), *AtFABD2* (using the primers 5'-CAAACCACCGATTAAGATGCCG-3' and 5'-CGCCCATAGAAGGTTGAGGAAGAATA-3'), the kanamycin resistance (with the primers

## Materials and Methods

5'-AGCCAACGCTATGTCCTGAT-3' and 5'-AAATGCTCCACTGACGTTCC-3'), and the left border region of the vector pK7WGF2 (with the primers 5'-GATGTTTCGCTTGGTGGTGGT-3' and 5'-AGAGGCTATTCGGCTATGA-3'). For the tested tubulin marker lines, insertion of *GFP* (using the primers 5'-ACTGGAGTTGTCCCAATTCTTG-3' and 5'-TCTTTTGTGTCTGCCGTGA-3'), *AtTUB6* (with the primers 5'-CGATGTTGTACGCAAAGAGGCTG-3' and 5'-GACGAGGGAAAGGAATGAGGTTTC-3'), and the left border region of vector pBI121 (primers 5'-GCAAACAATGAATCAACAAC-3' and 5'-AGAAAGGAAGGAAGAAAG-3') were used. The results were verified by non-radioactive Southern blotting (DIG DNA labeling and detection kit, Roche) according to the protocol of the manufacturer. The probe was cloned with a PCR-amplified DNA fragment locating at *eGFP*, and genomic DNA was digested with EcoRI overnight.

### 2.4 Quantitative phenotyping of transformed *Vitis* leaves

In order to eliminate phenotypical abnormalities arising from hormonal treatments during somatic embryogenesis, plants of line 10a were subjected to one period of overwintering in the greenhouse before analysing a venation phenotype manifest in the transformed leaves. Newly formed leaves were recorded using the programme Leafkit that had been generated by Benedikt Müller, a student of informatics in the course of the Master F2 module Plant Evolution. This self-learning image analysis program is based on common phenotypic traits of grapevine and yields quantitative outputs for several morphological parameters as defined in **Fig. 2.2B**.

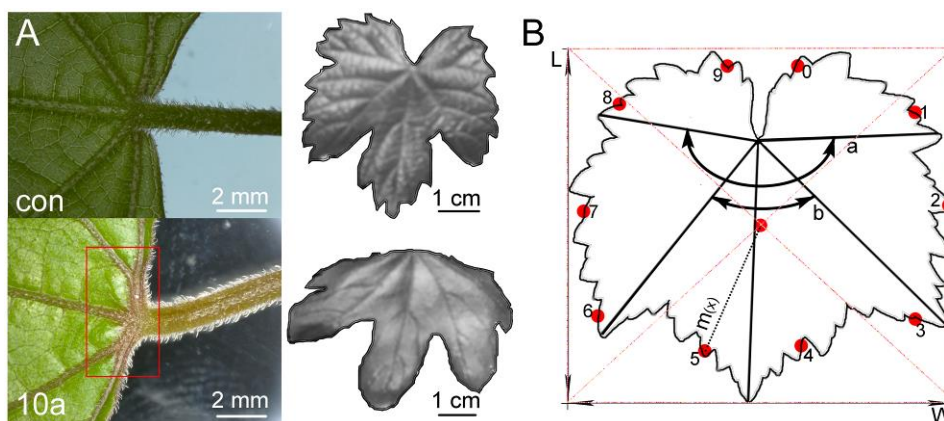


**Fig 2.2** Phenotypic analysis of greenhouse plant *Vitis vinifera* cv. 'Chardonnay' line 10a. **A** Overview of leaf base and petiole of leaves from an identical developmental state for wild type (WT) (upper image) and line 10a (lower image) recorded by deep-focus stereo microscopy (Keyence VHX-2000, objective lens 20 – 2000 fold). The red box indicates phenotypical changes characteristic for line 10a. **B** Schematic diagram of morphological parameters quantified by the Leafkit programme (Benedikt Müller). Angle a: angle between the two boarder veins of 5 main veins (V1 - V5, from left to right) in grapevine. Angle b: angle between V2-V4. W/L: max width over length of the leaf border (petiole is excluded). M0 to m9 are defined as the relative lengths from the reference point in the leaf center (the centre of the bounding box) to 10 marker points in leaf edge (red spots, length indicated as  $m_x$ ). The program registers all dots on the 28



exact margin of the leaf, and then divides these dots in 10 segments. For each dot it calculates the distance to the reference point in the leaf center, and determines the average of all distances from one segment yielding values  $m_0$  to  $m_9$ . 30 individual leaves from 10 plants were used for this analysis.

## 2.5 Tobacco BY-2 cell lines and cultivation

BY-2 (*Nicotiana tabacum* L. cv 'Bright Yellow-2) suspension cell lines (Nagata *et al.*, 1992) were cultivated in liquid medium containing 4.3 g L<sup>-1</sup> Murashige and Skoog salts (Duchefa Biochemie BV), 30 g L<sup>-1</sup> sucrose, 200 mg L<sup>-1</sup> KH<sub>2</sub>PO<sub>4</sub>, 100 mg L<sup>-1</sup> (myo)-inositol, 1 mg L<sup>-1</sup> thiamine, and 0.2 mg L<sup>-1</sup> 2,4-D, pH 5.8. In addition to the non-transformed BY-2 wild type (WT), transgenic lines were used in this study that expressed either the actin-binding domain 2 of plant fimbrin in fusion with GFP under control of the constitutive CaMV 35S promoter (AtFABD2, Sano *et al.*, 2005), and a transgenic line expressing the  $\beta$ -tubulin AtTUB6 from *Arabidopsis thaliana* in fusion with GFP driven by the CaMV 35S promoter (Hohenberger *et al.*, 2011). The cells were subcultivated weekly, inoculating 1.0 to 1.5 ml of stationary cells into fresh medium (30 ml) in 100-ml Erlenmeyer flasks. The cells were incubated in darkness at 27 °C under constant shaking on a KS260 basic orbital shaker (IKA Labortechnik) at 150 rpm. The media for the transgenic cell lines were complemented with either 30 mg L<sup>-1</sup> hygromycin (GFP-AtFABD2) or with 50 mg L<sup>-1</sup> kanamycin (GFP-AtTuB6), respectively.

## 2.6 Elicitors

The flg22 peptide QRLSTGSRINSAKDDAAGLQIA (Felix *et al.*, 1999) was purchased from a commercial source (Laboratoire de Biotechnologie du Luxembourg S.A.). The gene for the expression of HrpZ from *Pseudomonas syringae* p.v. *phaseolicola* (HrpZ<sub>p<sub>ph</sub></sub>) was cloned into the vector pET21a (Novagen, Darmstadt, Germany), and transferred into *E. coli* strain BL21 (DE3) RIL (Agilent Technologies, USA) by electroporation (Li *et al.* 2005). The recombinant protein was expressed and purified as follows: The transformed cells were grown at 30 °C in LB medium with 100 mg L<sup>-1</sup> ampicillin to an optical density at 600 nm approximately to 0.6-0.8. Then, expression was induced with 1 mM Isopropyl  $\beta$ -D-1-thiogalactopyranoside (IPTG) for about 6 h at 30 °C. Cells were spun down and the sediment resuspended in extraction buffer [50 mM Tris-HCl pH 8.0, 100 mM NaCl, 1 mM EDTA, 1 mM phenylmethanesulfonyl fluoride (PMSF, freshly added)]. Cells were lysed by sonication, and proteins denatured by boiling for 10 min. Cell debris and denatured proteins were removed by centrifugation (4 °C, 12000 rpm, 10 min) and the supernatant transferred to a fresh beaker. Then, solid ammonium sulphate was slowly added to 45% (w/v) of a saturated solution while stirring the mixture on ice. The precipitated protein was resuspended in 5 mM MES (pH 5.5), and desalted by dialysis using regenerated cellulose tubular membrane (size exclusion 6 kDa, wall thickness: 30  $\mu$ m; ZelluTrans/Roth dialysis membranes T2,

Roth, Karlsruhe, Germany). The concentration of purified HrpZ was quantified by the amido black protein dye assay (Popov *et al.*, 1975) against bovine serum albumin as calibration reference.

The short-term responses were elicited by 10  $\mu\text{M}$  (flg22) or 57.6  $\mu\text{M}$  (HrpZ). The long-term response was assessed at lower concentrations at 3 days (for flg22, 100 nM), and 2 days (for HrpZ, 2.59  $\mu\text{M}$ ) after treatment. Mock controls were done with the respective solvents (water for flg22, and 5 mM MES for HrpZ) and treated in exactly the same manner as the samples.

### **2.7 Inoculation with dTomato tagged Gram-negative bacteria: *Agrobacterium tumefaciens* EHA105, *Ewinia amylovora*, *Agrobacterium vitis* S4 and *Escherichia coli***

Marker lines of the phytopathogenic bacteria *E. amylovora*, *A. vitis* S4, and *A. tumefaciens* EHA105 expressing the red fluorescent protein (RFP) dTomato were kindly provided by Dr. Günther Buchholz (AlPlanta, Neustadt/W) (Buchholz *et al.*, manuscript in preparation).

#### **2.7.1 Leaves of *V. vinifera* ‘Chardonnay’ expressing GFP-AtFABD2**

For bacterial inoculation, the entire plant (line 10a, raised in the green house) was placed under a mild vacuum immersing the target leaves into a bacterial suspension (*A. tumefaciens* EHA105 dfr2 $\alpha$  dTomato-GFP, *E. amylovora* dTomato, and *A. vitis* S4 dTomato-GFP, respectively) for infiltration. 3 days later, the samples were examined by spinning disc microscopy. For this purpose, the fourth and fifth expanded leaves counted from the apex of the shoot were excised and rinsed under deionized water. Discs of 5 mm diameter were excised from the leaves with a cork borer and placed on wet filter paper in Petri dishes with the abaxial side up.

#### **2.7.2 Cells of *V. rupestris* expressing GFP-AtTUB6**

*V. rupestris* cells were placed on MS agar medium (pH 5.8), and co-cultivated with *E. amylovora* dTomato, *A. tumefaciens* EHA105 dfr2 $\alpha$  dTomato-GFP, *A. vitis* S4 dTomato-GFP, and *E. coli* S17- $\lambda$ pir dTomato, respectively. 2 days later, the samples were observed by spinning disc microscopy.

### **2.8 Inoculation and staining of *Plasmopara viticola***

The expanded leaves of line 10a were used for this experiment, using leaves 4 and 5 counted from the apex of plants raised in the greenhouse. Leaves were excised and rinsed under deionized water.

Mature sporangia of *P. viticola* frozen at -20 °C were suspended and shaken in sterile distilled water. Mobile zoospores hatched from 1.5-2.5 h after addition of distilled water, and were filtered by a custom-made column filled with 300 mg cottonwool in a 5-ml pipette tip (using 6 ml of suspension that contained hatched zoospores and empty sporangia). The filtrate was adjusted to a final concentration of ~500 000 cells per ml determined by a hemacytometer (Fuchs-Rosenthal, Germany), and used for inoculation. To propagate the *P. viticola* source population in the greenhouse, zoospores at a concentration of 5000-1000 cells per ml were used for inoculation.

3 d post inoculation, leaf discs of 5 mm diameter were excised from the inoculation sites using a cork borer and placed on wet filter paper in Petri dishes with the abaxial side up, before infiltration in Perfluorodecalin (PFD) for 3-5 min to increase transparency of the specimen. Subsequently, samples were stained for 5 min with 0.1% Calcofluor (Fluka), plus 0.01% break thrU (a commercial surfactant used to promote the penetrance of fungicides), and subsequently washed three times with 0.067% M KH<sub>2</sub>PO<sub>4</sub>, according to Díez-Navajas *et al.* (2007). Some samples were stained with 0.1% Diphenyl Brilliant Flavine (Sigma-Aldrich, Germany) for 5 min and washed three times with water.

## 2.9 Life-cell microtubule imaging in *V. rupestris* cells during stress

### 2.9.1 Biotic stress treatment

Elicitors: flg22 and HrpZ were chosen as biotic elicitors based on our previous studies. flg22 was used as a trigger for PTI; in contrast, HrpZ was used to trigger ETI-like responses. Cells were examined by microscopy after 3 days of treatment with 100 nM flg22 or 1.73 µM HrpZ, or with 500 µM of (±)-Jasmonic acid ((±)-JA) (Sigma-Aldrich, Germany). For short-term experiments, treatment, 10 µM of flg22, 28.8 µM and 57.6 µM of HrpZ and 1-50 mM JA were used.

### 2.9.2 Abiotic stress treatment

**Osmotic stress:** osmotic stress (to mimick salinity and drought) was administered by 64 mM of NaCl 64 mM or 20% PEG. For cold stress, cells were kept at 4 °C, for heat stress at 35 °C. EtOH (1% v/v) was tested as well. Cells were examined by microscopy 3 days after the onset of stress treatment. For short-term studies, NaCl was varied between 26 and 200 mM, PEG between 8.0 and 37.5 %, and EtOH was used at 0.5% and 1%.

**UV-C and UV-B treatment:** 2 ml of *V. rupestris* cells (corresponding to a PCV of 1.3 ml) collected at day 3 after subcultivation, were layered in a Petri dish (9 cm diameter) and exposed to UV-C irradiation (GEG1578 Germicidal, 15 W, 0.079 J cm<sup>-2</sup>, λ<sub>max</sub> 254 nm, distance 11 cm) for 10

min; to test the MT response to UV-B, cells were exposed in a 25 °C incubator for 10 min using a UV-B bulb (Philips TL40/12RS, 0.21 J cm<sup>-2</sup>, distance 11 cm) with three cut-off filters (WG 295, WG 302, WG 335) yielding UV-A+UV-B+UV-C, UV-A+UV-B alone, and UV-A alone as negative control (**Fig. 2.3**).

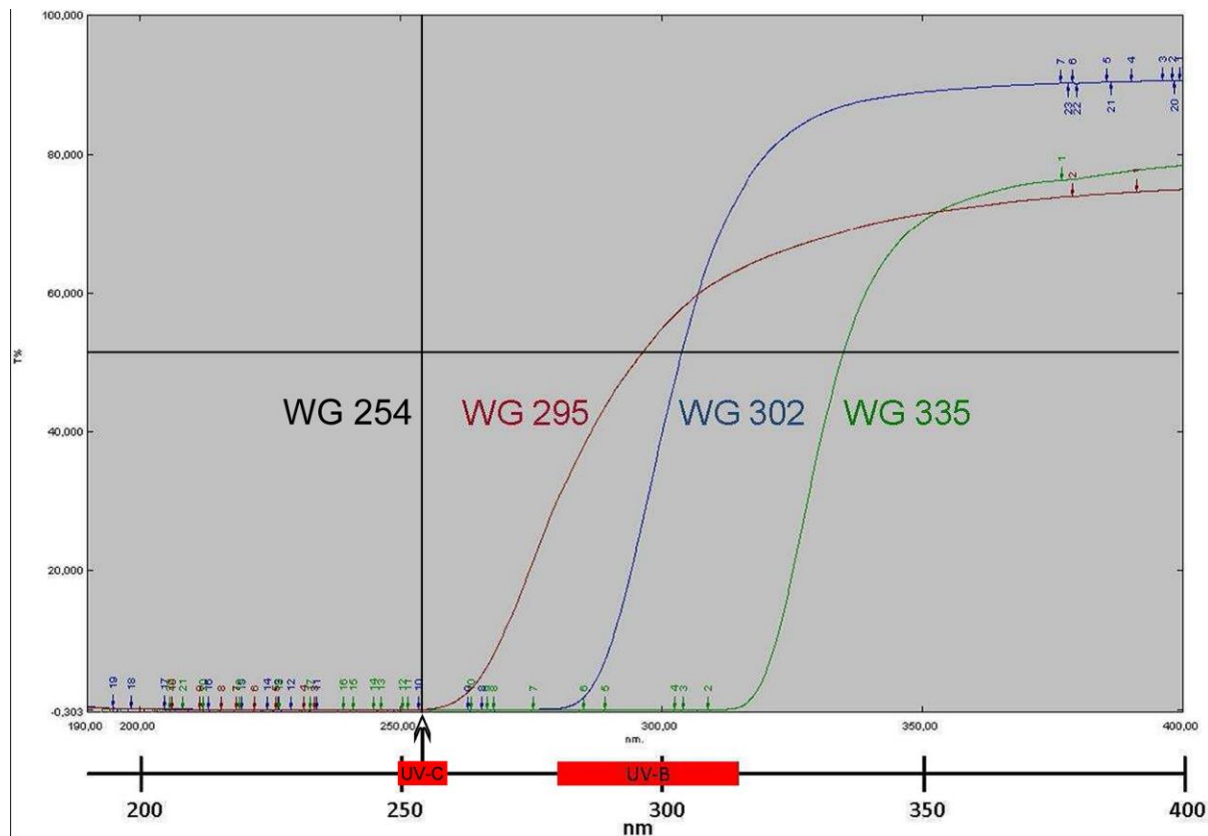


**Fig 2.3** transmission spectra of the UV cut-off filters used to administer different qualities of UV stress (adapted from Frühholz, 2011).

## 2.10 Microscopy

The responses of AFs (using the GFP-*At*FABD2 marker) and MTs (using the GFP-*At*TuB6 marker) to various biotic or abiotic stresses were followed over time in individual cells by spinning disc confocal microscopy. The cells on the slide were maintained at 27 °C using the temperature control stage integrated in the microscope, and time-lapse series were recorded by capturing z-stacks every two min over a period of at least 20 min.

Grapevine leaf discs were mounted on glass slides in a drop of water for observation by confocal microscopy. The response of AFs (using the GFP-*At*FABD2 marker) was followed over time focussing either on the guard cells or both upper and lower epidermal cells.

Confocal images were recorded with an AxioObserver.Z1 (Zeiss, Jena, Germany) using a glycerine immersion 63x LCI-Neofluar Imm Corr DIC objective (NA 1.3), the 488 nm emission line of an Ar-Kr laser, and a spinning disc device (YOKOGAWA CSU-X1 5000).

## 2.11 Quantitative image analysis of actin filaments and microtubules

To quantify cytoskeletal bundling and density, the original serial optical sections of the cell had to be preprocessed first. Fluorescent images were skeletonized using macros integrated in the quantitative image processing software ImageJ (For details see Hasezawa, <http://hasezawa.ib.k.u-tokyo.ac.jp/zp/Kbi/HigStomata>) (**Fig. 2.4**). Two parameters were used for quantification:

1) The skewness of intensity distribution of cytoskeletal pixels (reporting bundling of AFs/MTs): these values increase when the incidence of highly fluorescent pixels increases in consequence of AF/MT bundling:

$$skewness = \frac{1}{N} \sum_{i=1}^N \left( \frac{i_n - \bar{i}}{\sigma} \right)^3$$

$$\sigma = \frac{1}{N} \sum_{i=1}^N (i_n - \bar{i})^2$$

With N total number of cytoskeletal pixels,  $i_n$  intensity of a given pixel, and  $\bar{i}$  mean pixel intensity.

2) The occupancy of the GFP signal (used to estimate the density of AFs/MTs) measures the proportion of pixel numbers constituting the skeletonized AFs/MTs over the total pixel numbers in the region of interest:

$$occupancy = 100 \cdot \frac{n_{AF/MT}}{n_{Cell}}$$

With  $n_{AF/MT}$  number of cytoskeletal pixels and  $n_{Cell}$  total number of pixel in the region of interest.

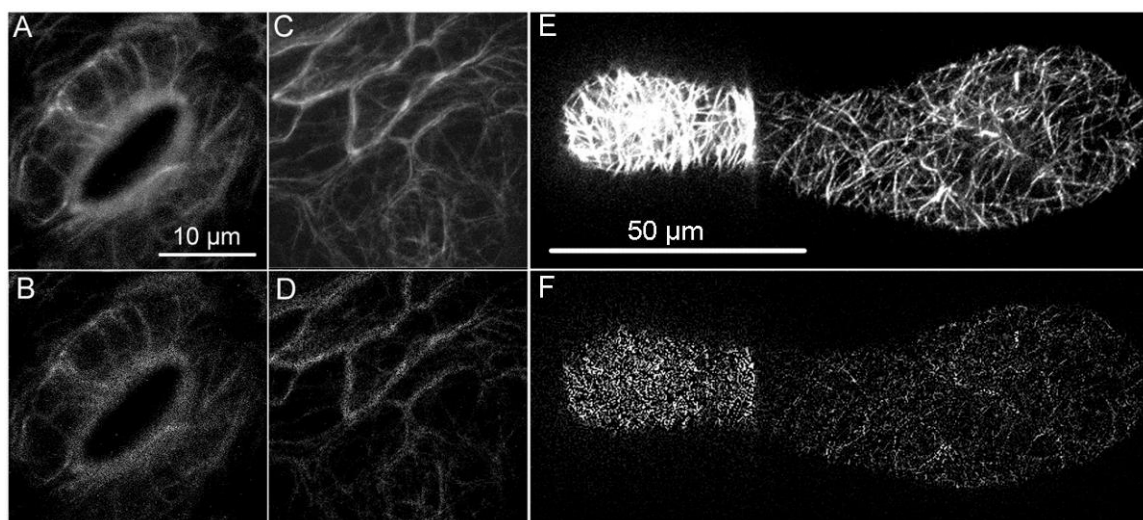


**Fig 2.4** Different stages of quantitative image analysis of the cytoskeleton using the method by Hasezawa. Guard cells expressing a fluorescent actin marker before (**A**), and after (**B**) skeletonization; lower epidermal cells before (**C**), and after (**D**) skeletonization. Suspension cells before (**E**) and after (**F**) skeletonization.

## 2.12 Measurement of extracellular alkalinisation

Extracellular alkalinisation was measured by combining a pH meter (pH 12, Schott handylab) with a pH electrode (LoT 403-M8-S7/120, Mettler Toledo). BY-2 cells were pre-equilibrated on an orbital shaker for around 30 min, and then treated by different concentrations of flg22 (1-500 nM) or HrpZ (0.26-14.4  $\mu$ M). Values for  $\Delta$ pH were calculated as differentials of treatment versus mock control. Peak values were used as estimate for  $\Delta$ pH<sub>max</sub> and reached at around 600 s (10 min) for flg22, and around 900-1200 s (15-20 min) for HrpZ. As positive controls for the activity of HrpZ, suspension cell lines from *Vitis rupestris* and *V. vinifera* cv. 'Pinot Noir' (Qiao *et al.*, 2010; Chang & Nick, 2012) were added to the study.

## 2.13 Phenotyping of cellular responses

PCV as indicator for growth was determined at day 3 after subcultivation/treatment. Aliquots of 2 ml were sampled from the culture flask with a sterile, scaled pipette (Greiner) while shaking to ensure a homogenous distribution of cells, the pipettes sealed with Nescofilm and positioned vertically at 4 °C till full sedimentation of the cells. The PCV was determined from the scale of the pipettes. Mitotic index was determined in aliquots of 500 mL at day 3 after subcultivation/treatment after staining for 2 min with 10 ng·mL<sup>-1</sup> Hoechst 33258 (Sigma-Aldrich, Neu-Ulm, Germany) and addition of one drop of 10% (v/v) Triton X-100 (Roth). Cells were immediately scored under a AxioImager Z.1 (Zeiss, Jena, Germany) using a DAPI filter set (excitation at 365 nm, beamsplitter at 395 nm, and emission at 445 nm) by means of a

Fuchs-Rosenthal hemacytometer (Thoma, Freiburg, Germany). For each data point, 2000 cells obtained from three independent experimental series were scored. To monitor changes in cell shape, differential interference contrast images of central sections were acquired by the AxioImager Z.1 in the ApoTome mode (Zeiss, Jena, Germany) at day 3 after subcultivation/treatment using the mosaic and length measurement tools of the AxioVision software (Zeiss, Jena, Germany). As measure of cell shape the ratio of cell width over cell length was measured and clustered into 11 classes increasing in steps of 0.2 and one class with values >2.0. Frequency distributions were constructed for three independent experimental series of 300-500 individual cells measured for each repeat. Mortality was assessed according to the method by Gaff and Okong'O-Ogola (1971) using 2.5% (w/v) Evans Blue (Sigma-Aldrich, Neu-Ulm, Germany) in aliquots of 200  $\mu$ l using custom-made staining chambers to remove the medium. The frequency of the dead cells (stained in blue) was scored using a Fuchs-Rosenthal hemacytometer under bright-field illumination with AxioImager Z.1/ApoTome microscope (Zeiss, Jena, Germany). Mortality values were determined from three independent experiments with 1500 cells scored for each data point. To evaluate division synchrony (Campanoni *et al.*, 2003), frequency distributions over the number of cells per individual file were constructed from approximately 2000 cell files from three independent experimental series.

## 3 Results

### 3.1 Actin responses to flg22 are subtle, those to HrpZ are drastic

To gain insight into the earlier stages of cytoskeleton remodeling in plant defence, we followed the response of AFs to flg22 and HrpZ in individual BY-2 cells expressing the GFP-AtFABD2 marker by spinning-disc confocal microscopy. To ensure saturation of possible responses even for early time points, we used 10  $\mu$ M flg22 based on dose-response studies discussed in detail below. We collected z-stacks through the entire cell every 2 min after addition of flg22 through the first 30 min (**Fig. 3.1A**). The transvacuolar network of actin cables emanating from the nucleus did not reveal any significant changes (**Fig. 3.1A**, upper row). However, a response of the fine meshwork of the cortical AFs underneath the cell membrane became detectable from ~5-10 min after elicitation (**Fig. 3.1A**, central and lower rows). Here, the finer filaments disappeared and cortical actin cables changed orientation and often became more prominent (compare for instance the images for 20 min versus 4 min in the central row of **Fig. 3.1A**). A responsiveness of the cortical actin meshwork was also observed in long-term studies using lower concentrations of flg22 such as 100 nM (**Fig. 3.1C**), where AFs in many (but not all) cells disintegrated into punctuate arrays, whereas the perinuclear network still persisted. None of these responses was observed in the mock control (**Fig. 3.1B**).



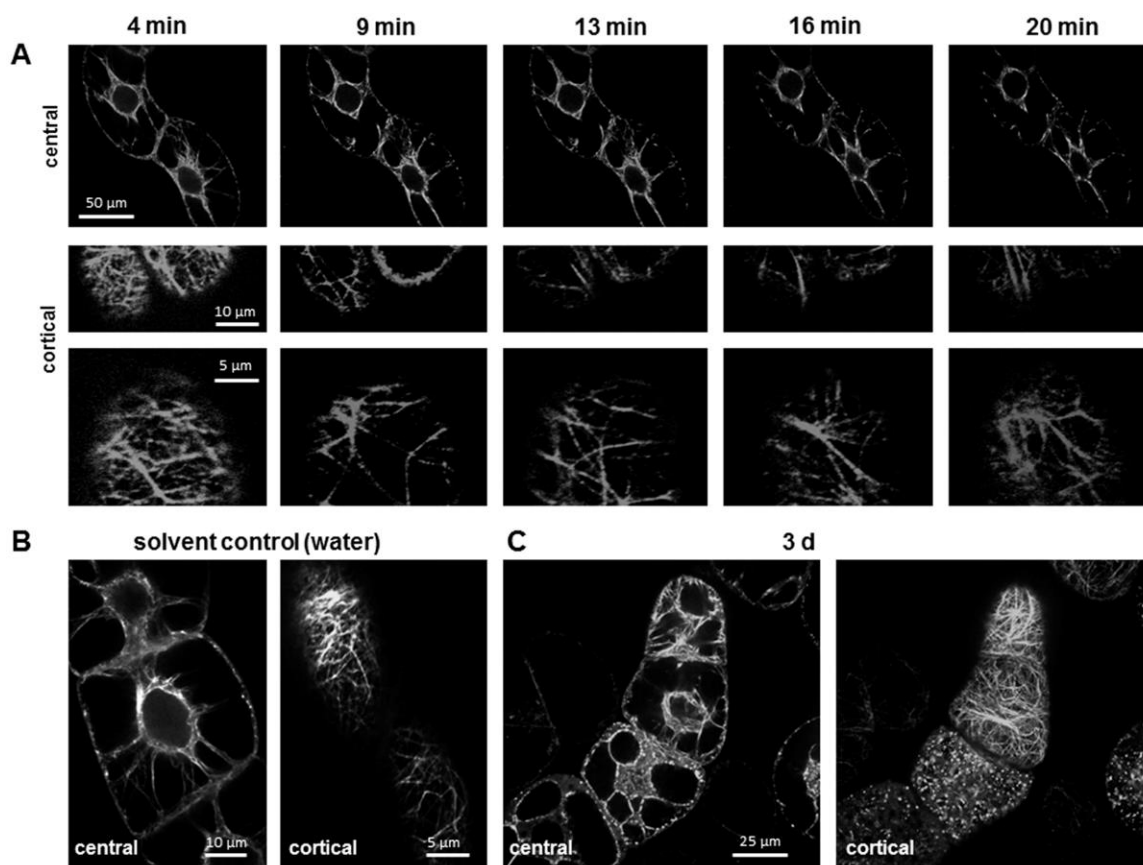


**Fig 3.1** Response of actin filaments in BY-2 to flg22 *in vivo* visualised by the GFP-AtFABD2 marker and spinning-disc confocal microscopy. **A** Time series after treatment with 10  $\mu$ M of flg22, confocal sections collected in the cell centre (upper row), and details from two cortical regions of the same cell (middle and lower rows). **B** solvent control (water). **C** long term response 3 d after elicitation with 100 nM of flg22. Observations are from at least five independent experimental series with a population of 100 individual cells for each treatment.

The rather subtle actin response to flg22 is contrasted by the drastic changes induced by HrpZ (**Fig. 3.2**). Confocal sections collected in the cell centre (upper row), and the cortical regions of the same cell (middle row) demonstrate that AFs have already undergone disruption at 20 min after elicitation with 57.6  $\mu$ M of HrpZ. Differential-interference contrast images of these cells show that this disruption is accompanied by a dramatic breakdown of cytoplasmic architecture manifest at 60 min after elicitation, and a disintegration of the vacuole (white arrows) visible at 90 min after elicitation. This was not observed in the solvent control (5 mM MES buffer). An inspection of earlier time points showed that AFs condensed into cortical aggregations that were clearly detectable at 10 min after elicitation (**Suppl. Fig. 1A**) followed by contraction of actin towards the nucleus. A long-term experiment conducted at a  $\sim$ 20-fold reduced concentration (2.59  $\mu$ M of HrpZ), where most cells survived, as deduced from mortality scores discussed in detail below, produced cortical AFs that were bundled and disorganised (**Suppl. Fig. 1B**).

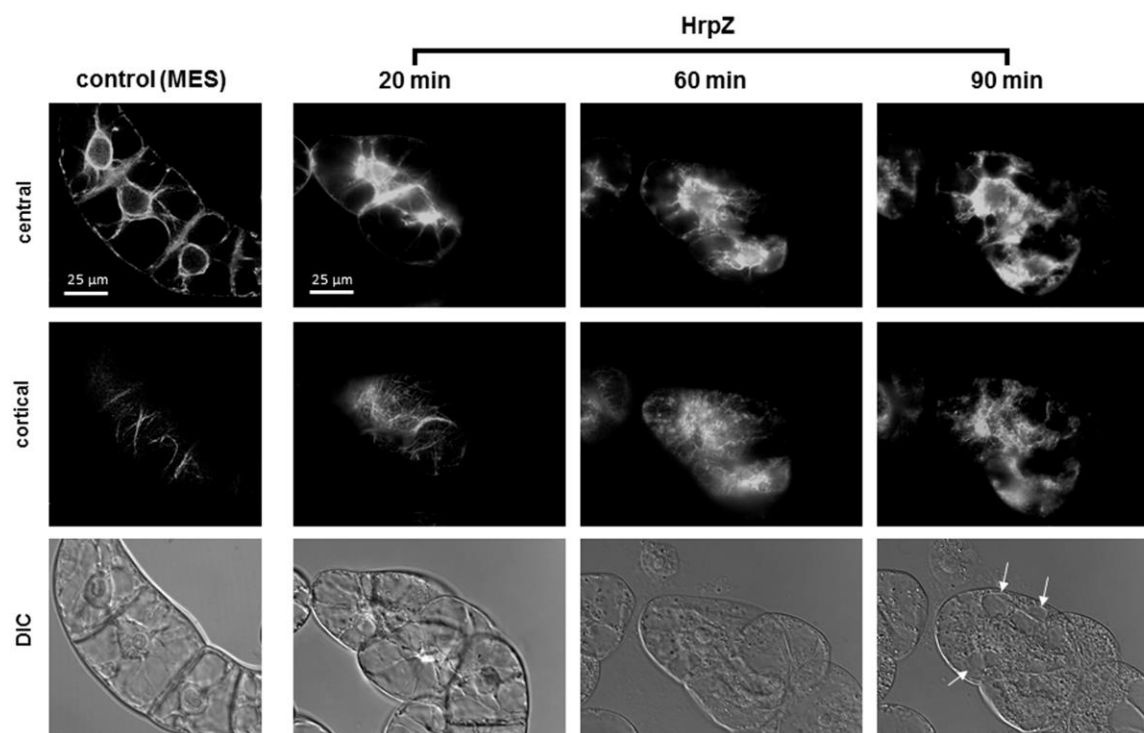


**Fig 3.2** Response of actin filaments in BY-2 to HrpZ *in vivo* visualised by the GFP-AtFABD2 marker and spinning-disc confocal microscopy. Time series after treatment with a saturating concentration of HrpZ (57.6  $\mu$ M), confocal sections collected in the cell centre (upper row), and the cortical regions of the same cell (middle and row). Differential-interference contrast images of this cells show the breakdown of cytoplasmic architecture manifest at 60 min after elicitation, and the disintegration of the vacuole (white arrows) visible at 90 min after elicitation. The solvent control consisted in 5 mM MES buffer. Observations are from at least five independent experimental series with a population of 100 individual cells for each treatment.

### 3.2 Microtubules respond to HrpZ, but not to flg22

Parallel to actin, we followed the response of MTs using the GFP-AtTUB6 marker (**Fig. 3.3**). In the vast majority of cells, a treatment with 10  $\mu$ M flg22 did not cause any changes, neither in the radial MTs emanating from the nucleus (**Fig. 3.3A**, upper row), nor in the cortical MTs underneath the membrane (**Fig. 3.3A**, lower row). Even for a long-term treatment, these MTs did not respond (data not shown). To be mentioned, however, that in rare cases aberrant microtubule structures could be observed (**Suppl. Fig. 2**). In these cells, plaque-like agglomerations of signals appeared in the vicinity of the nuclear envelope either as a transient stage in response to a high concentration of flg22 (10  $\mu$ M), or as long-term response to lower concentration (100 nM). As already found for actin, treatment with HrpZ (57.6  $\mu$ M) caused drastic changes, mainly in the radial microtubules that were found to be eliminated (**Fig. 3.3B**, upper row), whereas cortical microtubules became thinner as compared to the control, but still maintained their integrity (**Fig. 3.3B**, lower row).

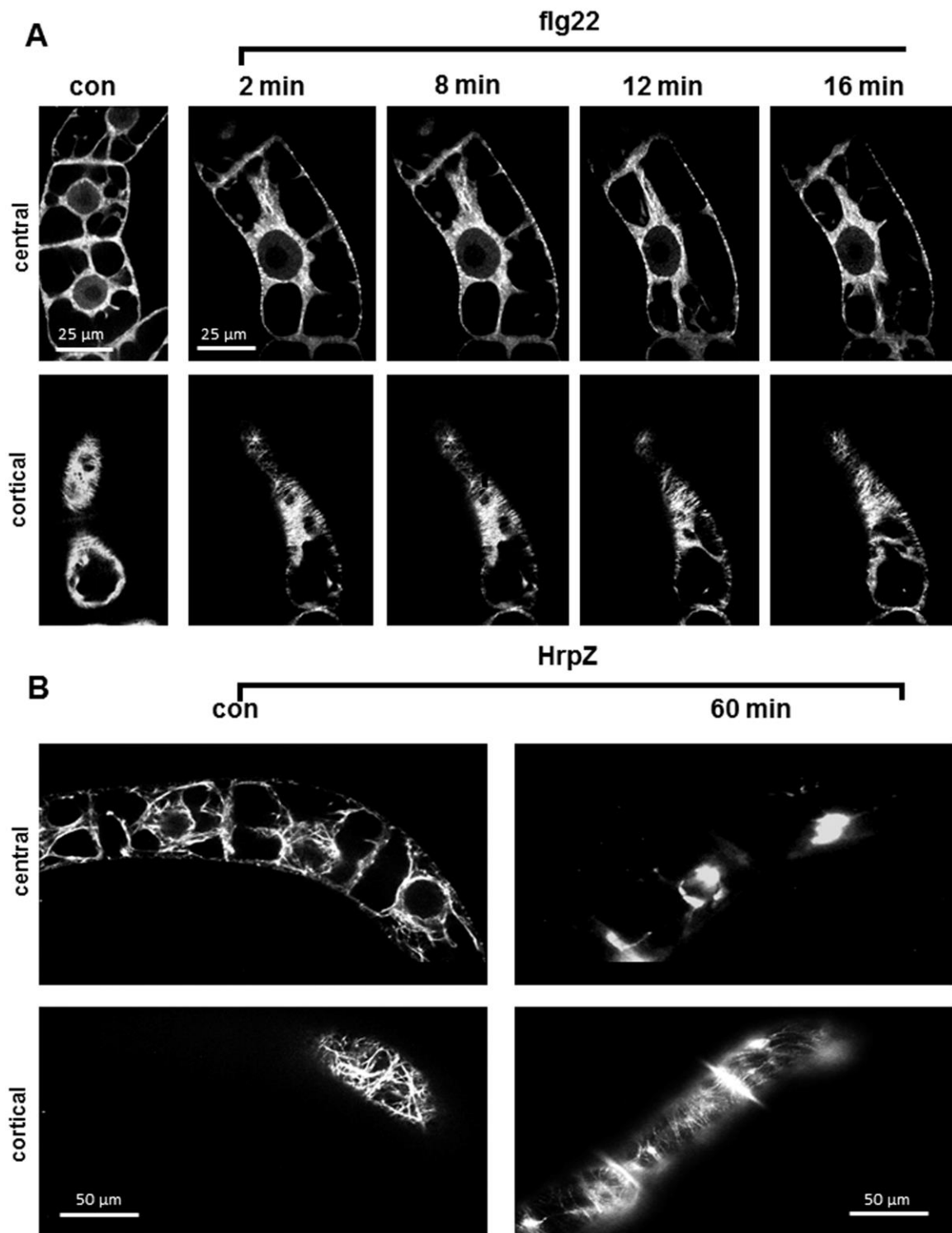


**Fig 3.3** Response of microtubules in BY-2 to 10  $\mu\text{M}$  flg22 (**A**) or 57.6  $\mu\text{M}$  HrpZ (**B**) *in vivo* visualised by the GFP-AtTUB6 marker and spinning-disc confocal microscopy. Confocal sections collected in the cell centre and the cortical regions of the same cell are shown. Controls show the response to the solvent (**A** water, **B** 5 mM MES buffer). Observations are from at least five independent experimental series with a population of 100 individual cells for each treatment.

### 3.3 Apoplastic alkalinisation as rapid defence readout is more sensitive to flg22 as compared to HrpZ

One of the earliest responses detected is a modification of plasma membrane permeability, in particular,  $\text{Ca}^{2+}$ ,  $\text{H}^+$  and  $\text{K}^+$ , and anion fluxes that can be conveniently followed as changes of extracellular pH (Jabs *et al.*, 1997; reviewed in Felix *et al.*, 1999; Nürnberger & Scheel, 2001). To test, whether the differential cytoskeletal response to flg22 versus HrpZ was caused by a lack of sensitivity of BY-2 cells to flg22, we therefore used extracellular alkalinisation as a fast cellular response monitoring plant defence. Already at a low concentrations (1 nM), flg22 could trigger a pH reaching a maximum at ~600 s after elicitation (**Fig. 3.4A**). This peak increased in amplitude, but was not advanced in time, when the concentration of flg22 was increased. A dose-response of maximal alkalinisation over the concentration of flg22 showed a saturation of the response from 200 nM at 0.27 pH units (**Fig. 3.4B**). HrpZ in a concentration of 1.73  $\mu\text{M}$  could trigger an alkalinisation that was comparable in amplitude (**Fig. 3.4C**). To verify that this recombinantly produced elicitor was biologically active, we tested the same concentration of HrpZ in the two grapevine cell lines. For the more responsive *Vitis rupestris*, up to almost 0.7 pH units were obtained, for the less responsive *Vitis vinifera* cv. ‘Pinot Noir’ the response was close to that found in BY-2. This pattern shows that the activity of HrpZ used in the current experiments was comparable to that of the commercial Harpin elicitor used in our previous studies (Qiao *et al.*, 2010; Chang & Nick, 2012). A dose response of maximal alkalinisation over the concentration of HrpZ in BY-2 (**Suppl. Fig. 3**) showed that stronger alkalinisation can be induced in BY-2 as well, but that this requires higher concentrations of the elicitor as compared to *V. rupestris* indicating differences in sensitivity between these cell lines. It should also be mentioned that the time point, when these maxima were reached were between 900 and 1500 s (depending on the concentration), which is significantly later than the timing found for flg22 (**Fig. 3.4A**).

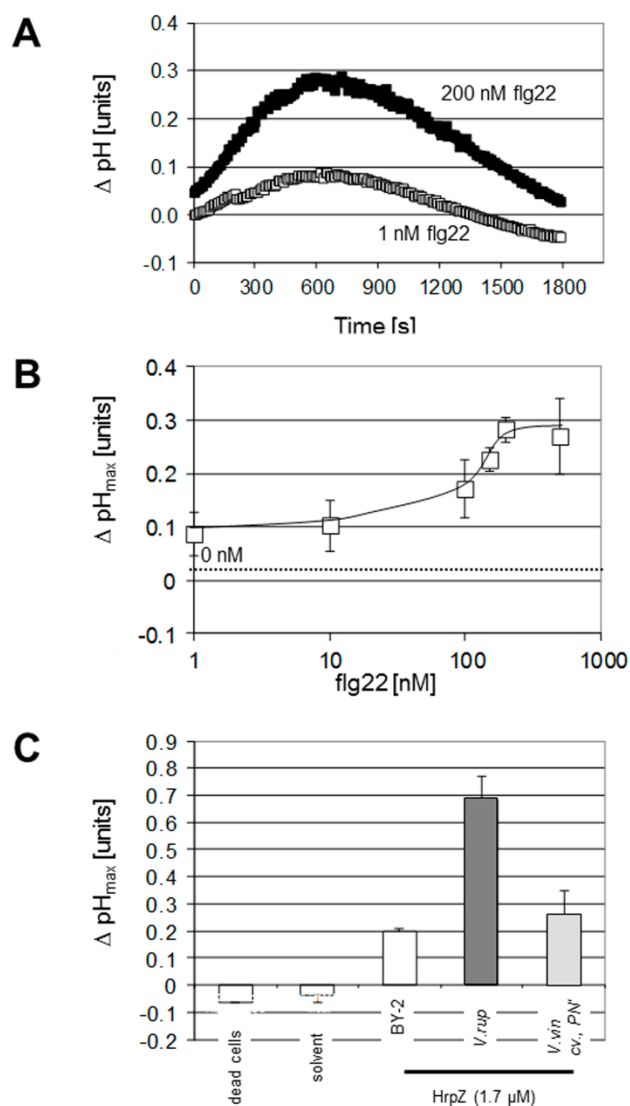


**Fig 3.4** Extracellular alkalinisation in response to flg22 (**A**, **B**) or HrpZ (**C**). **A** Representative time course of BY-2 cells to a low (1 nM) and a high (200 nM) concentration of flg22. **B** Dose response of maximal alkalinisation over the concentration of flg22 in BY-2. Dotted line shows the value obtained for solvent control water. **C** Maximal alkalinisation for treatment with 1.7  $\mu\text{M}$  HrpZ in BY-2 (white bars), the highly responsive *Vitis rupestris* cell line (dark grey) and the weakly responsive *Vitis vinifera* cv 'Pinot Noir' cell line (light grey). Negative controls include dead BY-2 cells challenged by the elicitor and a solvent control (5 mM MES). The response of the cells is recorded at the respective maxima (520 s after induction for BY-2, 1600 s after induction for the two *Vitis* cell lines). Data in **B** and **C** represent mean values and standard errors from three independent biological replicates.

### 3.4 Cell division and cellular morphogenesis are altered by HrpZ

The morphogenesis of plant cells depends on the cytoskeleton. The cytoskeletal responses induced by HrpZ should therefore, as a consequence, alter cellular morphogenesis. We therefore phenotyped growth, cell shape, and division synchrony as sensitive targets of cytoskeletal remodelling. A dose-response curve of PCV as reporter for culture growth over the concentration of elicitor (**Fig. 3.5A**) showed a significant inhibition with increasing concentration of flg22 or

## Results

---

HrpZ, respectively. This inhibition became more prominent with time (compare the curves for days 3 and 4 in **Fig. 3.5A**). To test, whether the decreased growth was caused by inhibition of cell division, we monitored the dose-responses of mitotic index at day 3 (at the peak of mitotic activity) after inoculation. For flg22, even for a high concentration of 1  $\mu\text{M}$  flg22, mitotic index was only partially reduced (by some third as compared to the control). In contrast, HrpZ reduced the mitotic index drastically to almost zero (**Fig. 3.5B**). In the following, we investigated the effects of flg22 and HrpZ on cell shape, since the axiality of cell expansion depends on the organisation of cortical MTs. Frequency distributions for the ratio between cell width over cell length were constructed (**Fig. 3.5C**). For high concentrations of flg22 such as 1  $\mu\text{M}$ , the frequency of cells with ratios of width/length 0.4-0.6 decreased, whereas cells with ratios  $>1$  increased. This means that elongated cells became rare; whereas broader cells became more frequent (a representative image is given in **Fig. 3.5D**, left). This trend became progressively evident from flg22-concentrations exceeding 10 nM. The situation was inverse for treatments with HrpZ. Here the frequency of cells with a ratio of width/length 0.2-0.4 increased for as the elicitor concentration reached 1.73  $\mu\text{M}$ , which means that cells became progressively elongated (for a representative image see **Fig. 3.5D**, right). Lower concentrations of HrpZ were not effective in affecting cell shape (data not shown).

Since the effects of flg22 on cellular morphogenesis were very subtle in comparison with those of HrpZ, we used division synchrony as most sensitive morphological marker. Cell divisions in tobacco suspension cells are synchronised by signals that depend on polar auxin transport which can be monitored as frequency peak of cells composed of six cells (Campanoni *et al.*, 2003). Since polar auxin transport is strongly dependent on actin organisation (reviewed in Nick, 2010), the division synchrony can be used as highly sensitive marker for actin-remodelling and had been used successfully to monitor cell-death related actin bundling (Chang *et al.*, 2011). In response to flg22, the amplitude of this peak increased progressively up to threefold as compared to the control (**Suppl. Fig. 4**), suggesting that flg22 can modulate the actin cytoskeleton although this is not accompanied by bulk changes. Conversely, as to be expected from its actin bundling effect, a permissive concentration of HrpZ (2.59  $\mu\text{M}$ ) elevates the frequency of hexacellular files (**Suppl. Fig. 4**).

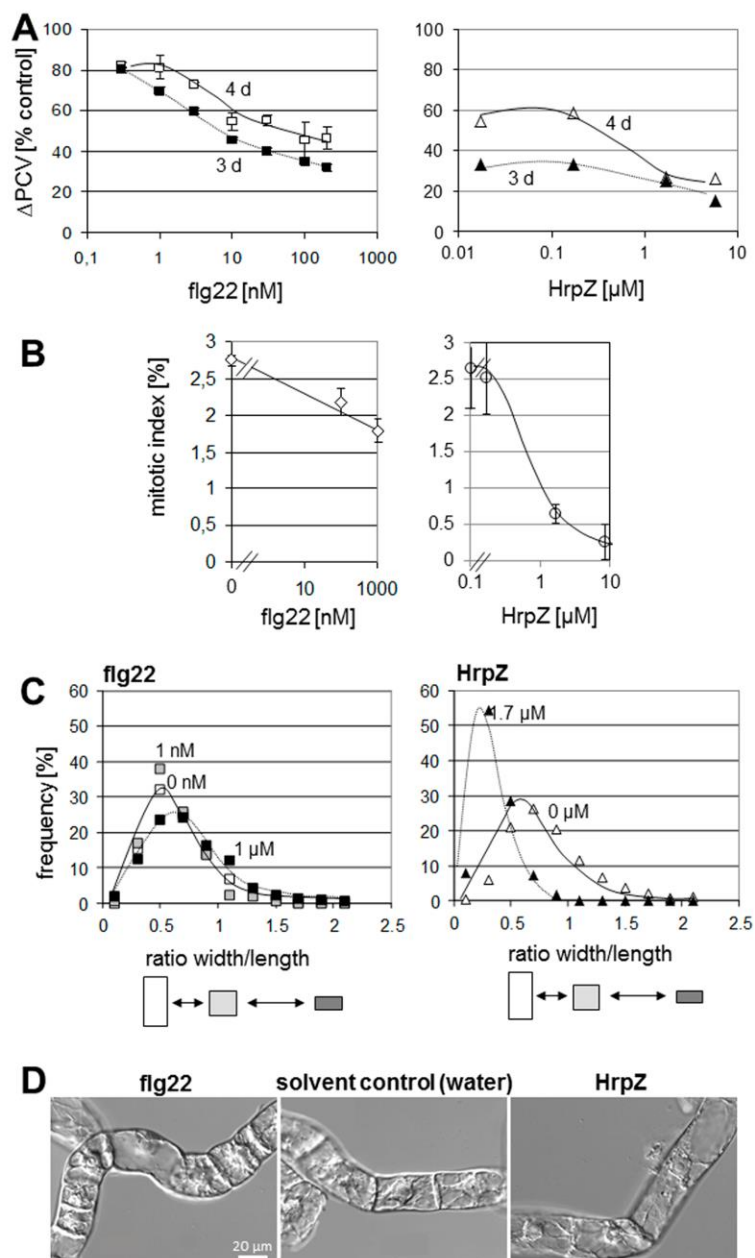


**Fig 3.5** Cellular responses to flg22 (left) and HrpZ (right). **A** Dose-responses of packed cell volume as indicator of culture growth at day 3 (peak of mitotic activity), and 4 d (at the onset of cell expansion) after inoculation, respectively. **B** Dose responses of mitotic index at day 3 after inoculation (scored from a population of 2000 individual cells for each data point). Data in **A** and **B** represent mean and standard errors from three biological replicates. **C** Effect on cell shape. Frequency distributions for the ratio between cell width over cell length were constructed from 2500 individual cells for each experiment. **D** Differential-interference contrast images of representative cells either raised under control conditions (centre) or after treatment with either 1  $\mu$ M flg22 or 1.73  $\mu$ M HrpZ.

### 3.5 HrpZ, but not flg22 can induce cell death

A characteristic feature of ETI is programmed cell death, leading to a hypersensitive response (HR) occurring at infection sites. We therefore, followed mortality in response to flg22 and HrpZ

## Results

over time. For flg22, we did not observe any elevated mortality (**Fig. 3.6**, left) for a range of concentrations. Even for treatment with 200 nM (data not shown), mortality was only 3.4% at day 3. On the contrary, HrpZ induced cell death from day 2, reaching nearly 70% at day 3 after treatment with 8.64  $\mu$ M HrpZ (**Fig. 3.6**, right).

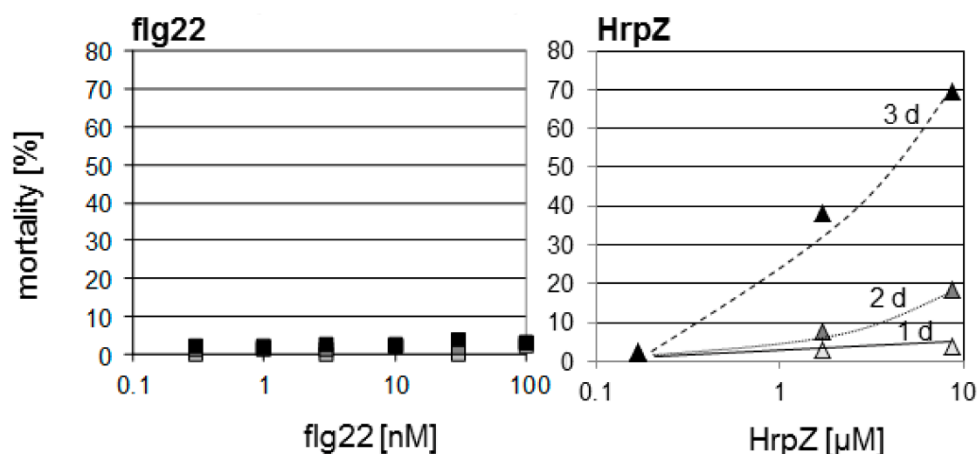


**Fig 3.6** Mortality in response to flg22 (left) and HrpZ (right). Data represent mean values and standard errors from three independent experimental series with a population of 2000 individual cells scored after staining with 2.5% Evans Blue for each value.

### 3.6 Phenotypic analysis of transformed plants

To our knowledge, stable fluorescent marker lines for AFs have been established only for the model plants *Arabidopsis thaliana* using the mouse talin marker (Kost *et al.*, 1998) or the less invasive FABD2 marker (Voigt *et al.*, 2004) and for the tobacco cell line BY-2 (Sano *et al.*, 2005). A limitation of previous studies on cytoskeleton in grapevine system was the need to visualize MTs by immunofluorescence, and AFs by fluorescent phalloidin, both protocols requiring chemical fixation. Since the cytoskeletal response could thus not be followed over time in individual cells, only bulk changes of cytoskeletal organization became evident, which means that the early stages of these responses were not detected. Grapevine genetic transformation is considered to be a risky and time consuming procedure. However, to establish a grapevine AF fluorescent protein marker line is necessary to better understand the role of the cytoskeleton in plant-pathogen interaction. So far, only few transgenic grapevines had been obtained by *Agrobacterium*-mediated genetic transformation originating from different organs via organogenesis or via somatic embryogenesis (Mullins *et al.*, 1990; Colby *et al.*, 1990; Martinelli *et al.*, 1993; Gambino *et al.*, 2007; Fan *et al.*, 2008). We therefore ventured to generate a fluorescent AF marker line in the important cultivar ‘Chardonnay’ using the non-invasive marker fimbrin actin-binding domain 2 (FABD2) representing the state-of-the art marker for plant actin (Voigt *et al.*, 2004).



*Vitis vinifera* ‘Chardonnay’ originated in the Burgundy wine region of eastern France, and is one of the most widely-planted grape varieties with over 160,000 hectares worldwide. It is cold hardy, and provides very high wine quality for both still and sparkling table wines, shows early and reliable fruit and wood maturity, and moderate vigor. However, these valuable traits are diminished by its high susceptibility to *Plasmopara viticola*, the causal agent of Grapevine Downy Mildew, in central Europe; and to *Botrytis cinerea*, the causal agent of Botrytis Bunch Rot in USA (Wine and juice grape varieties for cool climates, Cornell University. <http://www.hort.cornell.edu/reisch/grapegenetics/bulletin/wine/index2.html>; [www.Chardonnay-du-monde.com](http://www.Chardonnay-du-monde.com)). This high susceptibility is probably linked with the lack of effector-triggered immunity: European grapevines, in contrast to their North American wild counterparts, have evolved without contact to many pathogens that mostly originated in America. Since they were confronted with these pathogens only from the second part of the 19<sup>th</sup> century, they lack effective resistance (probably based on recognition of pathogen effectors by the production of host resistance genes) to pathogen attack (Terral *et al.*, 2010). For instance, hypersensitive cell death can be triggered by the bacterial effector Harpin in the American *Vitis rupestris* but not in the *Vitis vinifera* cultivar ‘Pinot Noir’ (Chang *et al.*, 2011).

1 month after line 10a was cultivated in green house. GFP-expression could be visually detected by irradiation with a long-wave UV-A lamp as a greenish hue on the red background of chlorophyll fluorescence (**Fig. 3.7A**). Already at this stage specific patterns of fluorescence were detectable in leaf and shoot tips by stereomicroscopical inspection under UVA (**Fig. 3.7B**). A closer examination by spinning disc confocal microscopy revealed fluorescent filaments that in all aspects of organisation, tissue-dependent changes, and morphological details appear as expected for the actin cytoskeleton (**Fig. 3.7C, D, E and F**).

The impression of a normal configuration of actin was supported by the completely normal morphology of the transgenic plants. Only a very close inspection revealed a phenotypical change between line 10a and non-transformed controls. Leaves were thinner, and their surface appeared rough because the intercostal fields protruded somewhat. Most importantly, leaf venation differed with the main vein converging distally of the petiole joint indicating a slight fasciation of leaf veins. This leaf phenotype persisted also after line 10a had undergone one period of overwintering and has remained persistent also in the newly formed leaves. A quantitative analysis of morphology, using our custom-made programme Leafkit (**Fig. 2.2; Suppl. Table. 1**) revealed that the angle between the central vein and the outer main veins was significantly steeper in line 10a. The value  $m_0$  is significantly larger in 10a.  $m_4$ - $m_6$  tested by multivariate analysis using oneway ANOSIM (analysis of similarity), based on a non-parametrical Duncan ranking algorithm

## Results

(Hammer *et al.*, 2001) is significantly smaller, which means that the leaves are significantly shorter in 10a and the proximal lobes more pronounced.

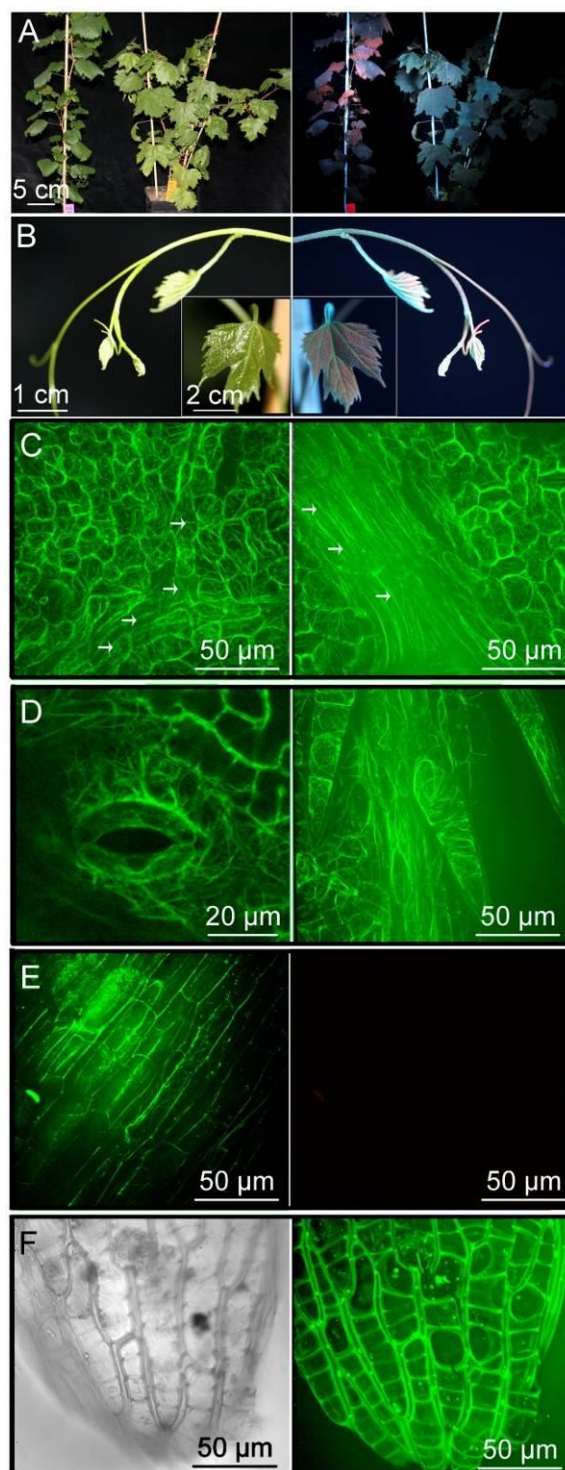


**Fig 3.7** Overview of transgenic *in vitro*-plants of *V. vinifera* 'Chardonnay' expressing *GFP-AtFABD2*. **A** Control (con) and *V. vinifera* 'Chardonnay' line 10a in greenhouse. **B** leaves and shoot tip (insert images) visualised by white light (left) and a long-wave UV lamp (right). **C** AFs in leaf tissue (adaxial, left; abaxial, right). Arrows indicate the leaf vein. **D** leaf stomata (left) and epidermal hairs (right). **E** root tissue (GFP-filter, left; CY3-filter, right). **F** root tip *in vivo* in DIC and GFP-filter.

Line 10a was selected from a total of 38 independent transgenic lines expressing *GFP-AtFABD2*. Only two of these lines, 5a and 10a, showed a normal structure of the GFP-labelled AFs. Unfortunately, line 5a grew very slowly, and produced only a tiny (of 4-5 cm in length) plantlet within 8 weeks (a size reached by the non-transformed control plantlets within two weeks), and thereafter arrested growth (despite the routine transfer were conducted as every four weeks). This line could not be rescued, and had died off. The attempt to obtain at least a callus line from 5a, failed as well. Only very few calli could be obtained from leaf tissue of line 5a, and after subculture, all of these calli were dying off. Even five attempts of propagation in tissue culture produced the same outcome indicating that the insertion of the transgene in line 5a impaired viability drastically. In parallel, to the generation of GFP-AtFABD2 lines, 20 independent lines expressing the GFP-AtTUB6 (from construct pH7WGF2-GFP-AtTUB6) marker had been generated, but none of them showed fluorescent patterns that appeared like normal MTs (**Suppl. Fig. 5**).

These observations illustrate that stable expression of cytoskeletal markers in grapevine requires a subtle balance between transgene expression, preserved cytoskeletal functionality and viability. Since the T-DNA is inserted randomly into the plant genome, the only strategy is to create a sufficient number of independent lines and to screen them for functionality and viability.

To understand, why only few lines were expressing normal cytoskeletal structures we genotyped several lines expressing GFP, but in aberrant patterns (**Suppl. Fig. 5**) Four of the 38 actin-marker lines produced fluorescent cell edges (9t, 16a, 31a, 9a), two showed fluorescent structures in the guard cells (13t, 33a), but only two (5a, 10a) produced AFs of normal appearance (**Suppl. Fig. 5A**). These lines did express a strong GFP signal that was stable even when examined after 1 year in the greenhouse (**Suppl. Fig. 5B**). Four lines (4t, 9a, 26a, 30a) expressed strong GFP signals, seven of them (23a, 30a, 9a, 4t, 7t, 15t, 26a) showed phenotypical aberrations compared to control plants.

### 3.7 PCR detection and southern blot of genomic DNA

Genomic DNA of 12 transformed plants (listed above) was extracted and analysed by genomic PCR reactions probing for *eGFP*, *AtFABD2*, the kanamycin resistance, and the left border region of the vector pK7WGF2. The actin marker lines yielded bands of the expected size when probed with the *eGFP* marker, but only the line 26a showed in addition bands reporting the presence of *AtFABD2* and the LB of the vector (**Suppl. Fig. 6A**). For the tested tubulin marker line 13t, insertion of of *GFP*, *AtTUB6*, and the left border region of vector pBI121 were used. Again, a band indicative of *GFP* could be amplified, but no band was amplified probing for *AtTUB6* (**Suppl. Fig. 6B**). Southern blot analysis, where genomic DNA were digested with EcoRI and

then hybridization (probe location was in eGFP) was in **Suppl. Fig. 6C**.

### 3.8 Response of actin filaments to *P. viticola*

The successful generation of the actin marker line *V. vinifera* ‘Chardonnay’ GFP-*AtFABD2* line 10a allowed to figure out the response of AFs to *P. viticola* infection. A precondition to conduct this experiment was the ability to visualize encysted zoospores, sporangiophores, and mycelia structures within the living leaf tissue. This could be achieved by staining with the fluorescent dyes Calcofluor and Diphenyl Brilliant Flavine in combination with Perfluorodecalin. 3 days after inoculation with zoospores of *P. viticola*, AFs in guard cells had disassembled, and perinuclear actin basket was observed in cells of the lower epidermis **Fig. 3.8**. To verify that these fluorescent structures were not caused by artificial autofluorescence or correspond to the endoplasmic reticulum, the non-transformed *Vitis vinifera* ‘Chardonnay’ wild type, and the fluorescent ER-marker line *Vitis vinifera* ‘Chardonnay’ GFP-ER, were used as negative controls (**Suppl. Fig. 7**).

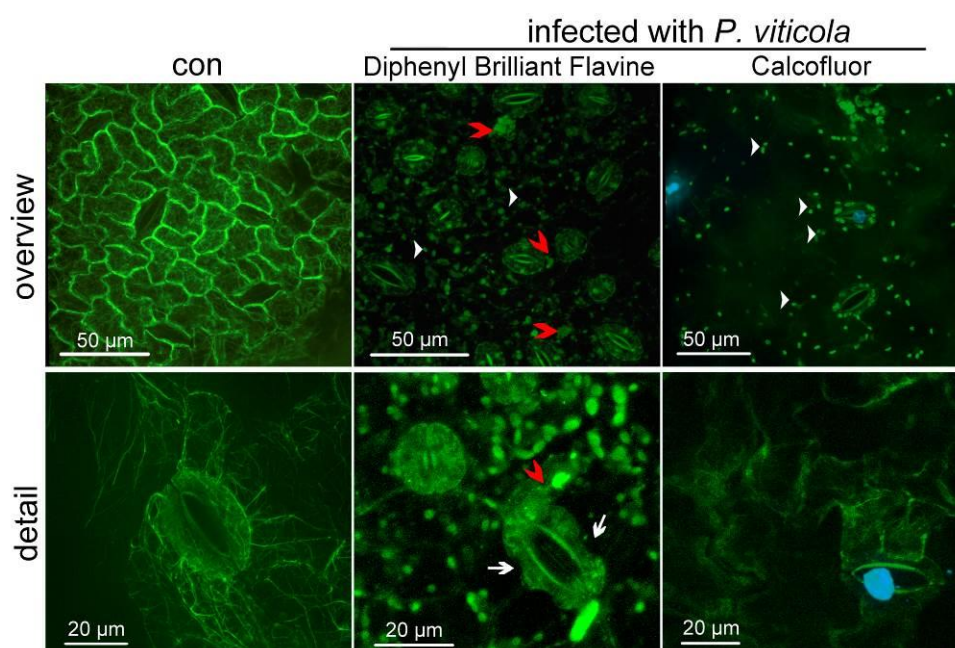


**Fig 3.8** Response of AFs in the lower leaf surface of *V. vinifera* ‘Chardonnay’ expressing *GFP-AtFABD2* to infection with *P.viticola* visualised by spinning-disc confocal microscopy. Encysted zoospores attached to the stomata were visualised by Calcofluor (emission in blue), intracellular hyphae by Diphenyl Brilliant Flavine (emission in green, red arrow heads). White arrow heads indicate the perinuclear AF baskets; White arrows indicate plasmolytic guard cells indicative of aberrant actin organisation.

### 3.9 Response of actin filaments to different Gram-negative bacteria.

Leaf discs of *Vitis vinifera* ‘Chardonnay’ line 10a were infiltrated with dTomato marker lines of the phytopathogenic bacteria *A. tumefaciens* EHA105, *E. amylovora*, and *A. vitis* S4, respectively, and co-cultivated for 3 days. Non-inoculated (but infiltrated with MOPS buffer (0.02 M MOPS, 2 mM sodium acetate trihydrate, 1 mM disodium EDTA, to final pH of 7.0)) *V. vinifera* ‘Chardonnay’ *GFP-AtFABD2* line 10a was used as control. Images were recorded in focal planes at the level of guard cells as well as at the level of upper and lower epidermal cells. Concentration series of the inoculum (with OD<sub>600</sub> ranging from 0.1 to 1.0) were tested to adjust optimal conditions. To visualize bacteria and host actin simultaneously, z-stacks were recorded at dual wavelengths (using both, the RFP- and GFP- filtersets). As compared to the negative control, inoculation of OD<sub>600</sub> 0.4 in MOPS buffer had caused a slight, but significant bundling of AFs at day 3 dpi at those sites, where the bacteria had attached (**Fig. 3.9**).

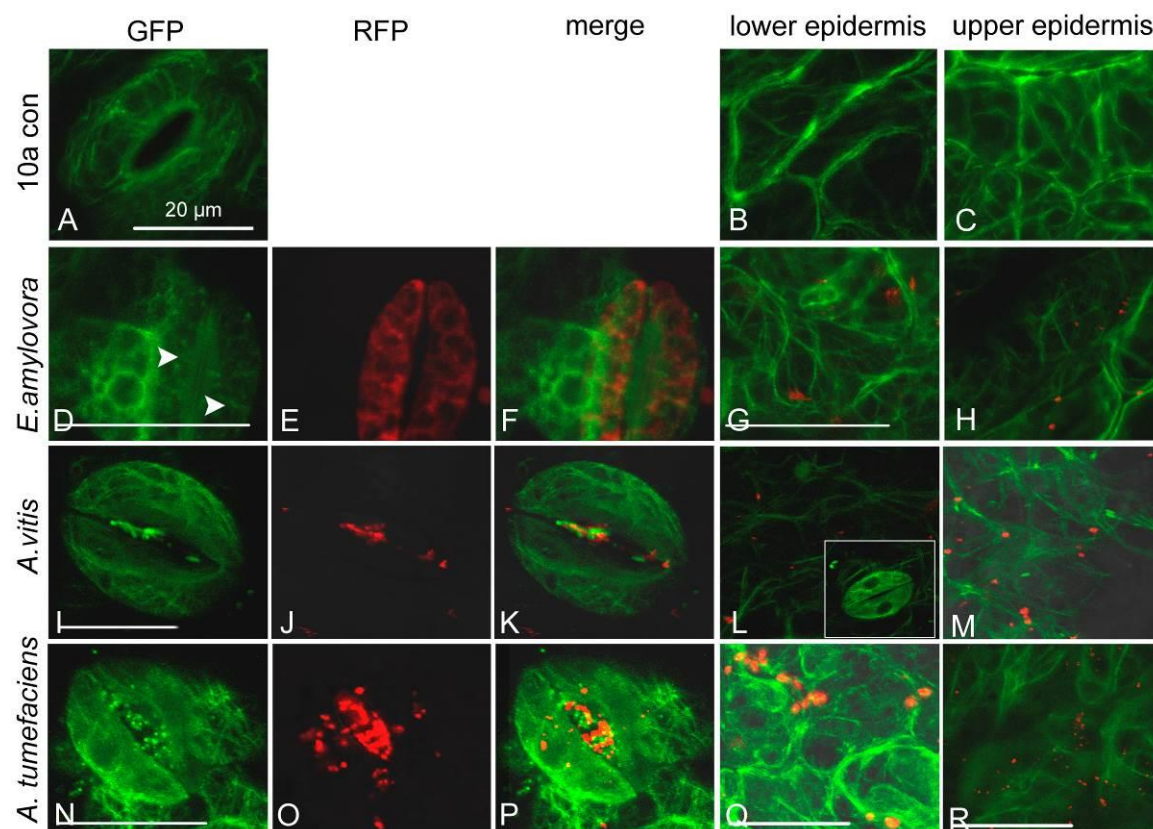


**Fig 3.9** Response of actin filaments to different Gram-negative bacteria visualised by spinning-disc confocal microscopy. AF structures in leaves of *V. vinifera* ‘Chardonnay’ line 10a expressing *GFP-AtFABD2* shown in green, the bacteria labelled red by the dTomato marker. *Ewinia amylovora* at guard cells (**D**, GFP, **E**, RFP, **F**, merge) and epidermal cells (**G**, lower; **H**, upper epidermal cells), *Agrobacterium vitis* S4 at guard cells (**I**, GFP, **J**, RFP, **K**, merge), exclusion of the signal from the nuclear region of guard cells (insert image in **L**) and epidermal cells (**L**, lower, **M**, upper epidermal cells) after inoculation with *A. vitis* S4, *Agrobacterium tumefaciens* EHA105 at guard cells (**N**, GFP, **O**, RFP, **P**, merge) and epidermal cells (**Q**, lower; **R**, upper epidermal cells). If not stated otherwise, images were recorded

## Results

3d post-inoculation with  $OD_{600} \sim 0.4$ , Non-inoculated *V. vinifera* 'Chardonnay' GFP-*AtFABD2* line 10a (**A**, guard cell, **B**, lower, **C**, upper epidermal cells) was used as control. White arrow heads indicate the disrupted AFs. Bar = 20  $\mu\text{m}$ .

To assess the extent of AF bundling, image series were analysed by quantitative image analysis following a specific skeletonization algorithm as described in 2.10 (see **Fig. 2.4A-D**). The skewness of the fluorescence intensity distribution is a useful indicator of AFs bundling, whereas AF density can be quantified using occupancy values of the GFP signal. For inoculation with *E. amylovora* AFs in the guard cells appeared fragmented at 3 dpi (**Fig. 3.9D-F**), but without altering their bundling state evident from a constant skewness of 96% (**Fig. 3.10A**) comparing to the non-infiltrated control (**Fig. 3.9A**). For inoculation with *A. vitis*, occasionally AF appeared to be excluded from the nuclear region of guard cells (**Fig. 3.9L** insert image). Here, guard cells showed a reduced skewness of 40% of controls indicating a significant thinning of AFs (**Fig. 3.10A**). Also, inoculation with *A. tumefaciens EHA105* reduced skewness to 46% of the control value (**Fig. 3.10A**). These changes of actin organisation were confined to the guard cells. In the other epidermal cells, neither inoculation with *E. amylovora*, nor with *A. tumefaciens EHA105* and *A. vitis* produced any significant difference (**Fig. 3.10B**). It should be mentioned that no indication of necrosis phenomena could be observed, when the leaves were monitored by stereo microscopy after infiltration.

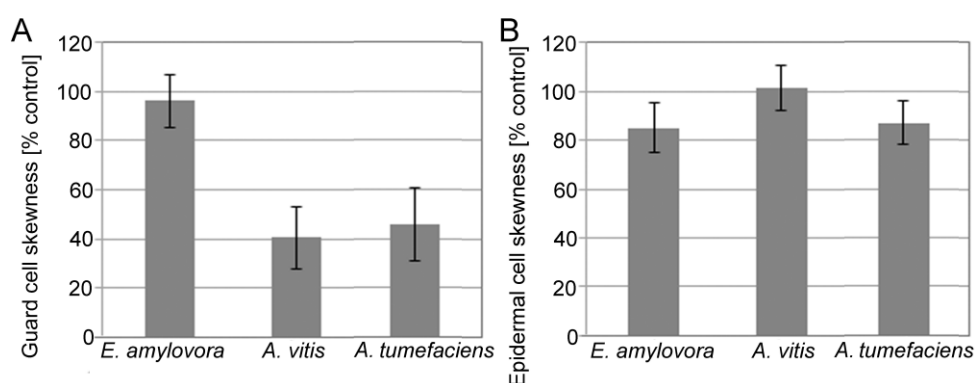


**Fig 3.10** AF bundling quantified by quantitative image analysis based on skewness values (for details refer to 2.10) in guard cells (**A**). And epidermal pavement cells (**B**). Data represent mean values and standard errors from a population of 30-50 individual cells.

### 3.10 Formation of *V. rupestris* calli and suspension cells expressing *GFP-AtTUB6*

Green fluorescent calli (**Fig. 3.11A** and **B**) with cells that showed microtubule structures were first examined 4 weeks after transformation, and then subcultured every 4 week, till enough callus was available after 12 weeks to generate a suspension cell line. Already in the callus stage clear cortical MTs were visible (**Fig. 3.11C** and **D**). In contrast, non-transformed (**Fig. 3.11Db**) and

dead cells (**Fig. 3.11Da**) only showed a faint unstructured autofluorescence. After transition to suspension growth, all cells of the stably transformed cell line exhibited clear cortical MTs and transvacuolar strands (**Fig. 3.11E**).

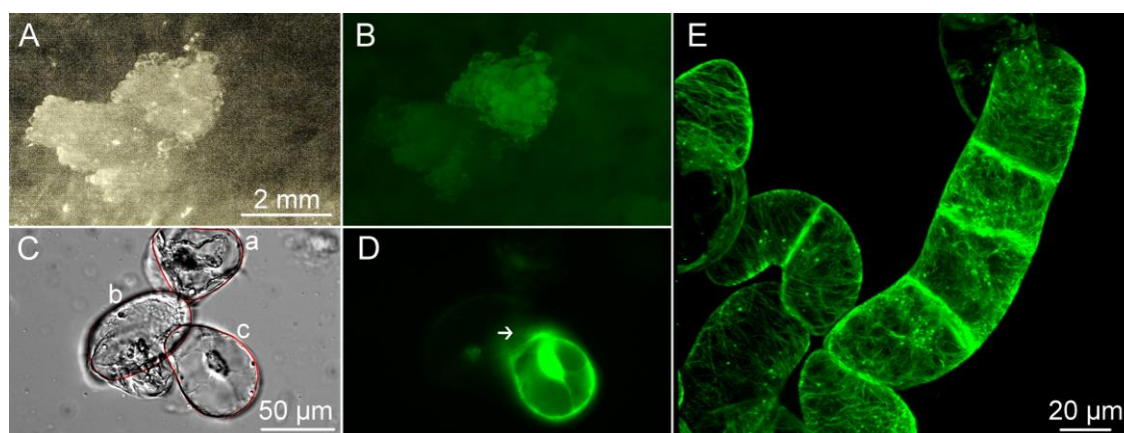


**Fig 3.11** Formation of *V. rupestris* calli (**A** differential interference contrast, dic; **B** GFP filterset) and suspension cells (**C** dic; **D** GFP filterset) expressing *GFP-AtTUB6* visualised by spinning-disc confocal microscopy. **C**: a: dead cell; b: untransformed cell; c: transformed cell. White arrow in **D** indicates cortical MTs. **E**, Stable transformed *V. rupestris* suspension cell line.

To verify the correct insertion of the transgene, the transgenic cells were genotyped. Total DNA from transformed and non-transformed cells was extracted (**Suppl. Fig. 8**) and used as template in subsequent genomic PCR probing for the presence of the Arabidopsis *TUB6* gene (Arabidopsis  $\beta$ -tubulin 6 (At5g12250)) (using primers 5'-CGATGTTGTACGCAAAGAGGCTG-3' and 5'-GACGAGGGAAAGGAATGAGGTTC-3') (**Suppl. Fig. 8**). As expected, only the transformed cells, not the non-transformed control yielded a band.

### 3.11 Morphogenetic response to biotic and abiotic stresses

The *Vitis rupestris* GFP-AtTUB6 suspension cell line provides a useful tool to investigate the response of MTs to biotic and abiotic stresses. Hence the effect of biotic stresses, mimicked by flg22 (PTI), HrpZ (ETI), and ( $\pm$ )-JA (wounding) and abiotic stresses, sodium chloride (salinity stress), polyethylene glycol 6000 (osmotic stress), ethanol (activation of G-protein dependent stress), UV-B, UV-C, cold and heat were studied.

Three days after the stress treatment, changes of PCV as measure of growth (**Suppl. Fig. 9A**), and mortality (**Suppl. Fig. 9B**) were estimated. The concentrations of active agents and incubation time were chosen according to previous experimental results from our group in this cell line and publications of other authors (Guan *et al.*, 2013; Ismail *et al.*, 2012; Hamayun *et al.*, 2010). All treatments affected cell growth as reflected by reduced increase of PCV. In case of

NaCl 79 mM, PEG 6000 25% and HrpZ 1.7  $\mu$ M the inhibition was most extreme and linked with a high rate of cell death. Treatment with flg22 reduced growth only slightly to 86% compared to the control. Interestingly, JA, cold and heat inhibited growth, while mortality was low, indicating that these cells remained viable, but arrested expansion.

### 3.12 Sustained microtubule response to biotic and abiotic stresses

To verify the results that had been obtained with tobacco BY-2 cells, 100 nM flg22 were administered to the grapevine tubulin marker line. This treatment did not cause any changes in the vast majority of cells neither in the radial MTs emanating from the nucleus, nor in the cortical MTs underneath the membrane (**Fig. 3.12**). In contrast, treatment with 1.7  $\mu$ M of HrpZ caused drastic changes, mainly in the radial MTs that were found to be eliminated, whereas cortical MTs became thinner as compared to the control, but still maintained their integrity (**Fig. 3.12**). These observations are in good agreement with those made for the BY-2 GFP-AtTUB6 marker line (chapter 3.2, Guan *et al.*, 2013). It should be mentioned that a small part of the fluorescent tubulin was present inside the nucleus, due to the use of confocal microscopy, which is clear that these tubulin speckles are truly intranuclear (for details on this point see **Suppl. Fig. 10**). Interestingly, these intranuclear tubulin speckles vanished during elicitor treatment most pronounced for flg22. In contrast, these speckles persisted during abiotic stress.

These experiments were accompanied by appropriate solvent controls. Here, cortical MTs formed clear parallel arrays in the majority of the cells; transvacuolar MTs formed thin equally spaced strands, and a part of the tubulin was present in form of intranuclear speckles. For treatment with 35  $^{\circ}$ C, ( $\pm$ )-JA, NaCl or PEG 6000 cortical MTs were found to be bundled 3 days after onset of stress (**Fig. 3.12**). Also 1% EtOH produced strong bundling, accompanied by an elevated number of large cells. When cells were exposed to 4  $^{\circ}$ C, tubulin was redistributed into the karyoplasm; for heat treatment (35  $^{\circ}$ C), the cells grew much bigger than control, and transvacuolar MTs bundled as well. When the effect of a UV-B pulse (10 min) was examined 3 days later, transvacuolar MTs were found to be partially eliminated, however, cortical MTs had persisted (shown exemplarily for the cut-off filter WG 302 in **Fig. 3.12**). There were no significant differences for different spectral ranges of UV-B established by the different cut-off filters. However, UV-C produced more drastic morphological changes when examined at day 3 after irradiation. Here, the transvacuolar MTs showed a net-like structure around disintegrated vacuoles, and the cortical MTs that persisted for a mild treatment with 2 min irradiation, were disrupted and fragmented for a longer irradiation (10 min).



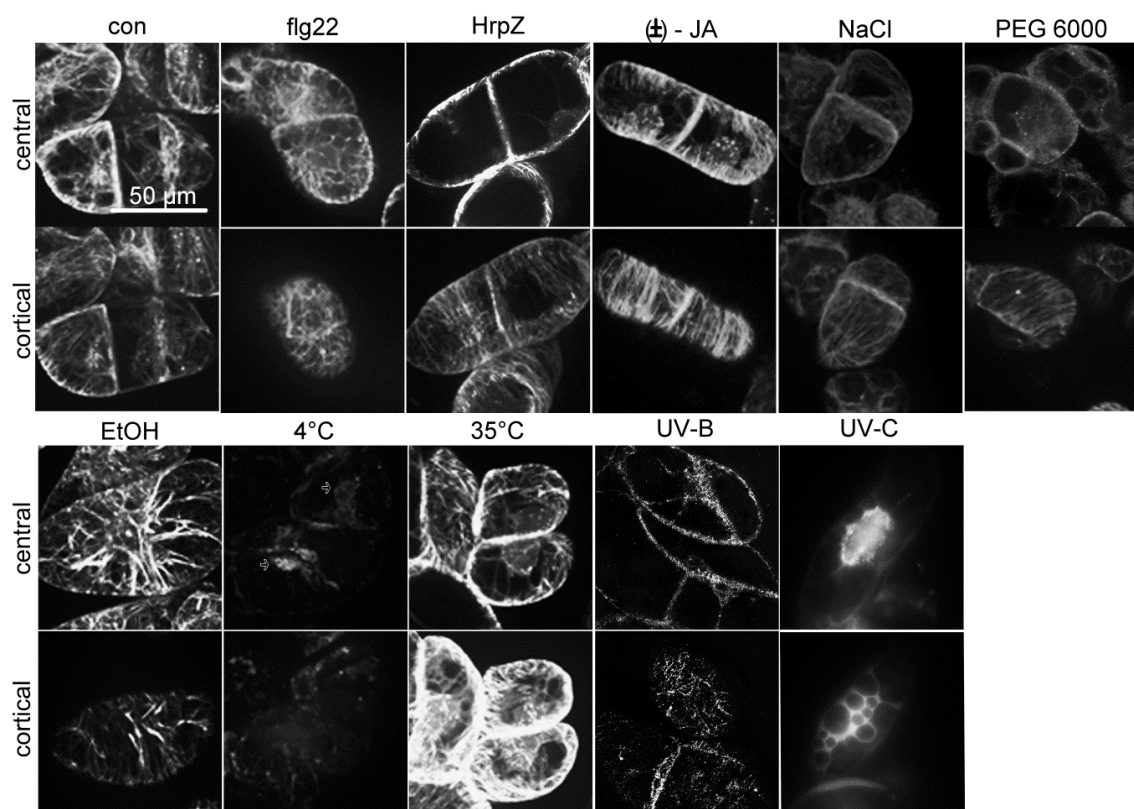


**Fig 3.12** Stress responses of microtubules *in vivo* in *V. rupestris* cells expressing the GFP-AtTuB6 marker 3 d after biotic (flg22, HrpZ, ( $\pm$ )-JA), and abiotic (NaCl, PEG 6000, EtOH, cold-, heat-treatment, UV-C- and UV-B-irradiation) stress treatments visualised by spinning-disc confocal microscopy (image of cells after UV-B-irradiation was taken by laser scanning confocal microscopy, ZEISS LSM 510, Germany). MTs in the cortical and central regions of the cell are shown in controls (con), and after the challenge with flg22 100 nM, HrpZ 1.7  $\mu$ M, ( $\pm$ )-JA 500  $\mu$ M, NaCl 64 mM, PEG 6000 20%, EtOH 1%, 4  $^{\circ}$ C, 35  $^{\circ}$ C, 10 min UV-B, or 10 min UV-C. White bordered arrows in the 4  $^{\circ}$ C experiment indicate intranuclear tubulin speckles observed in the central plane of the cell. Representative images from at least five independent experimental series with a population of 100 individual cells for each treatment are shown.

### 3.13 Rapid microtubule responses to biotic and abiotic stresses

The above results prompted the following questions: 1. Do MTs produce a higher response to abiotic stress than to biotic stress? 2. How to explain the extremely bundling of cortical MTs observed for treatment with ( $\pm$ )-JA, NaCl and PEG 6000? Therefore, short-term responses of MTs were analysed.

In order to investigate the short-term (<20 min) responses of MTs, time-series were recorded for individual cells that were mounted on slides and challenged directly under the microscope with the respective stress factor. In parallel, time series were conducted for mock controls to account for effects of the experimental set-up and possible effects of bleaching due to microscopical excitation. A treatment with flg22 10  $\mu$ M (up to 20 min) did not cause any changes, neither in the radial MTs emanating from the nucleus, nor in the cortical MTs underneath the membrane,

## Results

consistent with the findings in tobacco BY-2 (see chapter 3.2, Guan *et al.*, 2013). It should be mentioned, however, that flg22 challenge decreased the amount of intranuclear tubulin speckles compared to the untreated control (data not shown).

In contrast to flg22, HrpZ (at 28.8  $\mu\text{M}$  up to 30 min) or 57.6  $\mu\text{M}$  up to 20 min) induced rapid bundling of both radial and cortical MTs (**Suppl. Fig. 11**). Interestingly, here the intranuclear speckles that had been found to vanish if inspected 3d after addition of HrpZ, had increased within 30 min (data not shown).

As general transducer for biotic stress ( $\pm$ )-JA in progressively increasing concentrations was tested. Time-lapse series for treatment with 5 mM over 50 min showed disassembly of transvacuolar MTs (**Suppl. Fig. 12**), that initially were bundled more heavily as compared to the HrpZ treatment (28.8  $\mu\text{M}$ , 30 min).

For short-term responses to various concentrations of NaCl, there were no significant changes within a period of 20 min monitor (data not shown). For 200 mM, a lethal dose for *V. rupestris* (Ismail *et al.*, submitted) NaCl, plasmolysis became detectable from 5 min followed by detachment of the shrinking protoplast from the cell wall (**Fig. 3.13A**). For 79 mM of NaCl (a concentration where *V. rupestris* can survive due to efficient salt adaptation, Ismail *et al.*, submitted), a specific and rapid response of cortical microtubules was observed (**Fig. 3.13B**). Hereby, the original network disappeared, manifesting already 2 min after the addition of salt, and was then replaced by massive bundles of MTs detected as early as 7 min after addition of salt.

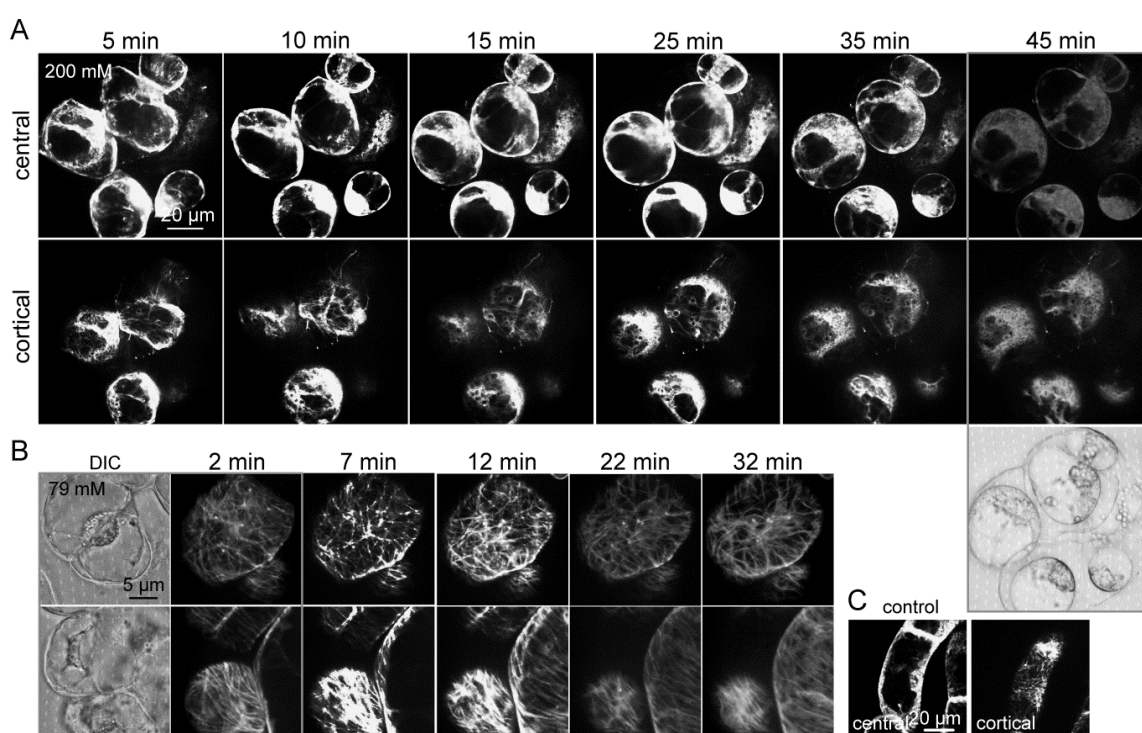


**Fig 3.13** Response of cortical and radial MTs to NaCl stress shown by time-lapse series recorded from the *V. rupestris*

GFP-TuB6 line. **A** plasmolysis and microtubule degradation in response to a lethal concentration of salt (200 mM NaCl), **B** adaptive formation of macro-tubules in response to intermediate salt stress (79 mM NaCl) Differential interference contrast images at the left show the same cell as taken with GFP channel. **C** Solvent control (water). Observations are representative of at least five independent experimental series with a population of 100 individual cells for each treatment.

To mimick drought stress, PEG 6000 at 8.0%, 12.5%, 18.75% and 37.5% was administered. A certain bundling could be observed for 18.75% of PEG 6000 (**Suppl. Fig. 13**) within 20 min, accompanied by plasmolysis evident from alteration in the central MTs.

In response to EtOH 0.5% and 1% produced diffuse, disordered microtubules (**Suppl. Fig. 14**). This apparent disorganisation of the cytoskeleton did not impair viability, mortality in 1% EtOH scored after 3 days was low (**Fig. 3.13**)

### **3.14 IAA effects on MTs in *V. rupestris* suspension cells expressing *GFP-AtTUB6***

Auxin is the most important activator of growth and therefore a primary target for defence-triggered growth inhibition, as worked out in the introduction. When the cells were exposed to IAA concentration from 0.1 to 100  $\mu\text{M}$ , neither cortical nor central MTs showed significant changes (**Fig. 3.14G**), whereas the intranuclear speckles differed significantly. The number of these speckles changed with increasing IAA concentration. This phenomenon was further analysed by scoring intranuclear speckles. Whereas the lowest concentration of auxin (0.1  $\mu\text{M}$ ) which is not sufficient to stimulate cell expansion (Campanoni & Nick, 2003) in suspension cells, showed a similar frequency distribution as the control, the frequency of cells with a high density of speckles was elevated for 1  $\mu\text{M}$  of IAA (a concentration that triggers auxin-dependent cell division), but decreased then drastically when IAA was raised to 10  $\mu\text{M}$  (a concentration that triggers auxin-dependent cell expansion), and increased again, when IAA reached 100  $\mu\text{M}$  (a concentration that is overoptimal for expansion, but still stimulates cell division). This specific dose-response pattern (**Fig. 3.14F, G**) shows an inverse correlation of the frequency of intranuclear speckles with the intensity of auxin-dependent cell expansion.

### **3.15 IAA effects on cell division, morphogenesis and mortality in *V. rupestris* suspension cells expressing *GFP-AtTUB6***

The cytoskeletal responses induced by IAA should, as a consequence, alter the morphogenetic responses of the cell that are dependent on the cytoskeleton. A dose-response curve of changes in PCV as reporter for culture growth over the concentration of IAA (**Fig. 3.14A**) showed a

## Results

---

significant increase with 10  $\mu\text{M}$  IAA, and a significant inhibition of ~20% as compared to control with superoptimal concentrations of 100  $\mu\text{M}$ . To test whether the increased growth at ~10  $\mu\text{M}$  IAA was caused by stimulation of cell division, we monitored the dose-responses of mitotic index at day 3 (at the peak of mitotic activity) after inoculation. Although there was a slight increase of mitotic activity, this was not significant and could not account for the stimulation of growth (**Fig. 3.14B**). In the following, we therefore investigated the effects of IAA on cell shape. Frequency distributions for the ratio between cell width over cell length were constructed. For 10  $\mu\text{M}$  concentrations of IAA, the frequency of cells with ratios of width/length 0.6-0.8 increased, whereas cells with ratios  $<0.5$  decreased. This means elongated cells became rare; whereas broader cells became more frequent (**Fig. 3.14C**). This trend became progressively evident from concentrations exceeding 1  $\mu\text{M}$  (shown exemplarily for 10  $\mu\text{M}$ ). Compared to the wild type of *V. rupestris*, the expression of GFP-AtTUB6 had a positive influence on culture growth (**Fig. 3.14A**). This increased growth seems not to be caused by a promotion of mitotic activity, on the contrary, cell division was reduced (**Fig. 3.14B**). Thus, the increase must be caused by cell expansion, which is linked with a widening of cells (**Fig. 3.14C**). The mean values of absolutely width and length are presented in **Fig. 3.14D** Mortality was low, independent of the concentration of IAA and thus is not relevant for the phenotype (**Fig. 3.14E**).

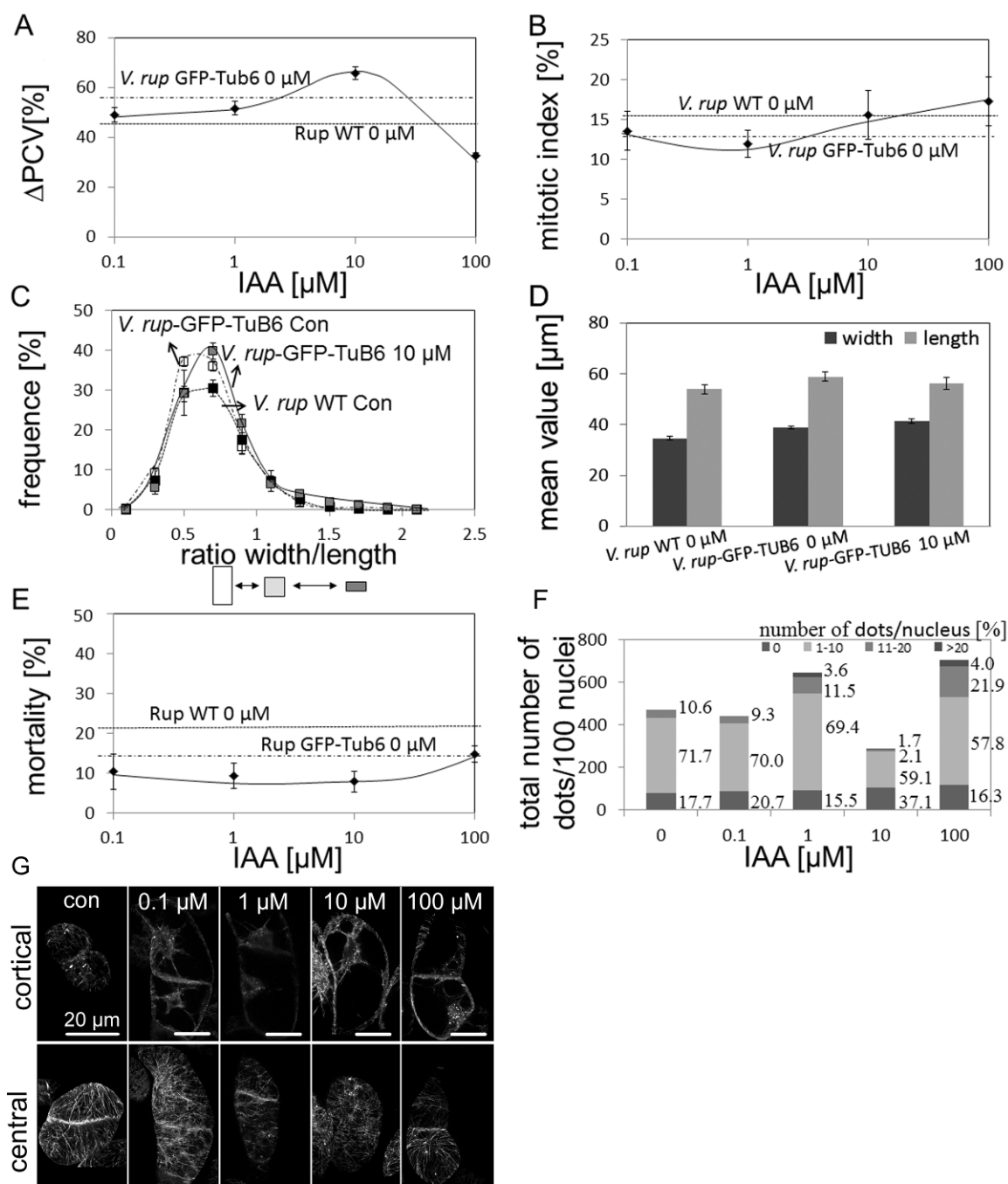


**Fig 3.14** Cellular responses to IAA. **A** Dose-responses of changes in packed cell volume as indicator of culture growth at day 3 (peak of mitotic activity). **B** Dose responses of mitotic index at day 3 after inoculation (scored from a population of 1000 individual cells for each data point). **C** Effect on cell shape. Frequency distributions for the ratio between cell width over cell length were constructed from 300 individual cells for each experiment. **D** Mortality in response to IAA. A population of 2000 individual cells scored after staining with 2.5% Evans Blue for each value. Data in **A**, **B**, **C** and **D** represent mean and standard errors from three biological replicates. **E** Total number of dots per 100 nuclei. **F** Response of MTs in *V. rupestris* cells to IAA *in vivo* visualised by the GFP-*AtTUB6* marker and spinning-disc confocal microscopy. Geometric projections from z-stacks collected in the cortical or the central region of the cells are shown.

### 3.16 IAA is antagonistic to JA, but not to HrpZ, with respect to the microtubular response

Since IAA and JA are antagonists for cell growth (see introduction), a response that depends on microtubules, we asked, whether IAA can counteract the microtubular response triggered by JA. A short-term treatment with a high dose of ( $\pm$ )-JA caused a bundling of cortical MTs (**Fig. 3.15A**). This JA-induced bundling could be rescued by 10  $\mu$ M of IAA. Both cortical and radial MTs even became finer within the 20 min of observation (**Fig. 3.15B**). For 20  $\mu$ M of IAA this debundling was tested also and was found to be accelerated to such an extent that it was not possible to record it in a time series due to limitations in experimental handling.

Since JA acts as general stress signal, we asked, whether IAA can also suppress the microtubular response triggered by HrpZ as elicitor for effector triggered immunity responses. We used a relatively mild treatment of HrpZ (15  $\mu$ M for 45 min). This concentration was chosen based on the responses observed in BY-2 with 57.6  $\mu$ M taking into account that the sensitivity of *V. rupestris* is  $\sim$ 2.5 fold that of BY-2 as monitored by apoplastic alkalinisation in response to HrpZ (Guan *et al.*, 2013). This HrpZ treatment impaired the parallel alignment of the cortical MTs that became progressively disordered, whereas at the same time, the transvacuolar MTs bundled and contracted towards to the nucleus (**Fig. 3.15C**). Additional application of IAA partially repaired the disorganisation of cortical MTs, but did not rescue the loss of transvacuolar MTs, even for prolonged incubation up to 40 min (**Fig. 3.15D**).

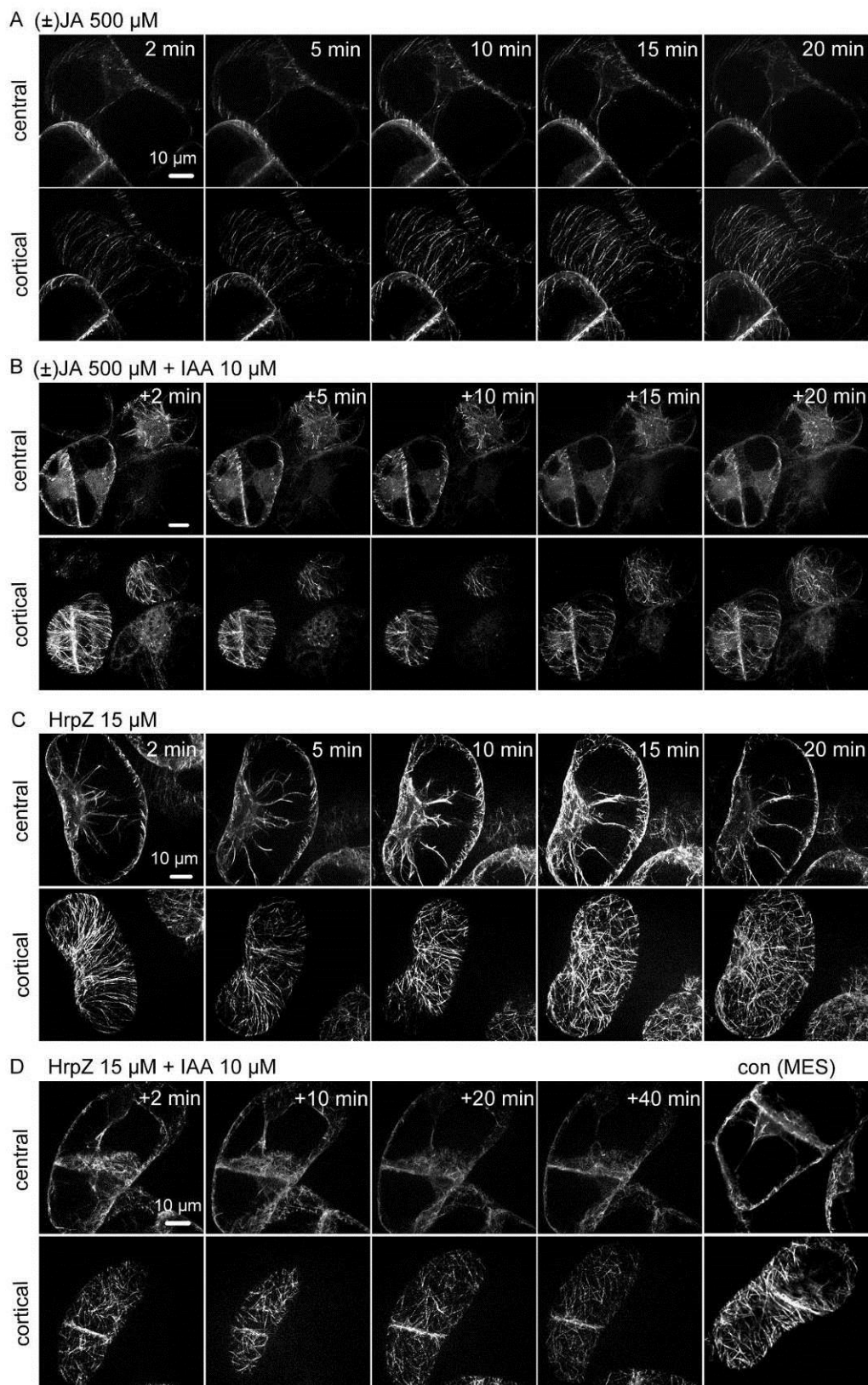


**Fig 3.15** Effect of IAA on the microtubular response to ( $\pm$ )-JA and HrpZ in *V. rupestris* *in vivo* visualised by the GFP-AtTUB6 marker and spinning-disc confocal microscopy. Confocal sections collected in the cell centre and the cortical regions of the same cell are shown. **A** MT response to 500  $\mu$ M ( $\pm$ )-JA over 20 min, **B** MT response to 500  $\mu$ M ( $\pm$ )-JA in combination with 10  $\mu$ M of IAA 10  $\mu$ M monitored for 20 min. **C** MT response to 15  $\mu$ M HrpZ over 20 min,

## Results

**D** MT response to 15  $\mu$ M HrpZ in combination with 10  $\mu$ M IAA monitored for 40 min). Controls show the response to the solvent (5 mM MES buffer).

### 3.17 Response of microtubules to different Gram-negative bacteria

*V. rupestris* cells were co-cultivated with dTomato-tagged marker lines for the phytopathogenic bacteria *E. amylovora* (**Fig. 3.16C**), *A. tumefaciens* EHA105 (**Fig. 3.16D**), and *A. vitis* S4 (**Fig. 3.16E**), *E. coli* S17- $\lambda$ pir (**Fig. 3.16F**), respectively, for 2 days. *V. rupestris* cells in liquid MS medium (sus con, **Fig. 3.16A**) and on agar-solidified MS medium (agar con **Fig. 3.16B**) were used as control. The extent of MT bundling was determined by quantitative image analysis as already described for actin filaments in the actin-marker plants (see 3.9) yielding statistical data on the MT response (see **Fig. 2.4E** and **F**).

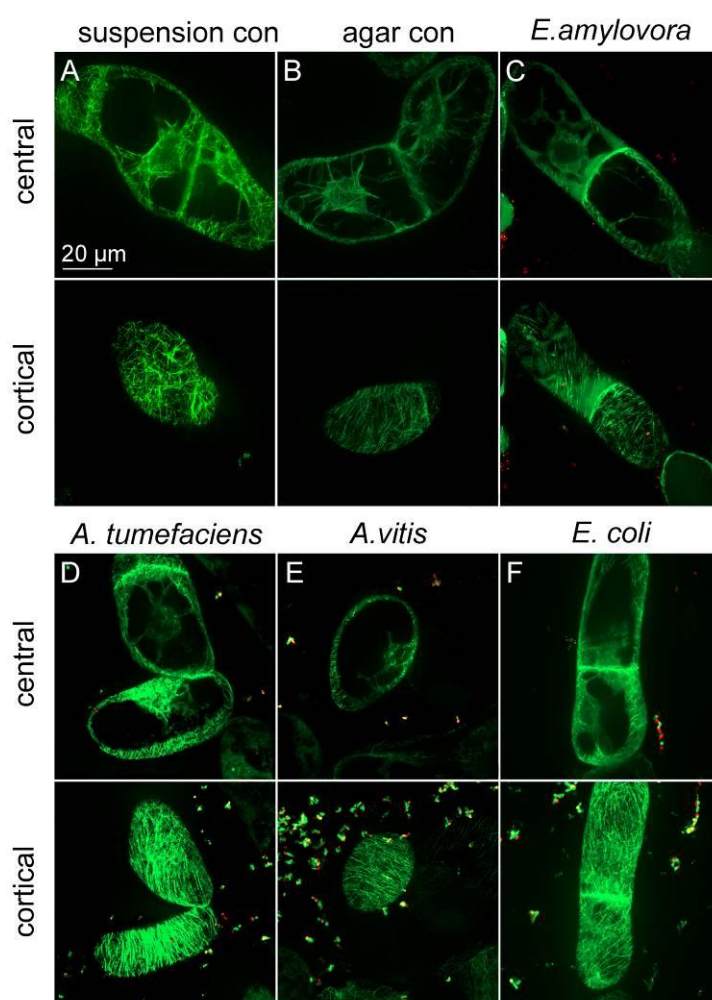


**Fig 3.16** Response of microtubules in *V. rupestris* to the phytopathogenic bacteria *Ewinia amylovora*-dTomato (*E. amylovora*, **C**), *Agrobacterium tumefaciens* EHA105 dfr2 $\alpha$ -dTomato-GFP (*A. tumefaciens* , **D**), *Agrobacterium vitis* S4-dTomato-GFP (*A. vitis*, **E**), and *Escherichia coli* S17- $\lambda$ pir-dTomato (*E. coli*, **F**) *in vivo*, visualised by the GFP-AtTUB6 marker and spinning-disc confocal microscopy. Confocal sections collected in the cell centre and the



---

cortical regions of the same cell are shown. Cells grown on MS agar medium, with the differences from suspension cells (**A**), are taken as controls (**B**).

The skewness of the fluorescence intensity distribution as indicator for MTs bundling was quantified. To evaluate MT density, the occupancy values of skeletonized images was assessed. Co-cultivation with *E. amylovora*-dTomato caused the increased density of both cortical MTs (148.7% to agar control in 60% cell population, **Fig. 3.17A**) and transvacuolar MTs (127% to agar control in 70% cell population **Fig. 3.17B**). The cortical MTs bundled strongly (30% cell population showed 9.91E+11% to agar control, 70% cell population showed 371.1% to agar control in **Fig. 3.17C**); with non-host *A. tumefaciens* EHA105 dfr2 $\alpha$ -dTomato-GFP, 60% transvacuolar MTs kept their thin structures and density as agar control (**Fig. 3.17A**), the occupancy of cortical MTs also remained as agar control (**Fig. 3.17B**), however the bundling of cortical MFs shown as skewness was 3 fold of agar control in around 40% cell population (**Fig. 3.17C**). In the case of co-culture with host pathogen *A. vitis* S4-dTomato-GFP, transvacuolar MTs increased their indensity to 183.% of agar control in 60% cells population (**Fig. 3.17A**), and cortical MTs slightly bundled to 6.5 times of agar control in 80% cell population (**Fig. 3.17C**). In co-cultivation with *E. coli* S17- $\lambda$ pir-dTomato only subtle changes were visible concerning the cortical skewness and central occupancy, whereas cortical MTs increased their density slightly in a cell population of 60% (**Fig. 3.17B**).

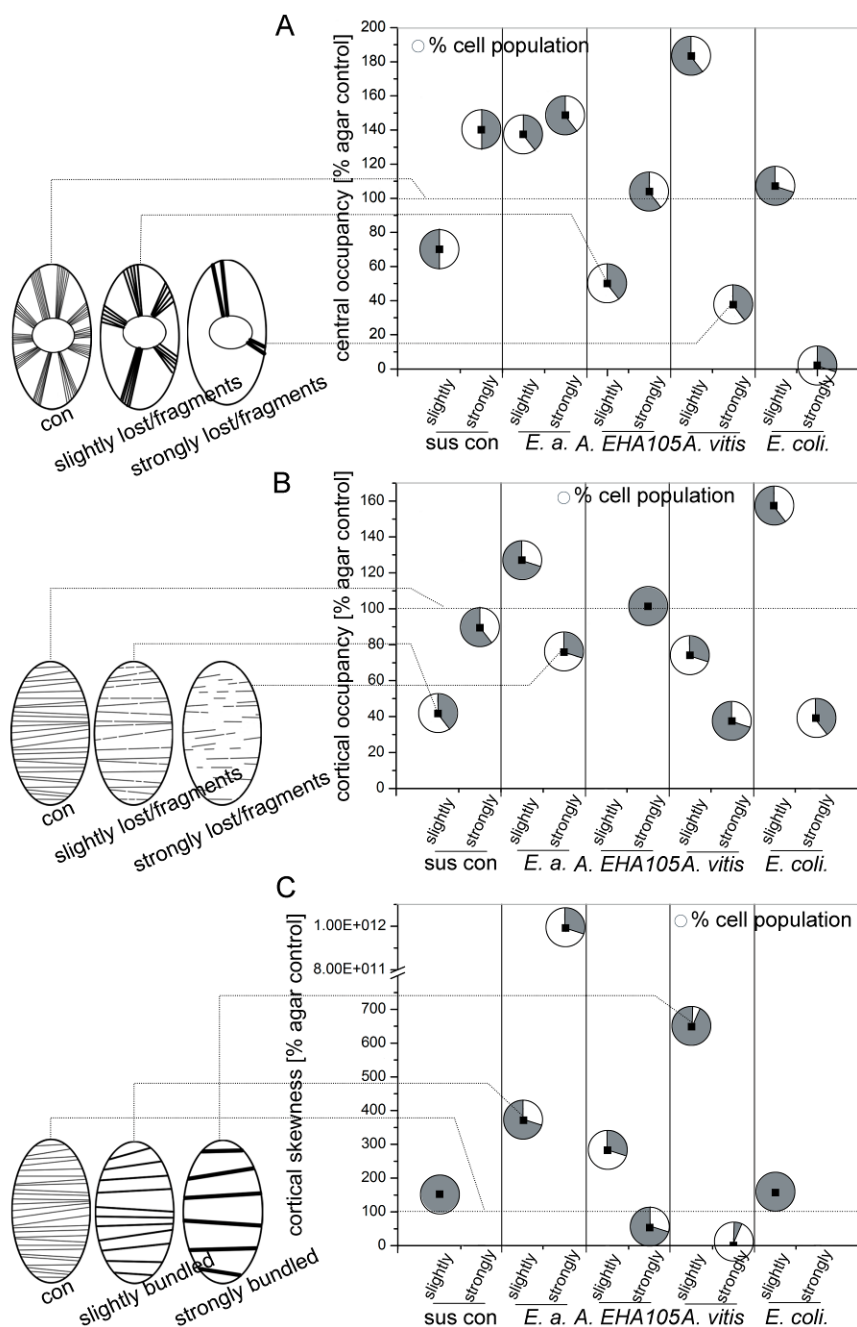


**Fig 3.17** Quantitative analysis of MTs bundling and MTs density using microscopic image analysis. Data are from a population of 30-50 individual *V. rupestris* cells for each Gram-negative bacteria co-cultivation. The serial optical sections by spinning disc confocal laser scanning microscopy were skeletonized, and then performed using JAVA plug-ins and macros: `hig_255counts` and `hig_skewness` (Hasezawa, <http://hasezawa.ib.k.u-tokyo.ac.jp/zp/Kbi/HigStomata>) on IMAGEJ. To evaluate MT density (using occupancy is as an indicator), cells are classified as two groups slightly lost/fragments (sl/f) and strongly lost/fragment (st/f) (central, **A**; cortical, **B**). To evaluate MTs bundling (using skewness is as an indicator) cells were classified as two groups slightly bundled (slb) and strongly bundled (stb) (cortical **C**). The percentages of each class (slightly or strongly) are presented as certain grey area in circles. Schematic illustrations are inserted in left bottom.

### 3.18 Summary

To gain insight into the earlier stages of cytoskeleton remodelling in plant defence, the BY-2 cells expressing the GPF-*AtFABD2* (AFs marker line) and GPF-*AtTUB6* (MTs marker line) were used to follow the cytoskeleton responses to flg22 and HrpZ. Challenged by 10  $\mu$ M flg22, the transvacuolar network of AFs did not reveal any significant changes; however, the cortical AFs lost their finer filaments, changed orientation and often became more prominent. On the contrary, the drastic changes of AFs induced by 57.6  $\mu$ M HrpZ, where AFs condensed into cortical aggregations, followed by contraction of actin towards the nucleus, a disruption of both cortical and transvacuolar AFs happened within 20 min. Parallel to AFs, the response of MTs under the treatment of 10  $\mu$ M flg22 did not cause any change, even for a long-term treatment; however, HrpZ (57.6  $\mu$ M) caused drastic changes mainly in the transvacuolar MTs that were found to be eliminated, whereas the cortical MTs became thinner as compared to the control, but still maintained their integrity. One of the earliest detectable responses is extracellular alkalinisation caused by modifying of plasma membrane permeability. flg22 triggered a pH reaching a maximum at ~600 s after elicitation (no variation between different concentrations, a saturation of the response from 200 nM reached at 0.27 pH units). HrpZ triggered the maxima pH significantly later than the timing found for flg22 (depending on the concentration, at 14  $\mu$ M, already reached 1.2 pH units). We next phenotyped growth, cell shape, and division synchrony which are as sensitive targets of cytoskeletal remodeling. HrpZ reduced the mitotic index drastically to almost zero (only partially reduced by flg22), cells became progressively elongated (cells became broader in the case of flg22 elicitation). flg22 and HrpZ can modulate the actin cytoskeleton indicating by impaired polar auxin transport. HrpZ (but not flg22) can induce cell death.

Since actin remodelling is as early event in ETI-like immunity in BY-2 suspension cell system, we tested whether this can be confirmed in a real plant with real pathogens with an economic important plant grapevine. A transgenic grapevine *Vitis vinifera* 'Chardonnay' expressing *GFP-AtFABD2* was established, where a normal configuration of actin was presented supporting by the completely normal morphology of the transgenic plants. Only a very close inspection revealed a phenotypical change between line 10a and non-transformed controls. The extent of AF bundling in response to Gram-negative bacteria was assessed. For inoculation with *E. amylovora*, AFs in the guard cells appeared fragmented at 3 dpi, but without altering their bundling state, which was in good agreement with the data on the effect of HrpZ in the AF marker line in BY-2. For inoculation with *A. vitis*, *A. tumefaciens EHA105*, guard cells showed a significant thinning of AFs. In the other epidermal cells, neither inoculation with *E. amylovora*, nor with *A. tumefaciens EHA105* and *A. vitis* produced any significant difference. If the specificity of actin responses in the guard cells are not caused by the specificity of pathogen effectors, but are innate to actin itself,

## Results

---

they should be triggered by completely different pathogens as well. Therefore, AFs response to *P. viticola* was tested. 3 days after inoculation with zoospores of *P. viticola*, AFs in guard cells had disassembled, and perinuclear actin baskets were observed in cells of the lower epidermis. Hereby, we proposed the guard cell gatekeeper model of AFs that with priority than in the epidermal pavement cells.

On the other hand, suspension cell line *V. rupestris* expressing *GFP-AtTUB6* was established that provides a useful tool to investigate the response of MTs to biotic (mimicked by flg22 (PTI), HrpZ (ETI), and ( $\pm$ )-JA (wounding)) and abiotic stresses (mimicked by sodium chloride (salinity stress), polyethylene glycol 6000 (osmotic stress), ethanol (activation of G-protein dependent stress), UV-B, UV-C, cold and heat). All treatments affected cell growth, especially in case of NaCl 79 mM, PEG 6000 25% and HrpZ 1.7  $\mu$ M, the inhibition was most extreme and linked with a high rate of cell death. When sustained and rapid microtubule responses were studied, some of the reorganization of MTs were observed, such as intranuclear tubulin speckles, tubulin was redistributed into the karyoplasm, formation of macrotubules. We found JA-induced bundling could be rescued by 10  $\mu$ M of IAA, leading to finer cortical and radial MTs; however, additional application of IAA did not rescue the loss of radial MTs, although partially repaired the disorganisation of cortical MTs. Furthermore, we tested such MTs reorganization with real phytopathogens. Under the inoculation of different Gram-negative bacteria (*E. amylovora*, *A. tumefaciens EHA105*, *A. vitis*, *E. coli*), the extent of MTs bundling and density were assessed. The density of cortical MTs was increased under *E. amylovora* inoculation. The density of transvacuolar MTs was increased under *E. amylovora*, *A. vitis* inoculation. The extent of cortical MTs bundling increased under all these four bacteria inoculation.

## 4 Discussion

### 4.1 Temporal signature of AFs and MTs in decoding elicitor signals of PTI and ETI

This work addressed the response of the cytoskeleton to flg22 (a canonical trigger for PTI), and HrpZ (a bacterial elicitor mimicking different aspects of ETI) by spinning-disc confocal microscopy and live-cell imaging in the BY-2 tobacco cell line, where GFP-tagged cytoskeletal marker lines are available. In our previous work, we had observed a remodelling of actin and a disintegration of cortical microtubules after treatment with a commercial Harpin elicitor in two grapevine cell lines that differ in their microtubular dynamics (Qiao *et al.*, 2010). A limitation of the grapevine system was the need to visualise microtubules by immunofluorescence, and actin by fluorescent phalloidin, both protocols requiring chemical fixation. Since the cytoskeletal response could thus not be followed over time in individual cells, only bulk changes of cytoskeletal organisation became evident, which means that the early stages of these responses were not detected. This limitation was circumvented in the current work by using tobacco BY-2 cells that are more readily transformed. As central point in the current work, we report now that the cytoskeletal responses differ depending on the nature of the elicitor and the nature of the cytoskeletal element: Whereas both actin and microtubules responded drastically and rapidly to HrpZ, the cytoskeletal responses to flg22 remained very subtle. Here, it was mainly a remodeling and slight bundling of the dynamic actin network underneath the cell membrane that could be detected from ~5-10 min after elicitation, whereas neither microtubules nor the transvacuolar actin cables revealed any change. For Harpin, a remodeling and bundling of both cortical and transvacuolar actin filaments was clearly evident already at 10 min after elicitation, which was followed by progressive disintegration, accompanied by a progressive disruption also of microtubules. For both elicitors, the time course for the actin response either accompanied (for flg22) or even preceded (for HrpZ) extracellular alkalinisation as rapid readout for defence. Generally, actin seems to respond more sensitively as compared to microtubules, although the microtubules in the cell centre disintegrate in response to HrpZ (parallel with actin filaments).

To understand the differential early cytoskeletal response to flg22 versus HrpZ, it is relevant to compare the perceptive mechanisms for these elicitors. The PAMP flg22 is a ligand of the leucine-rich repeat (LRR) receptor kinase FLS2 (Gómez-Gómez & Boller, 2000; Zipfel *et al.*, 2004; Chinchilla *et al.*, 2006). A dose-response curve using apoplastic alkalinisation as readout shows that around 100 nM were required to elicit a significant response (**Fig. 4B**), which places BY-2 into the less responsive systems. For comparison, cell lines of *V. rupestris* produce a

## Discussion

---

half-maximal response at <5 nM of flg22, whereas, on the other hand, *V. vinifera* cv. ‘Pinot Noir’ needs >800 nM of flg22 for half-activation (Chang & Nick, 2012). Although BY-2 does not classify for being highly flg22 sensitive, flg22 is clearly sensed at much lower concentrations as compared to HrpZ, where >5  $\mu$ M are required to get half-maximal alkalisation (**Supp. Fig. 2**). The differential sensitivity of BY-2 to flg22 versus HrpZ recalls the situation in grapevine cells, where flg22 acts in the nM range, but Harpin requires concentrations that are several magnitudes higher to trigger a comparable response (Chang & Nick, 2012). Moreover, the apoplastic alkalisation in response to HrpZ occurs in BY-2 about 5–10 min later as compared to flg22 leading to a model, where the link between flg22 and alkalisation is more direct, whereas the link between Harpin and alkalisation is indirect. Again, this difference in timing is not confined to BY-2, but has also been observed in the grapevine system.

The low sensitivity to Harpin indicates that Harpin proteins are not perceived through a canonical protein receptor. For HrpZPsph from *Pseudomonas syringae*, cation-permeable pores have been reported (Lee *et al.*, 2001a). HrpZ is highly conserved in the *P. syringae* strains and, unlike the harpin HrpN of *Erwinia amylovora* which is an essential pathogenicity factor (Wei *et al.* 1992), seems to act as helper protein supporting type-III secretion. Instead of being translocated into the plant cell cytoplasm, HrpZ has been localised in the apoplast (Brown *et al.*, 2001). HrpZ can bind to phosphatidic acid, and upon insertion into vesicles prepared from plant plasma membranes, it can cause vesicle disruption (Haapalainen *et al.*, 2011, Lee *et al.*, 2001b). Despite this obviously different mode of perception, there seems to be some sort of specificity: When HrpZ proteins originating from two different pathovars of *P. syringae* were administered to *Arabidopsis thaliana*, both HrpZ types caused cell death, but the modulation of anionic currents was specific and in a phage display screen for peptide-binding different motif preferences were observed (Haapalainen *et al.*, 2012).

Thus, whereas the flg22 signal is transduced through the membrane by a conformational change of the FLS2 receptor triggering an intracellular kinase activity, the HrpZ signal acts at the membrane barrier itself, and is transduced by pore formation, i.e. by a localised loss of membrane integrity, which will directly impinge upon cortical actin: Actin is known to stabilise membrane integrity in a great number of systems (for review, see Koivusalo *et al.*, 2009; Papakonstanti *et al.*, 2000). Cortical actin is extremely close to the plasma membrane – life-cell imaging by TIRF-microscopy in BY-2 protoplasts expressing the GFP-FABD2 marker revealed that cortical actin filaments converge upon rod like canters that approach the membrane well into the range of the evanescent wave (~50 nm) generated by TIRF excitation and presumably tether actin with the membrane (Hohenberger *et al.*, 2011). A generation of membrane pores similar to that of HrpZ can be mimicked in tobacco BY-2 by high-voltage pulsed electrical fields of extremely short

duration, in the range of ns (Flickinger *et al.*, 2010). This pore formation can be suppressed in BY-2 cells when actin is stabilised by either phalloidin (Berghöfer *et al.*, 2009) or by inducible expression of the actin-bundling WLIM-domain (Hohenberger *et al.*, 2011) as monitored by uptake of the membrane impermeable dye Trypan Blue. Analogous to the observations with HrpZ reported in the current work, nanosecond electrical pulses make cortical actin detach rapidly, within a few minutes, from the plasma membrane, which is then followed by bundling of actin cables and contraction towards the nucleus (Berghöfer *et al.*, 2009). And similar to treatment with HrpZ, the remodelling of actin triggered by the electrical field is followed by cell death. Thus, the responses induced by HrpZ resemble, in both timing and cellular details, the responses that are triggered by pore formation through nanosecond pulsed electrical fields and represent, to our knowledge, the earliest event heralding ensuing cell death (as a final output of ETI-like defence).

Our observations integrate well into the accumulating body of evidence linking actin remodelling with programmed cell death across eukaryotic cells in general (for review, see Gurlay & Ayscough, 2005; Franklin-Tong & Gurlay, 2008), and plant cells in particular (Smertenko & Franklin-Tong, 2011). For instance, during the programmed cell death of the male gametophyte that has been investigated in the context of self-incompatibility in poppy, actin remodelling is necessary and sufficient to activate programmed cell death (Thomas *et al.*, 2006). A similar conclusion can be drawn from the programmed cell death of embryonic suspensors during the somatic embryogenesis of conifers. Here, actin remodelling is required for the embryo proper to become committed for embryogenesis (Smertenko *et al.*, 2003). Whether it is a stabilisation or a depolymerisation of the actin cytoskeleton that induces programmed cell death seems to depend on cell type (Gurlay & Ayscough, 2005) indicating that the dynamic equilibrium of actin filaments regulates apoptotic signalling.

The link between impaired membrane integrity by HrpZ-induced pore formation and actin remodelling might be provided by reactive oxygen species. Reactive oxygen species modulate a variety of plant responses, including hormone signalling, growth, development, cell cycle, and the responses to abiotic and biotic stress (for review, see Apel & Hirt, 2004). In particular, they participate in the signalling culminating in programmed cell death (for review, see Gechev *et al.*, 2006). For instance, reactive oxygen species are induced rapidly and transiently in poppy self incompatibility, and are sufficient to trigger both actin reorganisation and programmed cell death (Wilkins *et al.*, 2011). As second player of oxidative stress, nitric oxide has emerged. Similar to reactive oxygen species, it can cause a remodelling of actin filaments (Kasproicz *et al.*, 2009), and was also found to be active in the poppy system (Wilkins *et al.*, 2011).

The remodelling of actin in response to changes of redox potential probably dates back to the early stages of eukaryotic evolution, since it is observed in all eukaryotic kingdoms

(Franklin-Tong & Gourlay, 2008). For instance, the textbook example of sickle-cell anemia could be recently explained by actin remodelling as consequence of reduced oxygen affinity of the mutated hemoglobin, which impairs the actin-dependent penetration of the malaria pathogen (Cyrklaff *et al.*, 2011). The relevance of reactive oxygen species in the context of Harpin triggered defence responses is also emphasised by two findings in the grapevine cell system: when the NADPH oxidase as major source of apoplastic oxidative burst is blocked by diphenylene iodonium chloride (DPI) or when apoplastic hydrogen peroxide is scavenged by addition of catalase, this impairs the induction of stilbene synthase, a key player for grapevine phytoalexin synthesis (Chang *et al.*, 2011). When the same system is challenged by either flg22 or Harpin, the accumulation of the active phytoalexins resveratrol (*trans*-3, 4', 5-trihydroxystilbene) and its oxidative highly toxic derivative - viniferin correlated with an early and strong oxidative burst (preceding even apoplastic alkalinisation) which could be observed for elicitation with Harpin, but not flg22 (Chang *et al.*, 2012).

Why should pore formation by HrpZ lead to an oxidative burst in the apoplast? Formation of pores will not only expose lipids to peroxidation by membrane-associated enzymes, but also alter the interaction of actin with the membrane and thus its dynamics. Changes in actin dynamics, in turn, have been recently shown to activate the NADPH oxidase generating an apoplastic burst (Liu *et al.*, 2012). The functional link might be provided by the membrane-associated phospholipase D that is not only activated upon mechanic perturbation of the plasma membrane (for review, see Munnik & Vermeer, 2010), but also recently has been shown to activate NADPH oxidase (Guo *et al.*, 2012). Interestingly, phosphatidic acid, the most active product of phospholipase D, can be bound by HrpZ (Haapalainen *et al.*, 2011), which would open the possibility of quelling defence signalling activated by oxidative burst. Actin and apoplastic oxidative burst seem to establish a self-amplifying circuit that should be able to transform even a minor disturbance of membrane integrity into a clear and robust output consisting in a peak of reactive oxygen species.

Compared to actin, the response of microtubules seems to be more indirect. Even at the time, when the actin cytoskeleton is breaking down in response to HrpZ, cortical microtubules, although disturbed in their orientation, still maintain a certain degree of integrity (**Fig. 3B**). Since plant microtubules have been recently shown to respond to oxidative disbalance (Livanos *et al.*, 2012), they might simply respond to the actin-dependent oxidative burst caused by pore formation. Microtubules modulate deformation-sensitive calcium channels (Ding & Pickard, 1993; Mazars *et al.*, 1997). Antimicrotubular compounds are therefore expected to modulate the activity of calcium channels and thus apoplastic alkalinisation. The delayed apoplastic alkalinisation in response to HrpZ as compared to that triggered by flg22 might be caused by the time span



required for the reactive oxygen species to disassemble the microtubules gating the calcium channel. It should be mentioned that the same temporal pattern has been observed in the direct comparison of flg22- versus Harpin-triggered alkalisation in the grapevine cell system (Chang *et al.*, 2012). In the grapevine system, pharmacological manipulation of microtubules could activate defence genes in the absence of a Harpin elicitor: Resveratrol synthase and stilbene synthase, as key genes of phytoalexin induction in grapevine, were induced by Oryzalin and Taxol, indicating a function of microtubules upstream of gene induction (Qiao *et al.*, 2010). Interestingly, Latrunculin B and Phalloidin were less effective, consistent with a more indirect mode of interaction.

This study arrives at a (speculative, but testable) model, where a dynamic population of cortical actin acts as a sensor for membrane damage and in response to HrpZ (or the membrane pores produced by HrpZ) triggers an oxidative burst that on the one hand causes bundling of actin followed by a contraction of actin cables towards the nucleus, on the other hand initiates a chain of event that culminates in cell death. In contrast, flg22 produces only a subtle cytoskeletal response, which might be related to the slower and weaker oxidative burst induced by flg22 as compared to Harpin elicitors (Chang & Nick, 2012). Apoplastic alkalisation, however, seems to be more closely linked with flg22 as compared to Harpin elicitors. Thus, although both elicitors are generating an oxidative burst and an apoplastic alkalisation, the temporal signature differs. The response of submembraneous actin might be responsible for the generation of this temporal signature. The role of the cortical cytoskeleton might therefore be best described as a kind of signature decoder leading to different outputs (cell death versus basal immunity).

## **4.2 A new tool to understand the role of cytoskeleton in biotic/abiotic defence**

Fluorescently tagged cytoskeletal transgenic marker lines have been generated for Arabidopsis (Kost *et al.*, 1998; Voigt *et al.*, 2004), rice (Frey *et al.*, 2009), and tobacco BY-2 cells (Sano *et al.*, 2005; Hasezawa *et al.*, 1997) and were useful to analyse cytoskeleton functions in virus movement, stomatal closure, motility of plant organelles and auxin transport, as well as for resistance to biotic and abiotic stress factors (Hofmann *et al.*, 2009; Zhao *et al.*, 2011; Holweg, 2007; Ruggenthaler *et al.*, 2008).

For grapevine, these tools have not been available, so far. Such tools would be highly desirable, however: Viticulture can only be conducted using intense protection by fungicides. For instance, fungicides are applied at an average rate of 19.5 kilograms per hectare throughout the E.U. with twelve to fifteen applications in each season (Gianessi & Williams, 2011). Defence against

pathogens is the central topic for sustainable viticulture. As discussed in the introduction, the cytoskeleton is central for plant defence, which has also been shown for grapevine cells (Chang *et al.*, 2011; Qiao *et al.*, 2010). To investigate the early responses of the cytoskeleton in decoding the stress signal and the subsequent reorganisation of the cytoskeleton is vital. This was to motivation to establish a fluorescent protein tagged cytoskeleton marker line in grapevine.

*Vitis vinifera* 'Chardonnay', *Vitis vinifera* 'Müller-Thurgau', and a root stock S04 (a commercial root stock from crosses with *Vitis berlandieri*) were utilized to establish transgenic plants expressing GFP-AtFABD2 and GFP-AtTUB6 via somatic embryogenesis, respectively. This approach has been successful for the AF marker line in using embryogenic suspension cells of *Vitis vinifera* cv 'Chardonnay'. However, the success rate was low: As mentioned, from 40 plantlets expressing *GFP-AtFABD2*, and 24 plantlets expressing *GFP-AtTUB6* that could be successfully regenerated, so far only one line could be obtained that reliably reports AFs and preserves a normal physiology. All successful regenerations were from the embryogenic suspension line of *Vitis vinifera* 'Chardonnay' (regenerants were neither obtained from *Vitis vinifera* 'Müller-Thurgau' nor from root stock S04). In the ~60 regenerated lines, the regeneration progress lasted at least 12 months, which is much longer comparing to previous work using other constructs that have no relation with the cytoskeleton. This indicates impaired functionality probably due to the overexpression of the marker that interferes with cytoskeletal function, giving rise to vital affects in cell development and plant morphogenesis (Giddings & Staehelin, 1991; Burgos-Rivera *et al.*, 2008; Deeks *et al.*, 2007). Other factors, such as somatoclonal variation (Schellenbaum *et al.*, 2008), histone modifications, DNA methylation and small RNA-directed DNA methylation can modulate somatic embryogenesis as well (for review, see Miguel & Marum, 2011), but these also occur in non-cytoskeletal transgenes, suggesting that marker visibility and the avoidance of cytoskeletal aberrations due to elevated expression of the marker have to reconciled in a subtle balance, which is achieved only in few of the transformed lines.

Although the FABD2-marker is generally discussed as non-invasive, it has a subtle effect on actin dynamics and cellular processes that depend on actin. Similar to the mouse-talin marker (Ketelaar *et al.*, 2004) it binds to the surface of actin at a site, where normally actin-depolymerizing factors would attach resulting in a reduced dynamics of actin. These changes of actin dynamics are minor in case of the FABD2-marker, but by sensitive assays they are detectable. For instance, there is a significant alteration of polar auxin transport observed in Arabidopsis lines expressing this marker (Holweg, 2007), and protoplasts from tobacco BY-2 cells expressing this marker show aberrations of cell polarity that can be mimicked by genetic or pharmacological stabilisation of actin (Zaban *et al.*, 2013). The specific venation phenotype in line 10a (partial fasciation, steeper angle of the

peripheral main veins) is indicative of accelerated polar auxin transport, which would be expected from a slightly elevated stability of actin filaments due to expression of this marker.

Also for the tubulin marker, impaired cytoskeletal function is likely the cause of the impaired regeneration and viability. Even slightly elevated levels of tubulin produce sublethal aberrations of numerous cellular functions. The few marker lines available for plants are usually based on expression of deviating tubulin isotypes that are integrated only to a small extent (for review, see Breviario & Nick, 2000). Overexpression of tubulin might also lead to silencing of endogenous tubulin leading to dominant-negative shut-down of the entire microtubular cytoskeleton. As a novel strategy to circumvent this drawback, we have therefore transformed with a different construct improved featuring with double terminators, aiming at to reduce the possible influence raised from the RNA silencing which can be induced by highly transcribed transgenes through a pathway dependent on RNA-DEPENDENT RNA POLYMERASE6 (RDR6) (Luo & Chen, 2007). This time embryo suspension cultures of root stock 110 Richter (a commercial root stock from *Vitis Berlandieri* crosses), and again *Vitis vinifera* 'Chardonnay' were used as candidates for transformation. So far (after 18 months from onset of transformation), some leaf-like structures have formed, but not yet plantlets.

Therefore, as fall-back strategy, suspension cell lines of *V. rupestris* expressing *GFP-AtTUB6* have been established successfully. Although this does not allow to test interaction with pathogens under natural conditions, this provides a useful tool for *in vivo* studies where the signalling of biotic or abiotic stress factors to MTs can be dissected.

### 4.3 The Actin Guard Cell Gatekeeper model

Plants are exposed to massive environment impacts, including infections by numerous pathogens. Cormophytic land plants have developed a water-impermeable cuticle as prerequisite for terrestrial life. This means that pathogens have to use openings in this cuticle, such as stomata, hydathodes, or lenticels, or they have to use specific feeding insects as vectors.

The cuticle is very efficient as structural barrier, but plants have to perforate this barrier to ensure the gas exchange necessary for photosynthesis by the stomata (Thordal-Christensen, 2003). It is therefore no surprise that numerous pathogens use the stomata as gateway for infection. Stomatal aperture is strictly regulated, which is important to balance the need for photosynthetic flow of gases with the need to reduce water loss by transpiration (Brodribb & Jordan, 2008). Therefore, guard cells can sense their environment and integrate this sensing into complex intracellular signalling (Kim *et al.*, 2010). This complex signalling network provides numerous targets for pathogen effectors directed to keep the stomata open in order to facilitate penetration. Stomatal

aperture and closure are mediated by ion fluxes driving consequent osmotic fluxes of water. Although AFs do not mediate the aperture and closure itself, they play an important role for the regulation of these fluxes, for instance by regulation of ion channels (Lee *et al.*, 1999) or by regulating dynamic changes of membrane material required to sustain membrane in plant cells integrity (Liu *et al.*, 2013). The signals upstream of AFs that are induced by factors such as ABA, elicitors, drought or salinity, might be the activation of ROS and NO, stimulating the MAPK pathway (Allègre *et al.*, 2009; Neill *et al.*, 2008). Numerous studies have demonstrated that both internal (e.g. hormones, Ca<sup>2+</sup>) and external (e.g. light, CO<sub>2</sub>, bacterial pathogens) stimuli modify the AFs in guard cells and that these changes correlate with opening and closing (Lucas *et al.*, 2006): in closed stomata, AFs are randomly oriented; in opened stomata, AFs are arranged in radial arrays or hoop- and ring- like structures (Wang *et al.*, 2011). The underlying mechanisms of stomatal AF reorganization are not known - there exist numerous possibilities such as elongation and shortening, buckling and straightening, bundling and branching, the activities possibly done by actin depolymerizing factors (Michelot *et al.*, 2007; Staiger *et al.*, 2010). Besides, AFs can form longer filaments by end-joining activity differing from the model of traditional treadmill (Smertenko *et al.*, 2010; Wang *et al.*, 2011). To discriminate between these possible events that can also act in combination is far from trivial, since the configuration of AFs is extremely complex, which obscurs any response that is not really drastical – usually observed only in non-physiological situations. To detect the more subtle responses characteristic for the physiological range, quantitative approaches are required. This has been a challenge for the complex actin cytoskeleton.

Higaki *et al.* (2010) established a methodology for quantitative image analysis using semiautomatic quantification and clustering of cytoskeletal structures. This framework allows to quantify cytoskeletal orientation, bundling and density by measurement of indicative parameters (skewness of the intensity distribution of cytoskeletal pixels as an indicator for cytoskeleton bundling; occupancy of the GFP signal to estimate cytoskeletal density) from microscopic images. Using this approach, the AF remodelling in *Arabidopsis* guard cells could be shown to undergo radial reorientation and transient bundling during diurnal stomatal aperture.

Based on this phenomenological framework it is then possible to make prediction on the underlying molecular events: for instance, dynamic remodelling of actin could be achieved by the cooperation of Arp2/3 complex, formins, ADFs, villins, AIP1 and CAP, but alternatively, long filaments can be severed into small fragments, which can form longer filaments by end-joining activities, which is a more rapid process (Michelot *et al.*, 2007; Staiger *et al.*, 2010). Thus, if the velocity of remodelling can be followed, it is possible to decide which of these two mechanisms is at work. It is relevant to identify these mechanisms, because the stomatal actin cytoskeleton

represents an important target for pathogen effectors. For instance, *Pseudomonas syringae* pv. tomato produces a toxin, coronatine, that stimulates the rapid opening of the stomata, facilitating pathogen entry, which requires dynamic remodelling of AFs.

These considerations brought us to have a closer look on the behaviour of AFs during pathogen attack. In our previous studies (Guan *et al.*, 2013; Qiao *et al.*, 2010) reorganization of AFs (bundling and disruption) were observed upon elicitation with Harpin in BY-2 and *Vitis* suspension cells as models. This prompted us to test whether the pathogen generating, Harpin, the phytopathogenic bacterium *E. amylovora* can cause a similar actin response in guard cells and whether this response is specific for guard cells? If so, HrpZ would be a real bacterial effector in *sensu strictu*. To increase the resolution of our analysis, we used quantitative image analysis of actin organization as strategy (Higaki *et al.*, 2010), which had already been used successfully to demonstrate that changes in density and bundling of the filaments into higher-order structures (rather than simple AFs disassembly) regulate guard cell shape changes. The analysis of skewness (measuring the extent of bundling of AFs) suggested that AFs showed a specific response in guard cells for inoculation with both *Agrobacteria* and *Emylovora*, but also revealed that different mechanisms must be at work.

For inoculation with *E. amylovora*, AFs in guard cells disrupted into fragments but did not change their bundling state (**Fig. 3.9**). This phenomenon was in good agreement with the data on the effect of HrpZ in the AF marker line in BY-2 (**Fig. 3.2**). This response was specific for the guard cells and not observed in the epidermal pavement cells. In contrast, inoculation with *A. vitis* and *A. tumefaciens* EHA105 detached actin cables in the guard cells by about the half reduced skewness values to 40% and 46% of the control, respectively. Again, there was no significant response of AFs in epidermal pavement cells.

From these data, two (speculative) conclusions can be drawn on the molecular mechanism: *E. amylovora* triggers the severing of actin bundles, but this is not followed by the next step of natural actin remodelling, the annealing of fragments to new actin cables such that actin is disrupted and stomatal closure suppressed. In contrast, the two *Agrobacteria* species trigger a detachment of actin bundles into finer strands, which is more likely caused by changes in the activity of nucleation regulators such as Arp2/3 and ADFs. Nevertheless, the reduction in bundling, should lead to the same outcome, suppression of stomatal closure. However, one should bear in mind that *Agrobacteria* do not use this route of infection in nature – they enter through the root system, in contrast to *E. amylovora* that infects the upper parts of the plants.

Although the pathogens trigger different types of actin responses in the guard cells, the response is confined to the guard cells and not observed in epidermal pavement cells, although the

pathogens were in contact with those cells as well. This is probably linked with the specific actin organisation of guard cells, where actin, due to its function in stomatal closure, differs in structure and probably decoration with actin-associated proteins.

If the specificity of actin responses in the guard cells are not caused by the specificity of pathogen effectors, but are innate to actin itself, they should be triggered by completely different pathogens as well. With respect to practical relevance, Downy Mildew (*Plasmopara viticola*), an oomycete and as eukaryotic organism not related with phytopathogenic bacteria was chosen.

In case of the phytopathogenic bacteria, tagging by red fluorescent proteins (dTomato) was useful to detect the sites of pathogen attachment. Due to its biotrophic lifestyle, transformation of *P. viticola* has not been successful so far. We had therefore to develop fluorescent staining techniques to observe infection structures of *P. viticola* on and in leaf tissues of grapevine plants expressing *GFP-AtFABD2*. Since oomycetes are related to algae, their cell walls contain mostly cellulose with additional  $\beta$ -1, 3-glucan polymers (Bartnicki-Garcia, 1968). Due to the attachment of the zoospores at the guard cells regenerate a cellulosic wall, the Calcofluor white M2R first reported as a dye useful for viewing cell walls of fungi and bacteria can be used, since, it binds to cell walls that are composed of chitin, cellulose or other  $\beta$ -1,4-linked carbohydrates (Darken, 1961; Maeda & Ishida, 1967). Solophenyl Flavine 7GFE 500 is not toxic to cells, but show a more durable of their fluorescence as compared to Calcofluor white M2R. It was not reported for wall components of higher plants, algae, bacteria. The improvements of staining techniques lead to high resolution and contrast between parasite structures and host-plant tissues (Hoch *et al.*, 2005).

Perfluorodecalin (PFD, C<sub>10</sub>F<sub>18</sub>) is a fluorocarbon, a derivative of decalin in which all of the hydrogen atoms are replaced by fluorine atoms. It is chemically and biologically inert, and stable up to 400 °C. Several applications make use of its ability to dissolve gases, for instance to dissolve large amounts of oxygen (100 ml of PFD at 25 °C will dissolve 49 ml of oxygen), and it is also studied for use in liquid breathing (Tawfic & Kausalya, 2011), bone regeneration (Tamimi *et al.*, 2013), and corneal toxicity (Wilbanks *et al.*, 1996). *In-vivo* imaging of leaves is impaired by airspaces in the spongy mesophyll subtending the lower epidermis of leaves. These airspaces may be several cell layers in depth causing heavy reflection in the mesophyll, strong attenuation of excitation light and total reflection of emission intensity. These aberrations impair confocal image quality. We therefore successfully used PFD (Littlejohn *et al.*, 2010) to improve the resolution of confocal imaging in grapevine leaves.

Based on these methodological advances we were able to study for the first time the response of AFs to infection with *P. viticola in vivo*. Similar to the case of *E. amylovora*, we observed

disruption of AFs in guard cells, suggesting a common molecular mechanism. There was, however, a decisive difference: Upon infection with *P. viticola* AFs rearranged into a perinuclear actin basket in epidermal pavement cells although they had not directly been in contact with the zoospores.

In the leaves of *V. vinifera* cv. 'Marselan' infected by *P. viticola*, stomata remained open in darkness and during water stress; however, can be induced to close by ABA; moreover, in excised infected leaves stomatal closure could not be induced by a water deficit or ABA treatment. To be mentioned, such *P. v.* induced stomatal lock-open was restricted to the colonized area, and no relation to mechanical forces resulting from the presence of the pathogen in the substomatal cavity (Allègre *et al.*, 2007). However, is there a reduction of the back-pressure exerted by epidermal cells?

Although the different mechanisms depending on AFs activities and the different roles AFs played among mammalian cells, plant cells, and fungi cells, the formation of AF perinuclear actin basket has been reported in each field. In the study of localization of F-actin in lens epithelial cells on bovine and human posterior capsules, the perinuclear basket of F-actin was found in cells away from the leading edge, whereas the AF in leading edge are thin and polarised along the length of the cells (Saxby *et al.*, 1998). Since the proliferative activity of the cells was greatest at or near the leading edge, the formation of AF perinuclear basket may indicate less cell activities. In human breast adenocarcinoma cells treated with taxol (a drug promoting tubulin assemble), AF perinuclear actin basket can be related to apoptosis, through indirect role of the taxoids on the microfilament network (Rosenblum & Shivers, 2000). Such MT and AF perinuclear actin basket connection was also reported in plant cells. In BY-2 cells overexpressing rice Kinesins containing a calponin homology domain (OsKCH1), the perinuclear actin basket were anchored to MTs that extend to the cell cortex by the static tobacco BY-2 cell KCH fraction at the nuclear periphery (Klotz & Nick, 2012). In fungi cells, perinuclear F-actin rings formed in *Cryptococcus neoformans* under treatment of microtubule inhibitor Nocodazole, which may be involved in the central positioning of yeast nucleus suspended and in nuclear movement. It may also be a temporary storage deposit of F-actin in slowly proliferating, resting or stressed cells (Kopecká *et al.*, 2012). Evidences from its counterpart plant are under treatment with cytochalasin D and cold stress. The rice mutant Yin-Yang, selected during a screen for resistance to cytoskeletal drugs and is highly sensitive to cytochalasin D for cell elongation, where the AFs bundles disintegrate partially and are replaced by a network of short AFs surrounding the nucleus in response to cytochalasin D (Wang & Nick, 1998). Basket-like structures around the nucleus were found as well in the perinuclear region shortly (5 min) after exposed cells to 25 °C from 0 °C in tobacco cells (Pokorná *et al.*, 2004).

Altogether, we proposed the guard cell gatekeeper role, where the AFs dynamic differs and priorities than in the epidermal cells in plant defense responses.

### 4.4 Formation of macrotubules in response to osmotic stress

As early as 1970s', a model on macrotubules formation was proposed based on pharmacological studies in plant. The MTs end split into protofilament pairs after treatment with  $10^{-4}$  vinblastine sulphate (VLB), following by longitudinal compacting of protofilament pairs into macrotubule. VLB can induce paracrystals which is the result of the lateral aggregation of macrotubules. Because the paracrystals and MTs both bind to colchicine, this high binding affinity for the same antibody probably indicate the macrotubules consist of microtubule protein (Warfield & Bouck, 1974). In regard to the formation of macrotubule, other evidences by immunolabel method are from the hyperosmotic stress where the MTs disappear, and soon replaced by massive bundles macrotubule. The macrotubules play roles in the regulatory mechanism of plasmolyzed protoplast volume in the root-tip cells of *Triticum turgidum* (Komis *et al.*, 2002).

In our present study, macrotubules were observed to form upon the treatment with ( $\pm$ )-JA, NaCl or PEG 6000 for three days. The progress in forming macrotubules can be followed within 32 min under the challenge with NaCl 200 mM.

PLD was considered to regulate the interaction between the plasma membrane and the cytoskeleton (for review, see Nick, 2013). Tubulin binds PA with a high affinity by a 90-kDa PLD $\delta$  isoform associated with MTs (Dhonukshe *et al.*, 2013). Under osmotic, the membrane will be deformed, which might render membrane lipids more accessible to PLD; on the other hand, the MTs will be unstable triggering by the detaching of SPR1 (Wang *et al.*, 2011), and MTs can be recovered from macrotubules when PLD inhibitor was removed. This provides a mechanism to transduce mechanical load on the membrane into changes of cytoskeletal dynamics.

The formation of macrotubules was reported by different agents. For instance, in crayfish nerve cords, volatile anaesthetic halothane was used as stimulation; on the contrary, glycerol pretreatment blocks macrotubule formation (Hinkley *et al.*, 1978). Moreover, low temperatures, colchicine, vinblastine, digitonin, hyaluronidase, isopropyl N-phenyl carbamate, and volatile anaesthetics; however, none of these agents routinely induces macotubules in all systems, moreover the promotion of macrotubule formation probably differs. It can happen by altering the confirmation of either MT subunits or MAPs; or it can affect the MTs environment (Hinkley *et al.*, 1978; Komis *et al.*, 2006). Among reports, the induced tubular structures were within arrangement of 30-60 nm in diameter (Warfield & Bouck, 1974; Komis *et al.*, 2002). So far, the triggering of macrotubules and their exactly formation progress are still open for speculation.



In the present study, antagonistic effects of IAA are observed on its rearrangement of microtubules that triggered by ( $\pm$ )-JA; however, this reformation of MTs cannot be found on the microtubules triggered by HrpZ.

This drove us to compare on the formation of the MTs disruption (then the formation of microtubules) caused by JA and HrpZ. Evidences can be shown as the JA-Me caused closing of *Avena* stomata, and inhibited opening of mimosa pulvinus (Zeiger, 1983). Abe *et al.* (1990) reported that JA could disrupt cortical MTs by inhibiting the efflux of protons in tobacco cultured cell. Since appropriate pH is required for polymerization of MTs, lower cytosolic pH caused by JA can promote de-polymerization of microtubules. The evidence from molecular level involved in MTs-microtubule formation can be the gene of *MARNERAL SYNTHASE (MRNI)*. *MRNI* is an oxidosqualene cyclase that produces the triterpene marneral, is highly upregulated when microtubule dynamics are disrupted in Arabidopsis. During methyl jasmonate induction, *MRNI* was expressed, suggesting the JA pathway is transcriptionally regulated through *MRNI*. It is interesting that both JA and osmotic stress can cause formation of microtubule (Johnson, 2012). Ismail *et al.* (2012) has demonstrated that the readout of salt stress signalling pathway is modulated by a parallel signal chain triggered by biotic factors downstream of jasmonate signalling. An activation of a calcium influx channel (monitored by apoplastic alkalination), could be triggered during biotic defense, can also be detected in salt stress (a marker for salt adaptation  $\text{Na}^+/\text{H}^+$ ) signaling. And the exogenous JA can rescue growth in the salt-sensitive cell line.

MTs can maintain transverse orientation under conditions favorable for elongation; otherwise will switch to longitudinal orientation. The IAA induced MTs reorientation has been studied widely. Cortical MTs oriented themselves transversely to the cell axis in maize coleoptiles by IAA inducing (Bergfeld *et al.*, 1988); however, induced by IAA in azuki bean epicotyls, the cortical MTs orientation does not alter (Katsumi *et al.*, 1989). Further evidence proposed IAA caused predominance of transverse MTs in cells possess a factor identical to a GA3-induced newly synthesized mRNA (Kancta *et al.*, 1993; for review, see Shibaoka, 1994). In the present study, cells exposed on IAA with concentration from 0.1 to 100  $\mu\text{M}$ , the structures of both cortical and central MTs didn't change dramatically; however, the dots in nucleus differed a lot. In the optimized concentration of IAA for cell elongation, the dots in nuclei disappeared dramatically. The explanation for the IAA induced MTs reorientation or the changes of number of MTs dots in nuclei may provide by studies on molecular level.

Concerning the MTs speckles in nuclei, one of the reports is from tobacco BY-2 cell after cold-induction where gradual tubulin accumulation was in a progressively growing proportion in interphase nuclei (Schwarzerová *et al.*, 2006). Interestingly, new MTs rapidly emerged from the

nuclear periphery and reconstituted new cortical arrays happened under rewarming. The requirement of MTs permeable to nuclear membrane is exist in species with closed mitosis, since their nuclear division takes place within an intact nuclear envelope (Heath, 1980). In higher plant, there is a so called MT-organizing centre, where  $\gamma$ -tubulin acts as a minus-end nucleator during microtubule assembling. Binarov *et al.* (2000) demonstrated the  $\gamma$ -tubulin can be transported through the intact nuclear envelope. Moreover, the nuclear pore complexes (NPC) that create passageways by forming aqueous channels through the nuclear envelope to connect the cytoplasm and the nucleoplasm. The macromolecules with a supper size limit of ~50 kDa are able to diffuse through the NPC; the macromolecules with larger size require specific interaction either with the NPC, e.g. the nuclear-export signal (NESs) or by an intermediary carrier. Highly conserved putative nuclear-export sequences were identified in tubulin sequences (Schwarzerov *et al.*, 2006) where tubulin was not present in the form of microtubules, but as nonassembled tubulin heterodimers. There are hypothesises, the transgenic cells expressing GFP-  $\beta$ TUB6 are somehow have a positive influence on cell growth (**Fig. 3.14A**), due to the delay of the dividing progress (**Fig. 3.14B**), upon IAA treatment, MTs are required abundantly to act their role for cell elongation; therefore such dots structures of MTs in nuclei might dissemble into free tubulin dimers, which pass thought the NPC by combining to certain receptor/carrier that can that can recognize NESs in either  $\alpha$ - or  $\beta$ - tubulin.

The classical relationship of JA and IAA is considered as antagonists, since JA is a well-characterized inhibitor of plant growth mainly involved in plant defence and developmental processes; in contrast, IAA is one of the growth promoters. However, they both have crosstalk as well to control plant responses and development (for review, see Hoffmann *et al.*, 2011). JA and IAA signalling pathway both share mechanism using ubiquitin-26S proteasome system. The hormone-governed gene activation is selectively expressed via the degradation of repressor proteins (for auxin signalling the Aux/IAA; for JA signalling the JAZ). Another cross-talk on early transduction is to share response factors during cytokinin and ethylene signaling, leading to cross talk or auxin and JA compete for AXR1 such that different complexes are recruited for the proteasome (Tiryaki & Staswick, 2002). Thus, activation of the IAA pathway by addition of IAA will recruit AXR1 such that AXR1 is not available for JA signalling, providing an environment for macrotubules recovered to MTs. Auxin Response Factor ARF6 and ARF8, DNA-binding transcription factors, can regulat a set of target JA biosynthesis genes during flower development. Moreover, the indirect across talk, such as spatiotemporally controlled in the developmental and environmental context. The jasmonate-mediated induction of auxin efflux and influx carriers, for instance, *PIN2* has been reported to proceed in an SCFCO11-dependent manner but through interaction with the auxin pathway for inhibits *PIN2* endocytosis (Sun *et al.*, 2011). In the case of HrpZ, as already discussed, it play roles as a helper protein in TypeIII secretion system, localizing

in apoplast, binding to phosphatidic acid cause vesicle disruption, and causing cation-permeable pores. To be mentioned as shown in **Suppl. Fig. 9** the mortality rate was as low as control after JA 500  $\mu\text{M}$  treatment, whereas, reached to around 90% after HrpZ 1.7  $\mu\text{M}$  treatment for three days. So such high mortality can be one of the reasons to explain the failing of IAA rescues, since such damage of phosphatidic acid binding exaggerate the damage in downstream PLD regulation of MTs dynamic.

As parallel, we tested the MTs response to various bacterial infections in MTs marker line of *Vitis* suspension cells. The MTs in the suspension cell line revealed with different behaviours after cocultivation with different bacteria. The variation of MTs reorganization between *Erwinia* and *Agrobacteria* may be due to their different infection mechanisms. *E. amylovora*, shown in 1878 to be associated with fire blight of apples and pears in Illinois and New York, USA, nowadays spreads throughout much of the temperate world (Burrill, 1878). The type III secretion system was utilized in *E. amylovora* infection. HrpN, a conserved effector in *E. Amylovora* belonging to Harpin family, is a subset of Type III secretion system. The needle-like structure is used as a sensory probe to detect the presence of plant organisms and to secrete proteins that help the bacteria to infect host, allowing proteins to secrete directly from the bacterial cell into the plant cell (Wei *et al.*, 1992).

During *A. tumefaciens* infection, the delivery of T-complex (made up of nucleoprotein) into the plant cell cytoplasm requires a specific export system that across both the bacterial envelope and the plant cell membrane (Howard & Citovsky, 1990). T-complex export occurs via a type IV secretion system, comprising of a filamentous pilus and a transporter (Salmond, 1994; Tzfira & Citovsky, 2000).

The mechanism for *E. coli* binding to plant surfaces may have more than one. The formation of curl that is long, thin, aggregative amyloid fibers made by many pathogenic strains of *E. coli* in the interaction mechanism was reported (Jeter & Matthysse, 2005; Chapman *et al.*, 2002). To be mentioned most laboratory strains of *E. coli* do not make curli.

## 4.5 Conclusion

Consistent with the results from tobacco BY-2 cells, strong and rapid cytoskeletal responses to HrpZ were observed, contrasting with very mild changes triggered by flg22. However, extending previous results by spinning-disc confocal microscopy and life-cell imaging, it is now shown that these responses initiate early and proceed in parallel with extracellular alkalinisation (so far, one of the most rapid readouts for defence). This shows that cytoskeletal remodeling might channel early signaling between HrpZ-triggered ETI-like defence and flg22-triggered PTI.

The formation of macrotubules triggered by JA, but not HrpZ could be rescued by addition of IAA, which were probably caused by the permanent damage of MTs dynamic in case of HrpZ. Moreover, MTs nuclei location and perinuclear AFs basket formation confirmed responses known from other plants. Comparing the AFs in guard cells and epidermal cells after inoculation of various bacteria and *P. viticola*, we proposed the stomata gatekeeper mechanism prior to epidermal cells. Together with the alternated arrangements of AFs in epidermal cells under *P. viticola* inoculation, but not by bacterial inoculation, raise a speculation that epidermal cells play roles differing than guard cells on sensing *P. viticola*.

### 4.6 Outlook

Future work will be directed to understand the relation between actin bundling and cell death. This link is expected to involve specific reprogramming of gene expression (Chang *et al.*, 2011). Remodeling of cortical actin in response to nanosecond electrical fields was observed to directly alter nuclear morphology (Berghöfer *et al.*, 2009), which can be easily explained by the tethering of the nucleus to actin and microtubules (Klotz & Nick, 2012). The role of actin in chromatin structure has been established in both yeast and mammalian cells (Pederson & Aebi, 2005) and could be meanwhile also confirmed in plant cells (Kandasamy *et al.*, 2010). It will therefore be interesting to test the impact of actin-dependent nuclear tension on the cellular response to pore-forming agents.

Since cortical cytoskeleton is involved in sensing and transduction of the early signals, to understanding their roles in decoding the temporal signature of defence activating different outputs (cell death versus basal immunity) is needed for further examining.

Several biotic and abiotic stresses were tested in this work. Some of the remodelling of AFs and MTs could be followed *in vivo* over time. However, the complex and delicate regulations in molecular level are still partially understood, for instance, the formation of macrotubules, the nuclei MTs, and the different output of MTs for treatments of JA-IAA and HrpZ-IAA. Future work will be interesting to focus on some of the stresses to reveal the molecular mechanisms.

## Acknowledgements

This work was supported by BACCHUS Interreg project; and a fellowship of the Chinese Scholarship Council (CSC) to Xin Guan. Kateřina Schwarzerová, Hashimoto-lab, Prague, Czech was acknowledged for providing Plasmid pBI121-GFP-*AtTUB6*. We would like to thank Dr. Günther Buchholz (RLP AgroScience/AIPlanta – Institute for Plant Research, Neustadt an der Weinstraße, Germany) for constructive advices through the whole progress, and critical reading; Dr. Yubin Kashef (Zoology Institute cell and developmental biology, Karlsruhe Institute of Technology, Karlsruhe) for training and support in spinning disc confocal microscopy; Thorsten Manthey and Mario Braun (RLP AgroScience/AIPlanta – Institute for Plant Research, Neustadt an der Weinstraße, Germany) for training and support in transformation and Laser scanning microscope (ZEISS LSM 510); Dr. Michael Riemann for helpful advices; Sabine Purper for technical support with the cell lines; Joachim Daumann for taking care of the transgenic plants in greenhouse. Use of the laboratory at RLP AgroScience/AIPlanta is gratefully acknowledged.

## References

- Abdrakhamanova, A., Wang, Q. Y., Khokhlova, L. & Nick, P. (2003).** Is microtubule disassembly a trigger for cold acclimation? *Plant Cell Physiol* **44**, 676–686.
- Abe, M., Shibaoka, H., Yamane, H. & Takahashi, N. (1990).** Cell cycle-dependent disruption of microtubules by methyl jasconate in tobacco BY-2 cells. *Protoplasma* **156**, 1–8.
- Akhmanova, A. & Steinmetz, M. O. (2008).** Tracking the ends: a dynamic protein network controls the fate of microtubule tips. *Nat Rev Mol Cell Biol* **9**, 309–322.
- Allègre, M., Daire, X., Hédouir, M. C., Trouvelot, S., Mercier, L., Adrian, M. & Pugin, A. (2007).** Stomatal deregulation in *Plasmopara viticola*-infected grapevine leaves. *New Phytol* **173**, 832–840.
- Allègre, M., Hédouir, M. C., Trouvelot, S., Daire, X., Pugin, A., Wendehenne, D. & Adrian, M. (2009).** Are grapevine stomata involved in the elicitor-induced protection against Downy Mildew? *Mol Plant Microbe Interact* **22**, 977–986.
- Apel, K. & Hirt, H. (2004).** Reactive oxygen species: metabolism, oxidative stress, and signal transduction. *Annu Rev Plant Biol* **55**, 373–399.
- Ascencio-Ibanez, J. T., Sozzani, R., Lee, T. J., Chu, T. M., Wolfinger, R. D., Cella, R. & Hanley-Bowdoin, L. (2008).** Global analysis of Arabidopsis gene expression uncovers a complex array of changes impacting pathogen response and cell cycle during geminivirus infection. *Plant Physiol* **148**, 436–454.
- Aslam, S. N., Erbs, G., Morrissey, K. L., Newman, M. A., Chinchilla, D., Boller, T., Molinaro, A., Jackson, R. W. & Cooper, R. M. (2009).** Microbe-associated molecular pattern (MAMP) signatures, synergy, size and charge: influences on perception or mobility and host defence responses. *Mol Plant Pathol* **10**, 375–387.
- Baluška, F., Šamaj, J., Wojtaszek, P., Volkmann, D. & Menzel, D. (2003).** Cytoskeleton-plasma membrane-cell wall continuum in plants. Emerging links revisited. *Plant Physiol.*, **133**, 482–491.
- Barrero, R. A., Umeda, M., Yamamura, S. & Uchimiya, H. (2002).** Arabidopsis CAP regulates the actin cytoskeleton necessary for plant cell elongation and division. *Plant Cell* **14**, 149–163.
- Bartnicki-Garcia, S. (1968).** Cell wall chemistry, morphogenesis and taxonomy of fungi. *Annu Rev Microbiol* **22**, 87–108.
- Baskin, T. I., & Cande, W. Z. (1990).** The structure and function of the mitotic spindle in flowering plants.

---

*Annu. Rev. Plant Physiol. Plant Mol Biol* **41**, 277–315.

**Bergfeld, R., Speth, V. & Schopfer, P. (1988).** Reorientation of microfibrils and microtubules at the outer epidermal wall of maize coleoptiles during auxin-mediated growth. *Bot Acta* **101**, 57–67.

**Berghöfer, T., Eing, C., Flickinger, B., Hohenberger, P., Wegner, L. H., Frey, W. & Nick, P. (2009).** Nanosecond electric pulses trigger actin responses in plant cells. *Biochem Biophys Res Commun* **387**, 590–595.

**Bertani G. (1951).** Studies on lysogenesis. I. The mode of phage liberation by lysogenic *Escherichia coli*. *J Bacteriol* **62**, 293–300.

**Bestwick, C. S., Bennett, M. H. & Mansfield, J. W. (1995).** Hrp mutant of *Pseudomonas syringae* pv *phaseolicola* induces cell wall alterations but not membrane damage leading to the hypersensitive reaction in lettuce. *Plant Physiol* **108**, 503–516.

**Binarová, P., Cenklová, V., Hause, B., Kubátová, E., Lysák, M., Doležal, J., Bogre, L. & Dráber, P. (2000).** Nuclear gamma-tubulin during acentriolar plant mitosis. *Plant Cell* **12**, 433–442.

**Boller, T. & Felix, G. (2009).** A renaissance of elicitors: perception of microbe-associated molecular patterns and danger signals by pattern-recognition receptors. *Annu Rev Plant Biol* **60**, 379–406.

**Boller, T. & He, S. Y. (2009).** Innate immunity in plants: an arms race between pattern recognition receptors in plants and effectors in microbial pathogens. *Science* **324**, 742–744.

**Bolwell, G. P. (1999).** Role of active oxygen species and NO in plant defence responses. *Curr Op Plant Biol* **2**, 287–294.

**Bonardi, V., Tang, S., Stallmann, A., Roberts, M., Cherkis, K. & Dangl, J. L. (2011).** Expanded functions for a family of plant intracellular immune receptors beyond specific recognition of pathogen effectors. *Proc Natl Acad Sci U S A* **108**, 16463–16468.

**Breviario, D. & Nick, P. (2000).** Plant tubulins: a melting pot for basic question and promising applications. *Transgenic Res* **9**, 383–393.

**Brodribb, T. J. & Jordan, G. J. (2008).** Internal coordination between hydraulics and stomatal control in leaves. *Plant Cell Environ* **31**, 1557–1564.

**Brown, I. R., Mansfield, J. W., Taira, S., Roine, E. & Romantschuk, M. (2001).** Immunocytochemical localization of HrpA and HrpZ supports a role for the transfer of effector proteins from *Pseudomonas syringae* pv. tomato across the host plant cell wall. *Mol Plant Microbe Interact* **14**, 394–404.

**Burgos-Rivera, B., Ruzicka, D. R., Deal, R. B., McKinney, E. C., King-Reid, L. & Meagher, R. B.**

## References

---

- (2008). ACTIN DEPOLYMERIZING FACTOR9 controls development and gene expression in Arabidopsis. *Plant Mol Biol* **68**, 619–632.
- Burrill, T. J. (1878)**. Pear blight. Trans III. *State Hort Soc* **11**, 114–116.
- Campanoni, P., Blasius, B. & Nick, P. (2003)**. Auxin transport synchronizes the pattern of cell division in a tobacco cell line. *Plant Physiol* **133**, 1251–1260.
- Cai, G. & Cresti, M. (2009)**. Organelle motility in the pollen tube: a tale of 20 years. *J Exp Bot* **60**, 495–508.
- Cecchini, M., Alexeev, Y. & Karplus, M. (2010)**. Pi release from myosin: A simulation analysis of possible pathways. *Structure* **18**, 458–470.
- Chapman, M. R., Robinson, L. S., Pinkner, J. S., Roth, R., Heuser, J., Hammar, M., Normark, S. & Hultgren, S. J. (2002)**. Role of Escherichia coli curli operons in directing amyloid fiber formation. *Science* **295**, 851–855.
- Chang, X. & Nick, P. (2012)**. Defence signalling triggered by Flg22 and Harpin is integrated into a different stilbene output in *Vitis* cells. *PLoS ONE* **7**, e40446.
- Chang, X., Heene, E., Qiao, F. & Nick, P. (2011)**. The Phytoalexin resveratrol regulates the Initiation of Hypersensitive cell death in *Vitis* cell. *PLoS One* **10**, e26405.
- Chen, H., Nelson, R. S. & Sherwood, J. L. (1994)**. Enhanced recovery of transformants of *Agrobacterium tumefaciens* after freeze-thaw transformation and drug selection. *Biotechniques* **16**, 664–670.
- Chen, X. (2010)**. Small RNAs—secrets and surprises of the genome. *Plant J* **61**, 941–958.
- Cheong, Y. H., Moon, B. C., Kim, J. K., Kim, C. Y., Kim, M. C., Kim, I. H., Park, C. Y., Kim, J. C., Park, B. O., Koo, S. C., Yoon, H. W., Chung, W. S., Lim, C. O., Lee, S. Y. & Cho, M. J. (2003)**. BWMK1, a rice mitogen-activated protein kinase, locates in the nucleus and mediates pathogenesis-related gene expression by activation of a transcription factor. *Plant Physiol* **132**, 1961–1972.
- Chinchilla, D., Bauer, Z., Regenass, M., Boller, T. & Felix, G. (2006)**. The Arabidopsis receptor kinase FLS2 binds flg22 and determines the specificity of flagellin perception. *Plant Cell* **18**, 465–476.
- Chisholm, S. T., Coaker, G., Day, B. & Staskawicz, B. J. (2006)**. Host-microbe interactions: shaping the evolution of the plant immune response. *Cell* **124**, 803–814.
- Chaudhry, F., Guérin, C., von Witsch, M., Blanchoin, L. & Staiger, C. J. (2007)**. Identification of Arabidopsis cyclase-associate protein 1 as the first nucleotide exchange factor for plant actin. *Mol Biol Cell* **18**, 3002–3014.



- Colby, S. M. & Meredith, C. P. (1990).** Kanamycin sensitivity of cultured tissues of *Vitis*. *Plant Cell Rep* **9**, 237–240.
- Collings, D. A. (2008).** Crossed-wires: interactions and cross-talk between the microtubule and microfilament networks in plants. *Plant Microtubules, Development and Flexibility*. Edited by Nick P. pp. 47–82. Springer-Verlag, Berlin.
- Collings, D. A., Asada, T. & Shibaoka, H. (1999).** Plasma membrane ghosts form differently when produced from microtubule-free tobacco BY-2 cells. *Plant Cell Physiol* **40**, 36–46.
- Collings, D. A., Carter, C. N., Rink, J. C., Scott, A. C., Wyatt, S. E. & Allen, N. S. (2000).** Plant nuclei can contain extensive grooves and invaginations. *Plant Cell* **12**, 2425–2439.
- Cossart, P. & Sansonetti, P. J. (2004).** Bacterial invasion: the paradigms of enteroinvasive pathogens. *Science* **304**, 242–248.
- Cyrklaff, M., Sanchez, C. P., Kilian, N., Bisseye, C., Simpire, J., Frischknecht, F. & Lanzer, M. (2011).** Hemoglobins S and C interfere with actin remodelling in *Plasmodium falciparum*-infected erythrocytes. *Science* **334**, 1283–1286.
- Darken, M. J. (1961).** Applications of fluorescent brighteners in biological techniques. *Science* **133**, 1704–1705.
- Day, B., Henty, J. L., Porter, K. J. & Staiger, C. J. (2011).** The pathogen-actin connection: A platform for defense signaling in plants. *Annu Rev Phytopathol* **49**, 483–506.
- Deeks, M. J., Rodrigues, C., Dimmock, S., Ketelaar, T., Maciver, S. K., Malhó R. & Hussey, P. J. (2007).** Arabidopsis CAP1—a key regulator of actin organisation and development. *J Cell Sci* **120**, 2609–2618.
- Del R ó, L. A. (2011).** Peroxisomes as a cellular source of reactive nitrogen species signal molecules. *Arch Biochem Biophys* **506**, 1–11.
- De Lumley, H. (1988).** La stratigraphie du remplissage de la Grotte du Vallonet. *L'Anthropologie* **92**, 407–428.
- DeYoung, B. J, Qi, D., Kim, S. H., Burke, T. P. & Innes, R. W. (2012).** Activation of a plant nucleotide binding-leucine rich repeat disease resistance protein by a modified self protein. *Cell Microbiol* **14**, 1071–1084.
- Dhonukshe, P., Laxalt, A. M., Goedhart, J., W. J. Gadella, T. W. J. & Munnik, T. (2003).** Phospholipase D Activation Correlates with Microtubule Reorganization in Living Plant Cells. *Plant Cell*

## References

---

15, 2666–2679.

**Ding, J. P. & Pickard, B. G. (1993).** Mechanosensory calcium-selective cation channels in epidermal cells. *Plant J* **3**, 83–110.

**Déz-Navajas, A. M., Greif, C., Poutaraud, A. & Merdinoglu, D. (2007).** Two simplified fluorescent staining techniques to observe infection structures of the oomycete *Plasmopara viticola* in grapevine leaf tissues. *Micron* **36**, 680–683.

**Dodds, P. N. & Rathjen, J. P. (2010).** Plant immunity: Towards an integrated view of plantpathogen interactions. *Nat Rev Genet* **11**, 539–548.

**Doyle, J. J. & Doyle, J. L. (1987).** A rapid DNA isolation procedure from small quantities of fresh leaf tissues. *Phytochem Bull* **19**, 11–15.

**Duncan, D. B. (1955).** Multiple range and multiple F test. *Biometrics* **11**, 1–42.

**Durst, S., Nick, P. & Maisch, J. (2013).** *Nicotiana tabacum* actin-depolymerizing factor 2 is involved in actin-driven, auxin-dependent patterning. *J Plant Physiol* doi: 10.1016/j.jplph.2013.03.002.

**Fan, C. H., Pu, N., Wang, X. P., Wang, Y. J., Fang, L., Xu, W. R., Zhang, J. X. (2008).** *Agrobacterium*-mediated genetic transformation of grapevine (*Vitis vinifera* L.) with a novel stilbene synthase gene from Chinese wild *Vitis pseudoreticulata*. *Plant Cell Tiss Organ Cult* **92**, 197–206.

**Felix, G., Duran, J. D., Volko, S. & Boller, T. (1999).** Plants have a sensitive perception system for the most conserved domain of bacterial flagellin. *Plant J* **18**, 265–276.

**Flickinger, B., Berghöfer, T., Hohenberger, P., Eing, C. & Frey, W. (2010).** Transmembrane potential measurements on plant cells using the voltage-sensitive dye ANNINE-6. *Protoplasma* **247**, 3–12.

**Flor, H. H. (1956).** The complementary genetic systems in flax and flax rust. *Adv Genet* **8**, 29–54.

**Foresi, N., Correa-Aragunde, N., Parisi, G., Calo, G., Salerno, G. & Lamattina, L. (2010).** Characterization of a nitric oxide synthase from the plant kingdom: NO generation from the green alga *Ostreococcus tauri* is light irradiance and growth phasedependent. *Plant Cell* **22**, 3816–3830.

**Franklin-Tong, V. E. & Gourlay, C. W. (2008).** A role for actin in regulating apoptosis/programmed cell death: evidence spanning yeast, plants and animals. *Biochem J* **413**, 389–404.

**Frey, N., Klotz, J. & Nick, P. (2009).** Dynamic Bridges—A Calponin-Domain Kinesin From Rice Links Actin Filaments and Microtubules in Both Cycling and Non-Cycling Cells. *Plant Cell Physiol* **50**, 1493–1506.

- Friml, J. (2003).** Auxin transport-shaping the plant. *Curr Opin Plant Biol* **6**, 7–12.
- Frühholz, S. (2011).** Untersuchung und optimierung induzierbarer promotoren im Cre/loxP-System zur erzeugung markergenfreier transgener pflanzen. Diplomarbeit. In Thesis: Universität Hohenheim.
- Gaff, D. F. & Okong'O-Ogola, O. (1971).** The use of non-permeating pigments for testing the survival of cells. *J Exp Bot* **22**, 756–758.
- Gambino, G., Ruffa, P., Vallania, R. & Gribaudo, I. (2007).** Somatic embryogenesis from whole flowers, anthers and ovaries of grapevine (*Vitis* spp.). *Plant Cell Tiss Organ Cult* **90**, 79–83.
- Gao, X., Chen, J., Wei, P., Ren, F., Chen, J. & Wang, X. (2006).** Array and distribution of actin filaments in guard cells contribute to the determination of stomatal aperture. *Plant Cell* **18**, 2194–2206.
- Gardiner, J. C., Harper, J. D. I., Weerakoon, N. D., Collings, D. A., Ritchie, S., Gilroy, S., Cyr, R. J. & Marc, J. (2011).** A 90-kD phospholipase D from tobacco binds to microtubules and the plasma membrane. *Plant Cell* **13**, 2143–2158.
- Garrido, I., Espinosa, F. & Alvarez-Tinaut, M. C. (2012).** Apoplastic superoxide production and peroxidase activity by intact and excised axenically grown seedling roots of sunflower, *Protoplasma* **249**, 1071–1080.
- Gechev, T. S., Van Breusegem, F., Stone, J. M., Denev, I. & Laloi, C. (2006).** Reactive oxygen species as signals that modulate plant stress responses and programmed cell death. *Bioessays* **28**, 1091–1101.
- Gianessi, L. & Williams, A. (2011).** Fungicides have protected European wine grapes for 150 years. International pesticide benefits case study No. 19. CropLife Foundation, Washington, DC.
- Giddings, T. H. & Staehelin, L. A. (1991).** Microtubule-mediated control of microfibril deposition: A re-examination of the hypothesis. *The Cytoskeletal Basis of Plant Form and Growth*. Edited by Lloyd, C. W. pp. 85–99. Academic Press, London.
- Gillespie, T., Boevink, P., Haupt, S., Roberts, A. G., Toth, R., Valentine, T., Chapman, S. & Oparka, K. J. (2002).** Functional analysis of a DNA-shuffled movement protein reveals that microtubules are dispensable for the cell to cell movement of Tobacco mosaic virus. *Plant Cell* **14**, 1207–1222.
- Gómez-Gómez, L. & Boller, T. (2000).** FLS2: an LRR receptor-like kinase involved in the perception of the bacterial elicitor flagellin in Arabidopsis. *Mol Cell* **5**, 1003–1011.
- Gourlay, C. W. & Ayscough, K. R. (2005).** The actin cytoskeleton: a key regulator of apoptosis and ageing? *Nat Rev Mol Cell Biol* **6**, 583–589.
- Green, P. B. (1962).** Mechanism for plant cellular morphogenesis. *Science* **138**, 1404–1405.

## References

---

- Guan, X., Buchholz, G. & Nick, P. (2013).** The cytoskeleton is disrupted by the bacterial effector HrpZ, but not by the bacterial PAMP flg22, in tobacco BY-2 cells. *J Exp Bot* doi:10.1093/jxb/ert042.
- Gunning, B. E. S. (1982).** The cytokinetic apparatus: its development and spatial regulation. *In* The Cytoskeleton. Edited by Lloyd, C. W. pp. 229–292. Academic Press, London.
- Guo, L., Devaiah, S. P., Narasimhan, R., Pan, X., Zhang, Y., Zhang, W. & Wang, X. (2012).** Cytosolic Glyceraldehyde-3-Phosphate dehydrogenases interact with phospholipase D $\delta$  to transduce hydrogen peroxide signals in the Arabidopsis response to stress. *Plant Cell* **24**, 2200–2212.
- Gupta, K.J., Igamberdiev, A. U. & Kaiser, W. M. (2010).** New insights into the mitochondrial nitric oxide production pathways *Plant Signal Behav* **5**, 999–1001.
- Haapalainen, M., Dauphin, A., Li, C. M., Bailly, G., Tran, D., Briand, J., Bouteau, F. & Taira, S. (2012).** HrpZ harpins from different *Pseudomonas syringae* pathovars differ in molecular interactions and in induction of anion channel responses in Arabidopsis thaliana suspension cells. *Plant Physiol Biochem* **51**, 168–174.
- Haapalainen, M., Engelhardt, S., Kűfner, I., Li, C. M., Nűrnberger, T., Lee, J., Romantschuk, M & Taira, S. (2011).** Functional mapping of harpin HrpZ of *Pseudomonas syringae* reveals the sites responsible for protein oligomerization, lipid interactions and plant defence induction. *Mol Plant Pathol* **12**, 151–166.
- Hammer, Ø., Harper, D. A. T. & Ryan, P. D. (2001).** PAST: Paleontological statistics software package for education and data analysis. *Palaeontol Electron* **4**, 9.
- Han, J., Zhong, C. Q. & Zhang, D. W. (2011).** Programmed necrosis: backup to and competitor with apoptosis in the immune system. *Nat Immunol* **12**, 1143–1149.
- Hancock, J. T. (2012).** NO synthase? Generation of nitric oxide in plants. *Period Biol* **114**, 19–24.
- Hasezawa, S., Kumagai, F. & Nagata, T. (1997).** Sites of microtubule reorganization in tobacco BY-2 cells during cell-cycle progression. *Protoplasma* **198**, 202–209.
- Ho, A. Y. Y., Day, D. A., Brown, M. H. & Marc, J. (2009).** Arabidopsis phospholipase D delta as an initiator of cytoskeleton-mediated signalling to fundamental cellular processes. *Funct Plant Biol* **36**, 190–198.
- Heath, I. B. (1980).** Variant mitoses in lower eucaryotes – indicators of the evolution of mitosis. *Int Rev Cytol* **64**, 1–80.
- Heinlein, M. (2002).** The spread of Tobacco mosaic virus infection: insights into the cellular mechanism of RNA transport. *Cell Mol Life Sci* **59**, 58–82.

- Heinlein, M. (2008).** Microtubules and viral movement. In *Plant Microtubules, Development and Flexibility*. Edited by Nick, P. pp. 141–173. Springer-Verlag, Berlin.
- Heinlein, M., Epel, B. L., Padgett, H. S., Beachy, R. N. (1995).** Interaction of tobamovirus movement proteins with the plant cytoskeleton. *Science* **270**, 1983–1985.
- Hess, D. T., Matsumoto, A., Kim, S. O., Marshall, H. E. & Stamler, J. S. (2005).** Protein S-nitrosylation: purview and parameters. *Nat Rev Mol Cell Biol* **6**, 150–166.
- Higaki, T., Kutsuna, N., Sano, T., Kondo, N. & Hasezawa, S. (2010).** Quantification and cluster analysis of actin cytoskeletal structures in plant cells: role of actin bundling in stomatal movement during diurnal cycles in *Arabidopsis* guard cells. *Plant J* **61**, 156–165.
- Hinkley, R. E. (1978).** Microtubules induced by halothane: *in vitro* assembly. *J Cell Sci* **32**, 99–108.
- Hoch, H. C., Galvani, C. D., Szarowski, D. H. & Turner, J. N. (2005).** Two new fluorescent dyes applicable for visualization of fungal cell walls. *Mycologia* **97**, 580–588.
- Hofmann, C., Nieh, A., Sambade, A., Steinmetz, A. & Heinlein, M. (2009).** Inhibition of tobacco mosaic virus movement by expression of an actin-binding protein. *Plant Physiol* **149**, 1810–1823.
- Hoffmann, M., Hentrich, M. & Pollmann, S. (2011).** Auxin-Oxylipin Crosstalk: Relationship of Antagonists. *J Integral Plant Biol* **6**, 429–445.
- Hohenberger, P., Eing, C., Straessner, R., Durst, S., Frey, W. & Nick, P. (2011).** Plant actin controls membrane permeability. *Biochem Biophys Acta* **1808**, 2304–2312.
- Holweg, C. L. (2007).** Living Markers for Actin Block Myosin-Dependent Motility of Plant Organelles and Auxin. *Cell Motil Cytoskel* **64**, 69–81.
- Holzinger, A. (2009).** Jasplakinolide: an actin-specific reagent that promotes actin polymerization. *Methods Mol Biol* **586**, 71–87.
- Howard, E. & Citovsky, V. (1990).** The emerging structure of the *Agrobacterium* T-DNA transfer complex. *BioEssays* **12**, 103–108.
- Hwang, J. U. & Lee, Y. (2001).** Abscisic acid-induced actin reorganization in guard cells of dayflower is mediated by cytosolic calcium levels and by protein kinase and protein phosphatase activities. *Plant Physiol* **125**, 2120–2128.
- Ismail, A., Riemann, M. & Nick, P. (2011).** The jasmonate pathway mediates salt tolerance in grapevines. *J Exp Bot* **63**, 2127–2139.

## References

---

- Jaillon, O., Aury, J. M., Noel, B., Policriti, A., Clepet, C., Casagrande, A., Choisne, N., Aubourg, S., Vitulo, N., Jubin, C., Vezzi, A., Legeai, F., Huguency, P., Dasilva, C., Horner, D., Mica, E., Jublot, D., Poulain, J., Bruyere, C., Billault, A., Segurens, B., Gouyvenoux, M., Ugarte, E., Cattonaro, F., Anthouard, V., Vico, V., Del Fabbro, C., Alaux, M., Di Gaspero, G., Dumas, V., Felice, N., Paillard, S., Juman, I., Moroldo, M., Scalabrin, S., Canaguier, A., Le Clainche, I., Malacrida, G., Durand, E., Pesole, G., Laucou, V., Chatelet, P., Merdinoglu, D., Delledonne, M., Pezzotti, M., Lecharny, A., Scarpelli, C., Artiguenave, F., P   E., Valle, G., Morgante, M., Caboche, M., Adam-Blondon, A. F., Weissenbach, J., Qu   tier, F. & Wincker, P. (2007).** The grapevine genome sequence suggests ancestral hexaploidization in major angiosperm phyla. *Nature* **449**, 463–468.
- Janda, M., Planchais, S., Djafi, N., Martinec, J., Burketova, L., Valentova, O., Zachowski, A. & Ruelland, E. (2013).** Phosphoglycerolipids are master players in plant hormone signal transduction. *Plant Cell Rep* DOI 10.1007/s00299-013-1399-0.
- Jasid, S., Simontacchi, M., Bartoli, C. G. & Puntarulo, S. (2006).** Chloroplasts as a nitric oxide cellular source. Effect of reactive nitrogen species on chloroplastic lipids and proteins. *Plant Physiol* **142**, 1246–1255.
- Johnson, E. E. (2012).** A profile of the expression of a metabolic gene cluster in Arabidopsis. In Thesis: University of British Columbia.
- Jones, A. M. (2001).** Programmed cell death in development and defense. *Plant Physiol* **125**, 94–97.
- Jones, J. D. & Dangl, J. L. (2006).** The plant immune system. *Nature* **444**, 323–329.
- Kadota, A., Yamada, N., Suetsugu, N., Hirose, M., Saito, C., Shoda, K., Ichikawa, S. Kagawa, T., Nakano, A. & Wada, M. (2009).** Short actin-based mechanism for light-directed chloroplast movement in Arabidopsis. *Proc Natl Acad Sci USA* **106**, 13106–13111.
- Kandasamy, M. K., McKinney, E. C. & Meagher, R. B. (2010).** Differential sub-localization of actin variants within the nucleus. *Cytoskel* **67**, 729–743.
- Kancta, T., Kakimoto, T. & Shibaoka, H. (1993).** Actinomycin D inhibits the GA3-induced elongation of azuki bean epicotyls and the reorientation of cortical microtubules. *Plant Cell Physiol* **34**, 1125–1132.
- Kasprowicz, A., Szuba, A., Volkmann, D., Baluska, F. & Wojtaszek, P. (2009).** Nitric oxide modulates dynamic actin cytoskeleton and vesicle trafficking in a cell type-specific manner in root apices *J Exp Bot* **60**, 1605–1617.
- Katsumi, M., Mori, S. & Ishida, K. (1989).** GA induced growth of cucumber seedlings under water stress. In *Plant Water Relations and Growth under Stress*, ed. M Tazawa, M Katsumi, Y Masuda, H Okamoto, pp. 349–356. Tokyo: Myn.

- Kawakami, S., Watanabe, Y. & Beachy, R. N. (2004).** Tobacco mosaic virus infection spreads cell to cell as intact replication complexes. *Proc Natl Acad Sci USA* **101**, 6291–6296.
- Ketelaar, T., Anthony, R. G. & Hussey, P. J. (2004).** Green fluorescent protein-mTalin cause defects in actin organization and cell expansion in Arabidopsis and inhibits actin depolymerizing factor's actin depolymerizing activity *in vitro*. *Plant Physiol* **136**, 3990–3998.
- Khurana, A. & Dey, C. S. (2003).** p38 MAPK interacts with actin and modulates filament assembly during skeletal muscle differentiation. *Differentiation* **71**, 42–50.
- Kiefer, B., Riemann, M., Büche, C., Kassemeyer, C. C. & Nick, P. (2002).** The host guides morphogenesis and stomatal targeting in the grapevine pathogen *Plasmopara viticola*. *Planta* **215**, 387–393.
- Kim, T. H. , Böhmer, M., Hu, H., Nishimura, N. & Schroeder, J. I. (2010).** Guard cell signal transduction network: advances in understanding abscisic acid, CO<sub>2</sub>, and Ca<sup>2+</sup> signaling. *Annu Rev Plant Biol* **61**, 561–591.
- Kirchheimer, F. (1938).** Beiträge zur näheren Kenntnis von Vitaceen-Samenformen tertiären Alters. *Planta* **28**, 582–598.
- Kleine-Vehn, J., Dhonukshe, P., Swarup, R., Bennett, M. & Friml, J. (2006).** Subcellular trafficking of the Arabidopsis auxin influx carrier AUX1 uses a novel pathway distinct from PIN1. *Plant Cell* **18**, 3171–3181.
- Klotz, J. & Nick, P. (2012).** A novel actin-microtubule cross-linking kinesin, NtKCH, functions in cell expansion and division. *New Phytol* **193**, 576–589.
- Knight, H. (2000).** Calcium signaling during abiotic stress in plants. *Int Rev Cytol* **195**, 269–324.
- Kobayashi, I. & Kobayashi, Y. (2008).** Microtubules and pathogen defence. Plant cell monographs: plant microtubules. Edited by Nick, P. pp. 121–140. Springer-Verlag, Berlin.
- Koivusalo, M., Kappus, A. & Grinstein, S. (2009).** Sensors, transducers, and effectors that regulate cell size and shape. *J Biol Chem* **284**, 6595–6599.
- Komis, G., Apostolakos, P. & Galatis, B. (2002).** Hyperosmotic stress induces formation of tubulin macrotubules in root-tip cells of *Triticum turgidum*: their probable involvement in protoplast volume control. *Plant Cell Physiol* **43**, 911–922.
- Komis, G., Quader, H., Galatis, B. & Apostolakos, P. (2006).** Macrotubule-dependent protoplast volume regulation in plasmolysed root-tip cells of *Triticum turgidum*: involvement of phospholipase D. *New Phytol* **171**, 131–150.

## References

---

- Konopka, C. A. & Bednarek, S. Y. (2008).** Variable-angle epifluorescence microscopy: a new way to look at protein dynamics in the plant cell cortex. *Plant J* **53**, 186–196.
- Kopecká, M., Kawamoto, S. & Yamaguchi, M. (2012).** A new F-actin structure in fungi: actin ring formation around the cell nucleus of *Cryptococcus neoformans*. *J Electron Microsc* doi: 10.1093/jmicro/dfs074.
- Kost, B., Spielhofer, P. & Chua, N. (1998).** A GFP-mouse talin fusion protein labels plant actin filaments *in vivo* and visualizes the actin cytoskeleton in growing pollen tubes. *Plant J* **16**, 393–401.
- Kusner, D. J., Barton, J. A., Wen, K. K., Wang, X., Rubenstein, P. A. & Iyer, S. S. (2002).** Regulation of phospholipase D activity by actin. Actin exerts bidirectional modulation of mammalian phospholipase D activity in a polymerization-dependent, isoform-specific manner. *J Biol Chem* **277**, 50683–50692.
- Lai, Z., Wang, F., Zheng, Z., Fan, B. & Chen, Z. (2011).** A critical role of autophagy in plant resistance to necrotrophic fungal pathogens. *Plant J* **66**, 953–968.
- Lecourieux, D., Mazars, C., Pauly, N., Ranjeva, R. & Pugin, A. (2002).** Analysis and effects of cytosolic free calcium increases in response to elicitors in *Nicotiana plumbaginifolia* cells. *Plant Cell* **14**, 2627–2641.
- Lee, J., Klüsener, B., Tsiamis, G., Stevens, C., Neyt, C., Tampakaki, A. P., Panopoulos, N. J., Nöller, J., Weiler, E. W., Cornelis, G. R., Mansfield, J. W. & Nürnberger, T. (2001a).** HrpZPspH from the plant pathogen *Pseudomonas syringae* pv. *phaseolicola* binds to lipid bilayers and forms an ion-conducting pore *in vitro*. *Proc Natl Acad Sci U S A* **98**, 289–294.
- Lee, J., Ishihara, A., Oxford, G., Johnson, B. & Jacobson, K. (1999).** Regulation of cell movement is mediated by stretch-activated calcium channels. *Nature* **400**, 382–386.
- Lee, J., Klessig, D. F. & Nürnberger, T. (2001b).** A harpin binding site in tobacco plasma membranes mediates activation of the pathogenesis-related gene HIN1 independent of extracellular calcium but dependent on mitogen-activated protein kinase activity. *Plant Cell* **13**, 1079–1093.
- Lee, Y. J., Szumlanski, A., Nielsen, E. & Yang, Z. (2008).** Rho-GTPase-dependent filamentous actin dynamics coordinate vesicle targeting and exocytosis during tip growth. *J Cell Biol* **181**, 1155–1168.
- Li, C. M., Haapalainen, M., Lee, J., Nürnberger, T., Romantschuk, M. & Taira, S. (2005).** Harpin of *Pseudomonas syringae* pv. *phaseolicola* harbors a protein binding site. *Mol Plant Microbe Interact* **18**, 60–66.
- Littlejohn, G. R., Gouveia, J. D., Edner, C., Smirnoff, N. & Love, J. (2010).** Perfluorodecalin enhances *in vivo* confocal microscopy resolution of *Arabidopsis thaliana* mesophyll. *New Phytol* **186**, 1018–1025.



- Liu, K. & Luan, S. (1998).** Voltage-dependent K<sup>+</sup>-channel as target of osmosensing in guard cells. *The Plant Cell* **10**, 1957–1970.
- Liu, Q., Qiao, F., Ismail, A., Chang, X. & Nick, P. (2013).** The plant cytoskeleton controls regulatory volume increase. *Biochim Biophys Acta* doi: 10.1016/j.bbamem.2013.04.027.
- Liu, S. G., Zhu, D. Z., Chen, G. H., Gao, X. Q. & Zhang, X. S. (2012).** Disrupted actin dynamics trigger an increment in the reactive oxygen species levels in the Arabidopsis root under salt stress. *Plant Cell Rep* **31**, 1219–1226.
- Livanos, P., Galatis, B., Quader, H. & Apostolakos, P. (2012).** Disturbance of reactive oxygen species homeostasis induces atypical tubulin polymer formation and affects mitosis in root-tip cells of *Triticum turgidum* and *Arabidopsis thaliana*. *Cytoskeleton* **69**, 1–21.
- Lloyd, C., & Hussey, P. (2001).** Microtubule-associated proteins in plants—Why we need a MAP. *Nat Rev Mol Cell Biol* **2**, 40–47.
- Lucas, J. R., Nadeau, J. A. & Sack, F. D. (2006).** Microtubule arrays and Arabidopsis stomatal development. *J Exp Bot* **57**, 71–79.
- Ludwig, A. A., Saitoh, H., Felix, G., Freymark, G., Miersch, O., Wasternack, C., Boller, T., Jones, J. D. & Romeis, T. (2005).** Ethylene-mediated cross-talk between calcium-dependent protein kinase and MAPK signaling controls stress responses in plants. *Proc Natl Acad Sci USA* **102**, 10736–10741.
- Luo, Z. & Chen, Z. (2007).** Improperly terminated, unpolyadenylated mRNA of sense transgenes is targeted by RDR6-mediated RNA silencing in Arabidopsis. *Plant Cell* **19**, 943–958.
- Lyons, J. M. (1973).** Chilling injury in plants. *Annu Rev Plant Physiol* **24**, 445–466.
- Machesky L. M. & Gould K. L. (1999).** The Arp2/3 complex: a multifunctional actin organizer. *Curr Opin Cell Biol* **11**, 117–121.
- MacLean-Fletcher, S. & Pollard, T. D. (1980).** Mechanism of action of cytochalasin B on actin. *Cell* **20**, 329–341.
- MacRobbie, E. A. & Kurup, S. (2007).** Signaling mechanisms in the regulation of vacuolar ion release in guard cells. *New Phytol* **175**, 630–640.
- Maeda, H. & Ishida, N. (1967).** Specificity of binding of hexopyranosyl polysaccharides with fluorescent brightener. *J Biochem* **62**, 276–278.
- Marantz, R. & Shelanski, M. L. (1970).** Structure of microtubular crystals induced by vinblastine *in vitro*. *J Cell Biol* **44**, 234–238.

## References

---

- Marc, J., Sharkey, D. E., Durso, N. A., Zhang, M., & Cyr, R. J. (1996).** Isolation of a 90-kD microtubule-associated protein from tobacco membranes. *Plant Cell* **8**, 2127–2138.
- Martinelli, L., Bragagna, P., Poletti, V. & Scienza, A. (1993).** Somatic embryogenesis from leaf- and petiole- derived callus of *Vitis rupestris*. *Plant Cell Rep* **12**, 207–210.
- Mathur, J., Mathur, N., Kernebeck, B. & Hulskamp, M. (2003).** Mutations in actin-related proteins 2 and 3 affect cell shape development in Arabidopsis. *Plant Cell* **15**, 1632–1645.
- Mazars, C., Thion, L., Thuleau, P., Graziana, A., Knight, M. R., Moreau, M. & Ranjeva, R. (1997).** Organization of cytoskeleton controls the changes in cytosolic calcium of cold-shocked *Nicotiana plumbaginifolia* protoplasts. *Cell Calcium* **22**, 413–420.
- Medina, J., Bargues, M., Terol, J., P érez-Alonso, M. & Salinas, J. (1999).** The Arabidopsis CBF gene family is composed of three genes encoding AP2 domain-containing proteins whose expression is regulated by low temperature temperature but not by abscisic acid or dehydration. *Plant Physiol* **119**, 463–469.
- Melcher, K., Xu, Y., Ng, L. M., Zhou, X. E., Soon, F. F., Chinnusamy, V., Suino-Powell, K. M., Kovach, A., Tham, F. S., Cutler, S. & R., Li, J., Yong, E. L., Zhu, J. K. & Xu, H. E. (2010).** Identification and mechanism of ABA receptor antagonism. *Nat Struct Mol Biol* **17**, 1102–1108.
- Michelot, A., Berro, J., Guerin, C., Boujemaa-Paterski, R., Staiger, C. J., Martiel, J. L. & Blanchoin, L. (2007).** Actin-filament stochastic dynamics mediated by ADF/cofilin. *Curr Biol* **17**, 825–833.
- Miguel, C., Marum, L. (2011).** An epigenetic view of plant cells cultured in vitro: somaclonal variation and beyond. *J Exp Bot* **62**, 3713–3725.
- Minibayeva, F., Gordon, L. K., Kolesnikov, O. P. & Chasov, A. V. (2001).** Role of extracellular peroxidase in the superoxide production by wheat root cells. *Protoplasma* **217**, 125–128.
- Miquel, C. & Marum, L. (2011).** An epigenetic view of plant cells cultured in vitro: somaclonal variation and beyond. *J Exp Bot* **62**, 3713–3725.
- Monteiro, H. P. (2002).** Signal transduction by protein tyrosine nitration: competition or cooperation with tyrosine phosphorylation-dependent signaling events? *Free Radical Biol Med* **33**, 765–773.
- Moon, J., Zhao, Y., Dai, X., Zhang, W., Gray, W. M., Huq, E. & Estelle, M. (2007).** A new CULLIN 1 mutant has altered responses to hormones and light in Arabidopsis. *Plant Physiol* **143**, 684–696.
- Moroldo, M., Paillard, S., Marconi, R., Fabrice, L., Canaguier, A., Cruaud, C., De Berardinis, V., Guichard, C., Brunaud, V., Le Clainche, I., Scalabrin, S., Testolin, R., Di Gaspero, G., Morgante, M. & Adam-Blondon, A. F. (2008).** A physical map of the heterozygous grapevine 'Cabernet Sauvignon'

- allows mapping candidate genes for disease resistance. *BMC Plant Biol* **8**, 66–80.
- Motes, C. M., Pechter, P., Yoo, C. M., Wang, Y. S., Chapman, K. D. & Blancaflor, E. B. (2005).** Differential effects of two phospholipase D inhibitors, 1-butanol and N-acylethanolamine, on in vivo cytoskeletal organization and Arabidopsis seedling growth. *Protoplasma* **226**, 109–123.
- Mullins, M. A., Tang, F. C. A. & Facciotti, D. (1990).** *Agrobacterium*-mediated transformation of grapevines: transgenic plants of *Vitis rupestris* SCHEELE and buds of *Vitis vinifera* L. *Nat Biotechnol* **18**, 1041–1045.
- Munnik, T. & Vermeer, J. E. M. (2010).** Osmotic stress-induced phosphoinositide and inositolphosphate signalling in plants. *Plant Cell Environ* **33**, 655–669.
- Nagata, T., Nemoto, Y. & Hasezawa, S. (1992).** Tobacco BY-2 cell line as the ‘HeLa’ cell in the cell biology of higher plants. *Int Rev Cytol* **132**, 1–30.
- Nakamura, M., Naoi, K., Shoji, T. & Hashimoto, T. (2004).** Low concentrations of propyzamide and oryzalin alter microtubule dynamics in Arabidopsis epidermal cells. *Plant Cell Physiol* **45**, 1330–1334.
- Navarro, L., Dunoyer, P., Jay, F., Arnold, B., Dharmasiri, N., Estelle, M., Voinnet, O. & Jones, J. D. (2006).** A plant miRNA contributes to antibacterial resistance by repressing auxin signaling. *Science* **312**, 436–439.
- Neill, S., Barros, R., Bright, J., Desikan, R., Hancock, J., Harrison, J., Morris, P., Ribeiro, D. & Wilson, I. (2008).** Nitric oxide, stomatal closure, and abiotic stress. *J Exp Bot* **59**, 165–176.
- Nick, P. (1998).** Signaling to the microtubular cytoskeleton in plants. *Int Rev Cytol* **184**, 33–81.
- Nick P. (2000).** Control of the response to low temperatures. *Plant Microtubules Potential for Biotechnology*. Edited by Nick, P. pp. 121–135. Springer-Verlag, Berlin.
- Nick, P. (2006).** Noise Yields Order – Auxin, Actin, and Polar Patterning. *Plant Biol* **8**, 360–370.
- Nick, P. (2008).** Control of cell axis. *Plant microtubules*. Edited by Nick, P. pp. 3–46. Springer-Verlag, Berlin.
- Nick, P. (2010).** Probing the actin-auxin oscillator. *Plant Signal Behav* **5**, 94–98.
- Nick, P. (2013).** Microtubules, signalling and abiotic stress. *Plant J* doi: 10.1111/tpj.12102.
- Nogales, E. (2000).** Structural insights into microtubule function. *Annu Rev Biochem* **69**, 277–302.
- Nühse, T. S., Peck, S. C., Hirt, H. & Boller, T. (2000).** Microbial elicitors induce activation and dual

## References

---

- phosphorylation of the *Arabidopsis thaliana* MAPK 6. *J Biol Chem* **275**, 7521–7526.
- Opalski, K. S., Schultheiss, H., Kogel, K. H. & Huckelhoven, R. (2005).** The receptor-like MLO protein and the RAC/ROP family G-protein RACB modulate actin reorganization in barley attacked by the biotrophic Powdery Mildew fungus *Blumeria graminis* f. sp. *hordei*. *Plant J* **41**, 291–303.
- Ouko, M. O., Sambade, A., Brandner, K., Niehl, A., Peña, E., Ahad, A., Heinlein, M. & Nick, P. (2010).** Tobacco mutants with reduced microtubule dynamics are less susceptible to TMV. *Plant J* **62**, 829–839.
- Papakonstanti, E. A., Vardaki, E. A. & Stournaras, C. (2000).** Actin cytoskeleton: a signaling sensor in cell volume regulation. *Cell Physiol Biochem* **10**, 257–264.
- Pauwels, L., Barbero, G. F., Geerinck, J., Tilleman, S., Grunewald, W., Perez, A. C., Chico, J. M., Bossche, R. V., Sewell, J., Gil, E., Garcia-Casado, G., Witters, E., Inze, D., Long, J. A., Jaeger, G. D., Solano, R. & Goossens, A. (2010).** NINJA connects the co-repressor TOPLESS to jasmonate signalling. *Nature* **464**, 788–791.
- Pederson, T. & Aebi, U. (2005).** Nuclear actin extends, with no contraction in sight. *Mol Biol Cell* **16**, 5055–5060.
- Petrásek J, Schwarzerová K. (2009).** Actin and microtubule cytoskeleton interactions. *Curr Opin Plant Biol* **12**, 728–734.
- Pickett-Heaps, J. D. (1967).** The effects of colchicine on the ultra-structure of dividing plant cells, xylem wall differentiation and distribution of cytoplasmic microtubules. *Dev Biol* **15**, 206–236.
- Pokorná J., Schwarzerová K., Zelenková S., Petráek, J., Janotová I., Apková V. & Opatrn, Z. (2004).** Sites of actin filament initiation and reorganization in cold treated tobacco cells. *Plant Cell Environ* **27**, 641–653.
- Pollard, T. D. & Cooper, J. A. (2009).** Actin, a central player in cell shape and movement. *Science* **27**, 1208–1212.
- Popov, N., Schmitt, S. & Matthies, H. (1975).** Eine stüungsfreie Mikromethode zur Bestimmung des Proteingehaltes in Gewebehomogenaten. *Acta Biol Med Ger* **34**, 1441–1446.
- Qiao, F., Chang, X. & Nick, P. (2010).** The cytoskeleton enhances gene expression in the response to the Harpin elicitor in grapevine. *J Exp Bot* **61**, 4021–4031.
- Ranf, S., Wunnenberg, P., Lee, J., Becker, D., Dunkel, M., Hedrich, R., Scheel, D. & Dietrich, P. (2008).** Loss of the vacuolar cation channel, AtTPC1, does not impair Ca<sup>2+</sup> signals induced by abiotic and biotic stresses. *Plant J* **53**, 287–299.

- Robatzek, S., Chinchilla, D. & Boller, T. (2006).** Ligand-induced endocytosis of the pattern recognition receptor FLS2 in Arabidopsis. *Genes Dev* **20**, 537–542.
- Rockel, P., Strube, F., Rockel, A., Wildt, J. & Kaiser, W. M. (2002).** Regulation of nitric oxide (NO) production by plant nitrate reductase *in vivo* and *in vitro*. *J Exp Bot* **53**, 103–110.
- Rodriguez, M. C., Petersen, M. & Mundy, J. (2010).** Mitogen-activated protein kinase signaling in plants. *Annu Rev Plant Biol* **61**, 621–649.
- Rosenblum, M. D. & Shivers, R. R. (2000).** Rings of F-actin form around the nucleus in cultures human MCF7 adenocarcinoma cells upon exposure to taxol and taxothere. *Comp Biochem Physiol C* **125**, 121–131.
- Ruggenthaler, P., Fichtenbauer, D., Krasensky, J., Jonak, C. & Waigmann, E. (2008).** Microtubule-associated protein ATMPB2C plays a role in organization of cortical microtubules, stomata patterning, and tobamovirus infectivity. *Plant Physiol* **149**, 1354–1365.
- Salmond, G. P. C. (1994).** Secretion of extracellular virulence factors by plant pathogenic bacteria. *Annu Rev Phytopathol* **32**, 181–200.
- Salzano, A. M., D'Ambrosio, C. & Scaloni, A. (2008).** Mass spectrometric characterization of proteins modified by nitric oxide-derived species. *Method Enzymol* **440**, 3–15.
- Samaj, J., Müller, J., Beck, M., Böhm, N. & Menzel, D. (2006).** Vesicular trafficking, cytoskeleton and signalling in root hairs and pollen tubes. *Trends Plant Sci* **11**, 1360–1385.
- Samaj, J., Ovecka, M., Hlavacka, A., Lecourieux, F., Meskiene, I., Lichtscheid, I., Lenart, P., Salaj, J., Volkmann, D., Bögre, L., Baluska, F. & Hirt, H. (2003).** Involvement of MAP kinase SIMK and actin cytoskeleton in the regulation of root hair tip growth. *Cell Biol Int* **27**, 257–259.
- Sano, T., Higaki, T., Oda, Y., Hayashi, T. & Hasezawa, S. (2005).** Appearance of actin microfilament ‘twin peaks’ in mitosis and their function in cell plate formation, as visualized in tobacco BY-2 cells expressing GFP-fimbrin. *Plant J* **44**, 595–605.
- Saxby, L., Rosen, E. & Boulton, M. (1998).** Lens epithelial cells proliferation, migration, and metaplasia following capsulorhexis. *Br J Ophthalmol* **82**, 945–952.
- Schellenbaum, P., Mohler, V., Wenzel, G. & Walter, B. (2008).** Variation in DNA methylation patterns of grapevine somaclones (*Vitis vinifera* L.). *BMC Plant Biol* **8**, 78–88.
- Schellmann, S. & Hülskamp, M. (2005).** Epidermal differentiation: trichomes in Arabidopsis as a model system. *Int J Dev Biol* **49**, 579–584.

## References

---

- Schmelzer, E. (2002).** Cell polarization, a crucial process in fungal defence. *Trends Plant Sci* **7**, 411–415.
- Schmit, A. C. & Lambert, A. M. (1988).** Plant actin filament and microtubule interactions during anaphase--telophase transition: effects of antagonist drugs. *Biol Cell* **64**, 309–319.
- Schmit, A. C. & Nick, P. (2008).** Microtubules and the evolution of mitosis. Plant cell monograph. Edited by Nick, P. pp. 234–266. Springer, Berlin.
- Schwarzerová1, K., Petrásěk, J., Panigrahi, K. C. S., Zelenková1, S. Opatrny, Z & Nick, P. (2006).** Intranuclear accumulation of plant tubulin in response to low temperature *Protoplasma* **227**, 185–196.
- Sheard, L. B., Tan, X., Mao, H., Withers, J., Ben-Nissan, G., Hinds, T. R., Kobayashi, Y., Hsu, F. F., Sharon, M., Browse, J., He, S. Y., Rizo, J., Howe, G. A. & Zheng, N. (2010).** Jasmonate perception by inositolphosphate- potentiated COI1-JAZ co-receptor. *Nature* **468**, 400–405.
- Shibaoka, H. (1994).** Plant hormone-induced changes in the orientation of cortical microtubules: Alterations in the cross-linking between microtubules and the plasma membrane. *Annu Rev Plant Physiol Plant Mol Biol* **45**, 527–544.
- Singh, D. P., Moore, C. A., Gilliland, A. & Carr, J. P. (2004).** Activation of multiple antiviral defence mechanisms by salicylic acid. *Mol Plant Pathol* **5**, 57–63.
- Smertenko, A. P., Bozhkov, P. V., Filonova, L. H., von Arnold, S. & Hussey, P. J. (2003).** Re-organisation of the cytoskeleton during developmental programmed cell death in *Picea abies* embryos. *Plant J* **33**, 813–824.
- Smertenko, A. P., & Franklin-Tong, V. E. (2011).** Organisation and regulation of the cytoskeleton in plant programmed cell death. *Cell Death Differ* **18**, 1263–1270.
- Smertenko, A. P., Deeks, M. J. & Hussey, P. J. (2010).** Strategies of actin reorganisation in plant cells. *J Cell Science* **123**, 3019–3028.
- Staiger, C. J., Poulter, N. S., Henty, J. L., Franklin-Tong, V. E. & Blanchoin, L. (2010).** Regulation of actin dynamics by actin-binding proteins in pollen. *J Exp Bot* **61**, 1969–1986.
- Sun, J., Chen, Q., Qi, L., Jiang, H., Li, S., Xu, Y., Liu, F., Zhou, W., Pan, J., Li, X., Palme, K. & Li, C. (2011).** Jasmonate modulates endocytosis and plasma membrane accumulation of the Arabidopsis PIN2 protein. *New Phytol* **191**, 360–375.
- Takemoto, D. & Hardham, A. R. (2004).** The cytoskeleton as a regulator and target of biotic interactions in plants. *Plant Physiol* **136**, 3864–3876.
- Tamimi, F., Comeau, P., Le Nihouannen, D., Zhang, Y. L., Bassett, D. C., Khalili, S., Gbureck, U.,**

- Tran, S. D., Komarova, S. & Barralet, J. E. (2013).** Perfluorodecalin and bone regeneration. *Eur Cell Mater* **25**, 22–36.
- Tampakaki, A. P., Skandalis, N., Gazi, A. D., Bastaki, M. N., Sarris, P. F., Charova, S. N., Kokkinidis, M. & Panopoulos, N. J. (2010).** Playing the ‘Harp’: evolution of our understanding of hrp/hrc genes. *Annu Rev Phytopathol* **48**, 347–370.
- Tan, X., Calderon-Villalobos, L. I., Sharon, M., Zheng, C., Robinson, C. V., Estelle, M. & Zheng, N. (2007).** Mechanism of auxin perception by the TIR1 ubiquitin ligase. *Nature* **446**, 640–645.
- Tawfic, Q. A. & Kausalya, R. (2011).** *Liquid Ventilation*. *Oman Med J* **26**, 4–9.
- Terral, J., Tabard, E., Bouby, L., Ivorra, S., Pastor, T., Figueiral, I., Picq, S., Chevance, J., Jung, C., Fabre, L., Tardy, C., Compan, M., Bacilieri, R., Lacombe, T. & This, P. (2010).** Evolution and history of grapevine (*Vitis vinifera*) under domestication: new morphometric perspectives to understand seed domestication syndrome and reveal origins of ancient European cultivars. *Ann Bot* **105**, 443–455.
- Thimann, K. V. & Biradivolu, R. (1994).** Actin and the elongation of plant cells II: the role of divalent ions. *Protoplasma* **183**, 5–9.
- Thion, L., Mazars, C., Thuleau, P., Graziana, A., Rossignol, M., Moreau, M. & Ranjeva, R. (1996).** Activation of plasma membrane voltage-dependent calcium-permeable channels by disruption of microtubules in carrot cells. *FEBS Lett* **393**, 13–18.
- Thomas, C., Hoffmann, C., Dieterle, M., Van Troys, M., Ampe, C. & Steinmetz, A. (2006).** Tobacco WLIM1 is a novel F-actin binding protein involved in actin cytoskeleton remodeling. *Plant Cell* **18**, 2194–2206.
- Thomma, B. P., Nürnberger, T. & Joosten, M. H. (2011).** Of PAMPs and effectors: the blurred PTI-ETI dichotomy. *Plant Cell* **23**, 4–15.
- Thordal-Christensen, H. (2003).** Fresh insight into processes of nonhost resistance. *Curr Opin Plant Biol* **6**, 351–357.
- Tian, M., Chaudhry, F., Ruzicka, D. R., Meagher, R. B., Staiger, C. J. & Day, B. (2009).** Arabidopsis actin depolymerizing factor AtADF4 mediates defense signal transduction triggered by the *Pseudomonas syringae* effector AvrPphB. *Plant Physiol* **150**, 815–824.
- Tiryaki, I. & Staswick, P. E. (2002).** An Arabidopsis mutant defective in jasmonate response is allelic to the auxin-signaling mutant *axr11*. *Plant Physiol* **130**, 887–894.
- Torres, M. A., Jones, J. D. G. & Dangl, J. L. (2006).** Reactive oxygen species signaling in response to

## References

---

pathogens. *Plant Physiol* **141**, 373–378.

**Tsuda, K. & Katagiri, F. (2010).** Comparing signalling mechanisms engaged in pattern-triggered and effector-triggered immunity. *Curr Opin Plant Biol* **13**, 459–465.

**Tzfira, T. & Citovsky, V. (2000).** From host recognition to T-DNA integration: the function of bacterial and plant genes in the Agrobacterium-plant cell interaction. *Mol Plant Pathol* **1**, 201–212.

**Ueguchi-Tanaka, M., Ashikari, M., Nakajima, M., Itoh, H., Katoh, E., Kobayashi, M., Chow, T. Y., Hsing, Y. I., Kitano, H., Yamaguchi, I. & Matsuoka, M. (2005).** GIBBERELLIN INSENSITIVE DWARF1 encodes a soluble receptor for gibberellin. *Nature* **437**, 693–698.

**Vance, V. & Vaucheret, H. (2001).** RNA silencing in plants—defense and counterdefense. *Science* **292**, 2277–2280.

**Velasco, R., Zharkikh, A., Troggio, M., Cartwright, D. A., Cestaro, A., Pruss, D., Pindo, M., Fitzgerald, L. M., Vezzulli, S., Reid, J., Malacarne, G., Iliev, D., Coppola, G., Wardell, B., Micheletti, D., Macalma, T., Facci, M., Mitchell, J. T., Perazzoli, M., Eldredge, G., Gatto, P., Oyzerski, R., Moretto, M., Gutin, N., Stefanini, M., Chen, Y., Segala, C., Davenport, C., Demattè, L., Mraz, A., Battilana, J., Stormo, K., Costa, F., Tao, Q., Si-Ammour, A., Harkins, T., Lackey, A., Perbost, C., Taillon, B., Stella, A., Solovyev, V., Fawcett, J. A., Sterck, L., Vandepoele, K., Grando, S. M., Toppo, S., Moser, C., Lanchbury, J., Bogden, R., Skolnick, M., Sgaramella, V., Bhatnagar, S. K., Fontana, P., Gutin, A., Peer, Y. Van de Salamini, F. & Viola, R. (2007).** A high quality draft consensus sequence of the genome of a heterozygous grapevine variety. *PLoS ONE* **2**, e1326.

**Verma, D. P. (2001).** Cytokinesis and building of the cell plates in plants. *Annu. Rev Plant Physiol Plant Mol Biol* **52**, 751–784.

**Voigt, B., Timmers, A. C. J., Samaj, J., Müller, J., Baluška, F. & Menzel, D. (2004).** GFP-FABD2 fusion construct allows *in vivo* visualization of the dynamic actin cytoskeleton in all cells of *Arabidopsis* seedlings. *Eur J Cell Biol* **84**, 595–608.

**Wakatsuki, T., Schwab, B., Thompson, N. C. & Elson, E. L. (2001).** Effects of cytochalasin D and latrunculin B on mechanical properties of cells. *J Cell Sci* **114**, 1025–1036.

**Waller, F., Furuya, M., & Nick, P. (2002).** Expression of OsARF1 an auxin response factor from rice (*Oryza sativa* L.) correlates positively with auxin-regulated differential growth. *Plant Mol Biol* **50**, 415–425.

**Wang, C., Li, J. & Yuan, M. (2007).** Salt tolerance requires cortical microtubule reorganization in *Arabidopsis*. *Plant Cell Physiol* **48**, 1534–1547.



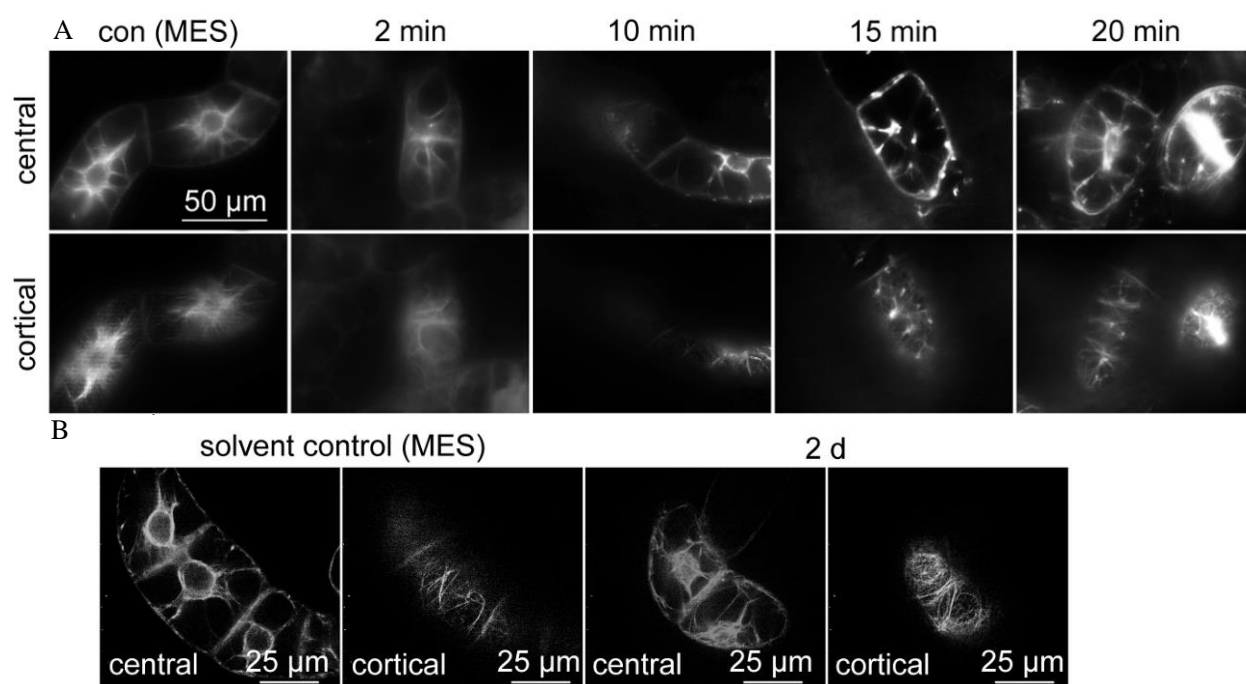
- Wang, Q. Y. & Nick, P. (1998).** The auxin response of actin is altered in the rice mutant Yin-Yang. *Protoplasma* **204**, 22–33.
- Wang, S., Kurepa, J., Hashimoto, T. & Smalle, J. A. (2011).** Salt stress-induced disassembly of Arabidopsis cortical microtubule arrays involves 26S proteasome-dependent degradation of SPIRAL1. *Plant Cell* **23**, 3412–3427.
- Wang, X. (2001).** Plant phospholipases. *Annu Rev Plant Physiol Plant Mol Biol* **52**, 211–231.
- Warfield, R. K. & Bouck, G. B. (1974).** Microtubule-macrotubule transitions: intermediates after exposure to the mitotic inhibitor vinblastine. *Science* **4170**, 1219–1221.
- Wasteneys, G. O. (1992).** The characean cytoskeleton: spatial control in the cortical cytoplasm. In *The Cytoskeleton of the Algae*. Edited by Menzel, D. pp. 273–295. CRC Press, Boca Raton.
- Wei, Z. M., Laby, R. J., Zumoff, C. H., Bauer, D. W., He, S. Y., Collmer, A. & Beer, S. V. (1992).** Harpin, elicitor of the hypersensitive response produced by the plant pathogen *Erwinia amylovora*. *Science* **257**, 85–88.
- Wendehenne, D., Lamotte, O., Frachisse, J. M., Barbier-Brygoo, H. & Pugin, A. (2002).** Nitrate efflux is an essential component of the cryptogein signaling pathway leading to defense responses and hypersensitive cell death in tobacco. *Plant Cell* **14**, 1937–1951.
- Wilbanks, G. A., Apel, A. J., Jolly, S. S., Devenyi, R. G. & Rootman, D. S. (1996).** Perfluorodecalin corneal toxicity: five case reports. *Cornea* **15**, 329–334.
- Wilkins, K. A., Bancroft, J., Bosch, M., Ings, J., Smirnoff, N. & Franklin-Tong, V. E. (2011).** ROS and NO mediate actin reorganization and programmed cell death in the self-incompatibility response of *Papaver*. *Plant Physiol* **156**, 404–416.
- Wolfe, J., Dowgert, M.F. & Steponkus, P.L. (1986).** Mechanical study of the deformation and rupture of the plasma membranes of protoplasts during osmotic expansions. *J Membrane Biol* **93**, 63–74.
- Woods, C. M., Reids, M. S. & Patterson, B. D. (1984).** Response to chilling stress in plant cells. I. Changes in cyclosis and cytoplasmic structure. *Protoplasma* **121**, 8–16.
- Wymer, C. & Lloyd, C. (1996).** Dynamic microtubules: implications for cell wall patterns. *Trends Plant Sci.* **1**, 222–228.
- Yang, Z. & Fu, Y. (2007).** ROP/RAC GTPase signaling. *Curr Opin Plant Biol* **10**, 490–494.
- Yarm F, Sagot I & Pellman, D. (2001).** The social life of actin and microtubules: interaction versus cooperation. *Curr Opin Microbiol* **4**, 696–702.

## References

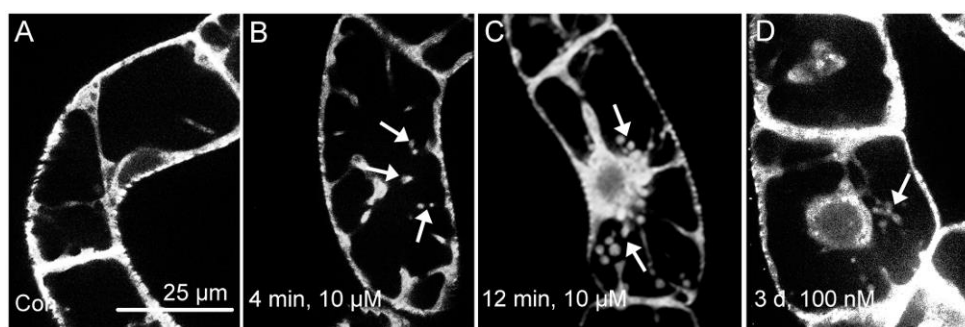
---

- Ye, J., Zhang, W. & Guo, Y. (2013).** Arabidopsis SOS3 plays an important role in salt tolerance by mediating calcium-dependent microfilament reorganization. *Plant Cell Rep* **32**, 139–148.
- Zaban, B., Maisch, J., Nick, P. (2013).** Dynamic actin controls polarity induction de novo in protoplasts. *J Int Plant Biol* **55**, 142–159.
- Zhao, J., Davis, L. C. & Verpoorte, R. (2005).** Elicitor signal transduction leading to production of plant secondary metabolites. *Biotechnol Adv* **23**, 283–333.
- Zhao, Y., Zhao, S., Mao, T., Qu, X., Cao, W., Zhang, L., Zhang, W., He, L., Li, S., Ren, S., Zhao, J., Zhu, G., Huang, S., Ye, K., Yuan, M. & Guo, Y. (2011).** The plant-specific actin binding protein SCAB1 stabilizes actin filaments and regulates stomatal movement in Arabidopsis. *Plant Cell* **23**, 2314–2330.
- Zeiger, E. (1983).** The biology of stomatal guard cells. *Annu Rev Plant Physiol* **34**, 441–475.
- Zipfel, C., Robatzek, S., Navarro, L., Oakeley, E. J., Jones, J. D., Felix, G. & Boller, T. (2004).** Bacterial disease resistance in Arabidopsis through flagellin perception. *Nature* **428**, 764–767.

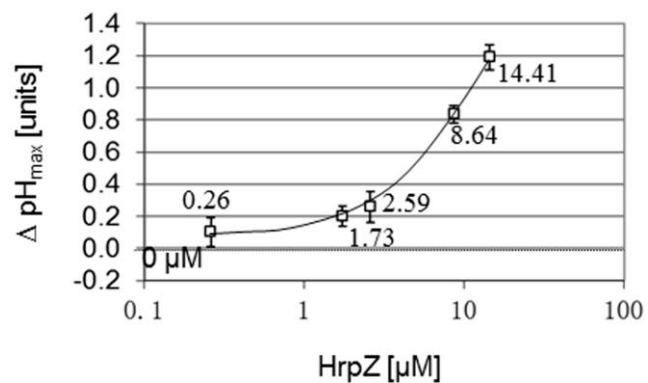
## Appendix



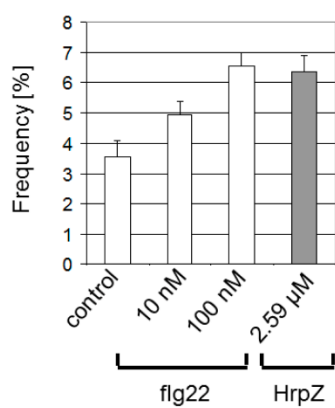
**Supplementary Fig 1 A** Early response of actin filaments in BY-2 to HrpZ *in vivo* visualised by the GFP-AtFABD2 marker and spinning-disc confocal microscopy. Time series after treatment with 57.6  $\mu\text{M}$  of HrpZ, confocal sections collected in the cell centre (upper row), and details from two cortical regions of the same cell (lower row). **B** Bundling of cortical actin filaments in BY-2 in response to a long-term treatment over 2 d with a permissive concentration of HrpZ (2.59  $\mu\text{M}$ , compare **Supplementary Fig 11**).



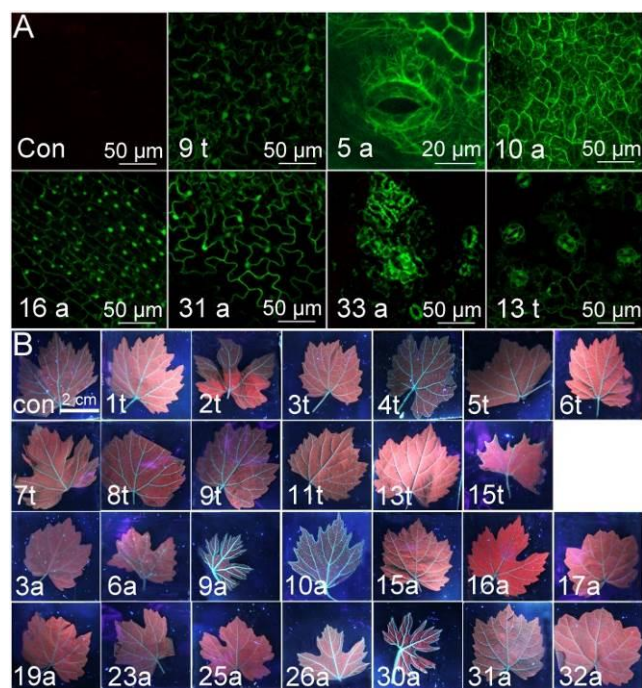
**Supplementary Fig 2** Aberrant microtubule structures in response to flg22. **A** control cell, **B** 4 min after addition of 10  $\mu\text{M}$  flg22, **C** 12 min after addition of 10  $\mu\text{M}$  flg22, **D** 3 days after addition of 100 nM flg22. Visualisation *in vivo* by the GFP-AtTUB6 marker and spinning-disc confocal microscopy. Confocal sections were collected in the cell centre, where the aberrant structures appear.



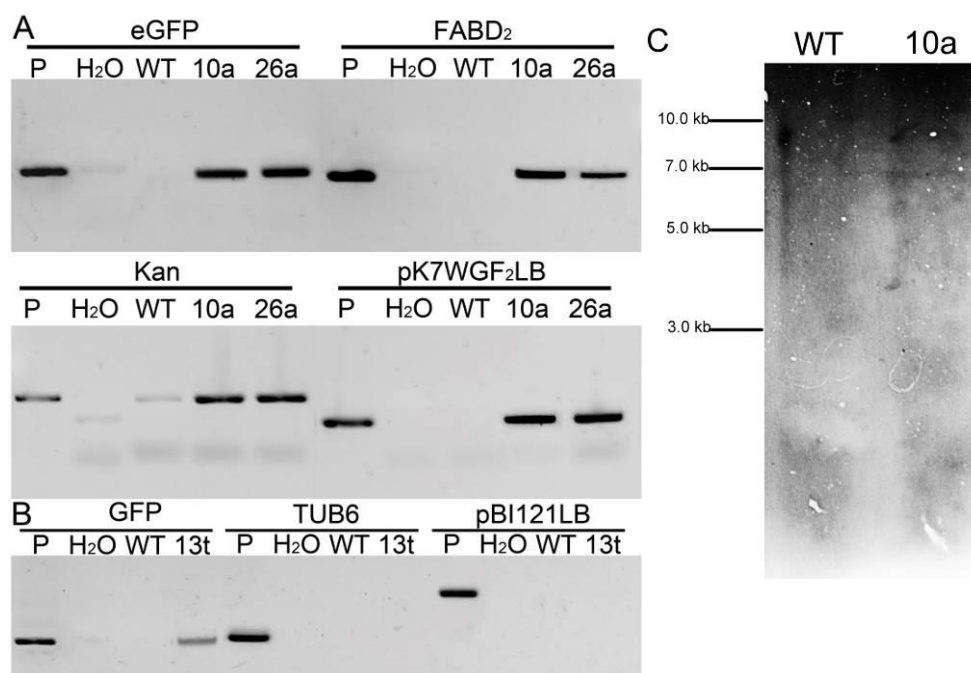
**Supplementary Fig 3** Dose response of maximal alkalisation over the concentration of HrpZ in BY-2. Dotted line shows the value obtained for solvent control of 5 mM MES buffer.



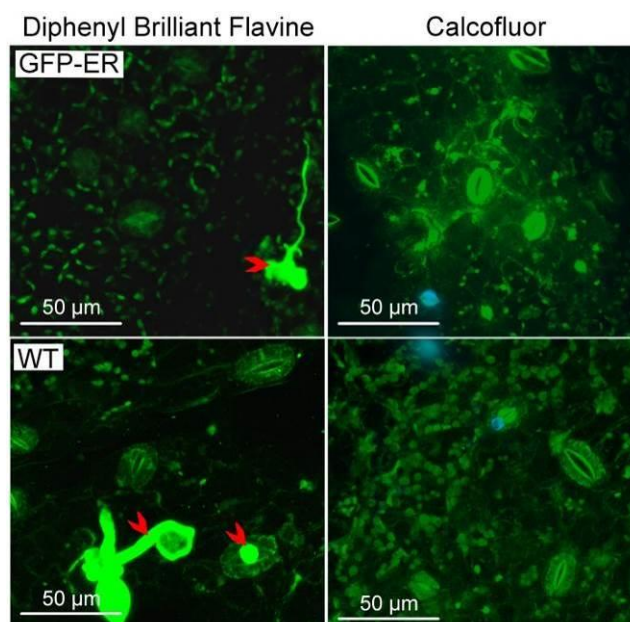
**Supplementary Fig 4** Division synchrony at the end of cell division phase (day 3 after subcultivation) using the frequency of files composed of 6 cells as diagnostic marker for treatment with flg22 (left) or HrpZ (right).



**Supplementary Fig 5** Leaf tissue of transgenic *Vitis vinifera* cv. 'Chardonnay' lines expressing *GFP-AtTUB6* and *GFP-AtFABD2* observed by confocal microscopy. **A** *V. vinifera* cv. 'Chardonnay' somatic embryogenesis and transformation with pBI121 *GFP-AtTUB6* (lines: 13t, 9t) and pK7WGF2-*AtFABD2* (lines: 10 a, 33 a, 16 a, 31a, 5a). **B** Different intensities of GFP signal in leaves of green house plant. Control (con) is non-transformed line.



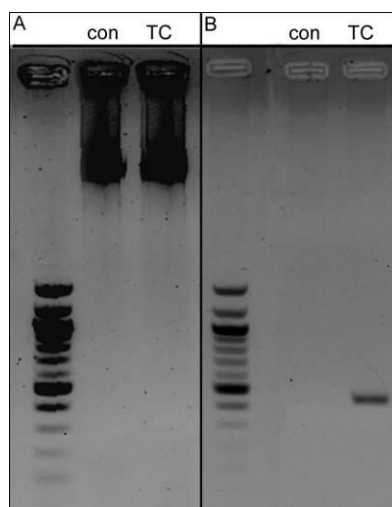
**Supplementary Fig 6** Detection of transgene in DNA extracted from leaves of *V. vinifera* 'Chardonnay' expressing *GFP-AtFABD2* and of *V. vinifera* 'Chardonnay' expressing *GFP-TUB6*. *eGFP*, *AtFABD2*, Kanamycin region, and left border of vector pK7WGF2 (**A**), *GFP*, *TUB6*, left border region of vector pBI121 (**B**) were amplified respectively. Controls are from plasmid, ddH<sub>2</sub>O, and wild type *V. vinifera* 'Chardonnay'. **C** Southern blot analysis, genomic DNA were digested with EcoRI and then hybridization (probe location was in *eGFP*).



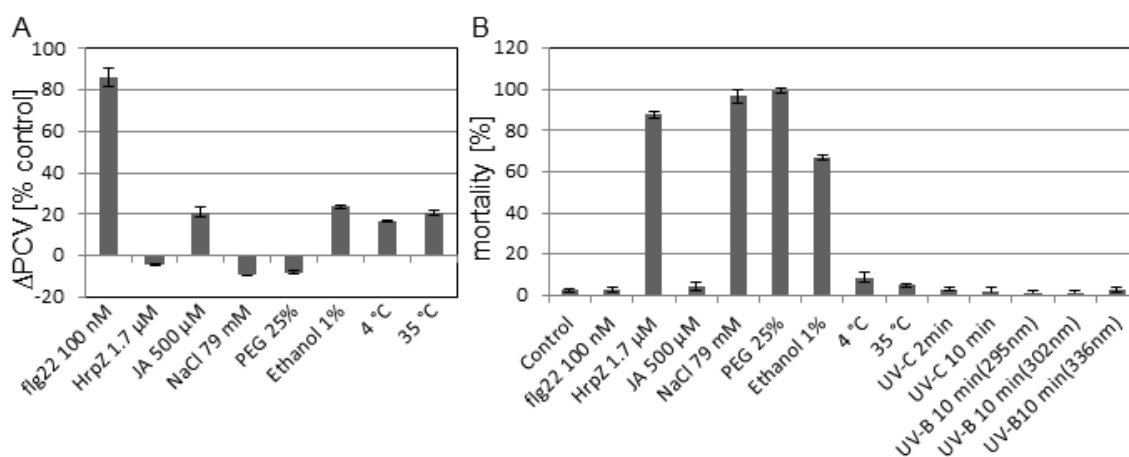
**Supplementary Fig 7** *P.v.* structures visualised by confocal microscopy inoculated in 'Chardonnay' line GFP – ER and wild type (WT). Encysted zoospores in stomata 0 - 3 day post-inoculation and developed hypha, sporangiophore

## Appendix

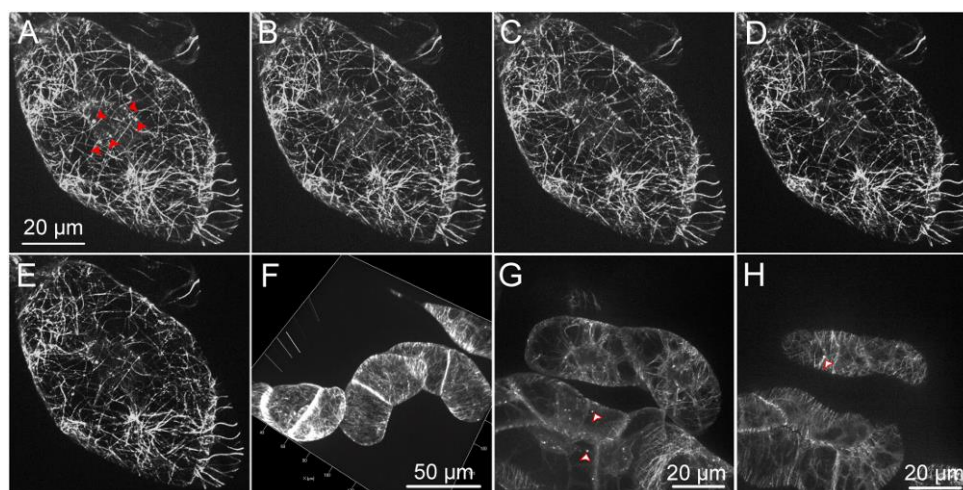
structures 4 - 12 d post-inoculation were visualised by Calcofluor (emission in blue) and Diphenyl Brilliant Flavine (emission in green) staining. Red arrow head indicates the *P. v.* structures emission in green.



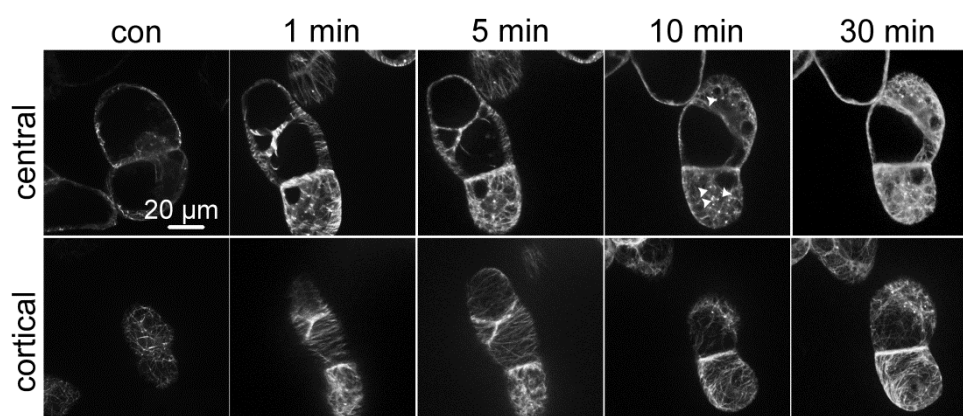
**Supplementary Fig 8** *V. rupestris* suspension cell line expressing *GFP-AtTUB6*. **A** DNA from non-transformed suspension cell line (con) and transformed suspension cell line (TC); **B** PCR with the respective genomic DNA as template, con and TC.



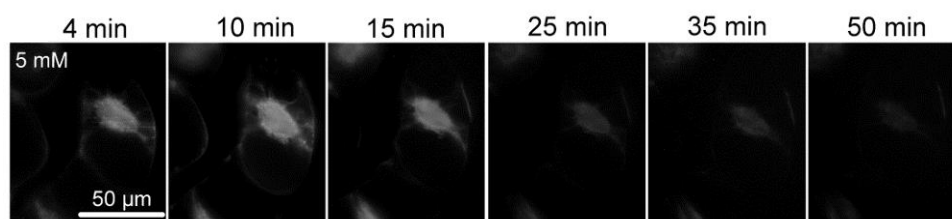
**Supplementary Fig 9** Cellular responses to flg22 and HrpZ, jasmonic acid (JA), sodium chloride (NaCl), polyethylene glycol (PEG 6000), ethanol (EtOH), cold and heat stress. **A** Packed cell volume as indicator of culture growth Dose-responses at day 3 (peak of mitotic activity) after inoculation. **B** Mortality in response to flg22, HrpZ, ( $\pm$ ) - JA, NaCl, PEG 6000, EtOH, cold-, heat-treatment, UV-C- and UV-B- irradiation. Data represent mean values and standard errors from three independent experimental series with a population of 2000 individual cells each, scored after staining with 2.5% Evans Blue for each value.



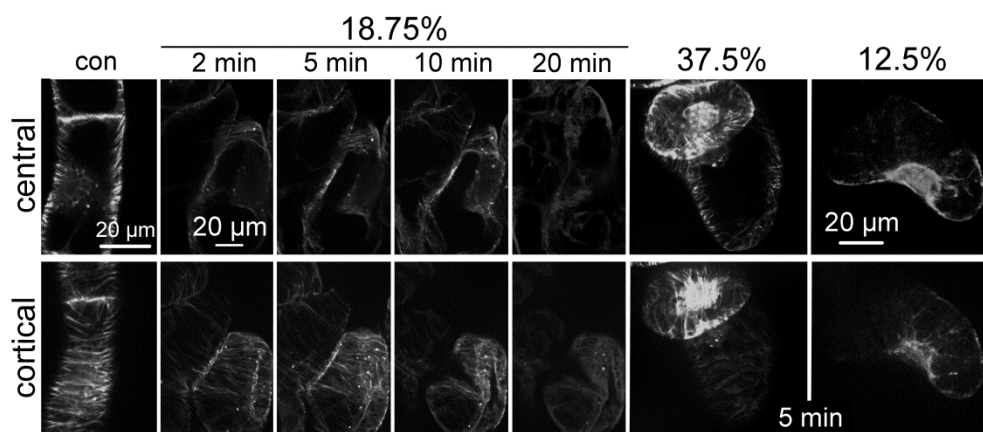
**Supplementary Fig 12** Z-stacks and 3-Dimensions of *V. rupestris* suspension cell line expressing *GFP-AtTUB6* to show the nuclear dots of MTs. **A – E** Z-stacks of one cell (1  $\mu\text{m}$  intervals). Dots are indicated in white arrows. **F** 3-Dimensions of an overview of the suspension cell lines. Some cells also with dots out of nuclei regions: central layers **G**; and cortical layer **H** of the same scope. Dots are indicated in white arrows with red edge.



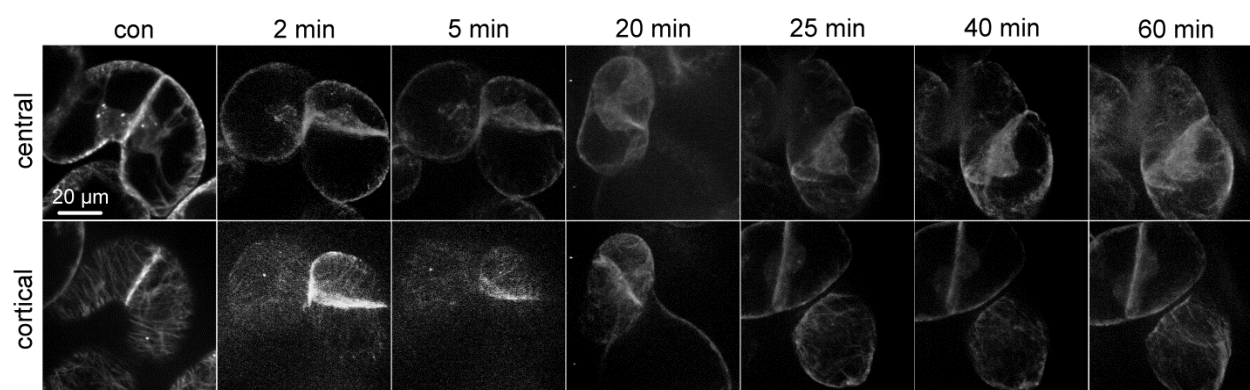
**Supplementary Fig 11** Response of microtubules in *V. rupestris* cells to HrpZ *in vivo* visualised by the *GFP-AtTUB6* marker and spinning-disc confocal microscopy. Time series after treatment with 28.8  $\mu\text{M}$  of HrpZ, confocal sections collected in the cell centre (upper row), and details from cortical regions of the same cell (lower row). Solvent control consisted in 5 mM MES buffer. White solid arrows in control and HrpZ central indicate MTs dots in the nuclei. Observations are representative of at least five independent experimental series with a population of 100 individual cells for each treatment.



**Supplementary Fig 12** Response of microtubules in *V. rupestris* cells to ( $\pm$ ) - JA *in vivo* visualised by the *GFP-AtTUB6* marker and spinning-disc confocal microscopy showing merged Z-stack of confocal sections. The layers in cell centre after the challenge with ( $\pm$ ) JA 5 mM for 50 min.



**Supplementary Fig 13** Response of microtubules in *V. rupestris* cells to PEG 6000 *in vivo* visualised by the GFP-AtTUB6 marker and spinning-disc confocal microscopy showing merged Z-stack of confocal sections. The cortical and central regions of MTs were shown after the challenge of PEG 6000 12.5%, 18.75% and 37.5%. Solvent control (water). Observations are representative of at least five independent experimental series with a population of 100 individual cells for each treatment.



**Supplementary Fig 14** Response of microtubules in *V. rupestris* cells to EtOH *in vivo* visualised by the GFP-AtTUB6 marker and spinning-disc confocal microscopy showing merged Z-stack of confocal sections. The cortical and central regions of MTs were shown after the challenge of EtOH 0.5%. Solvent control (water).

**Supplementary Table 1** Statistical analysis of *V. vinifera* ‘Chardonnay’ expressing *GFP-AtFABD2* line 10a.

	a/radian	b/radian	W/L	Relative length <sup>a</sup>									
				m0	m1	m2	m3	m4	m5	m6	m7	m8	m9
WT	3.18 A	1.45 A	1.02 A	0.74 BCDEF	0.95 A	0.91 AB	0.58 EFGHI	0.70 HI	0.72 FGHI	0.63 I	0.83 ABC	0.96 A	0.85 CDEFG
10a	2.43 B	1.46 A	1.47 B	0.82 ABCDE	0.96 A	0.89 A	0.66 GHI	0.55 DEFGH	0.63 CDEFG	0.54 FGHI	0.87 ABCD	0.96 A	0.73 ABCD

<sup>a</sup> Data are presented as relative length from the leaf centre of the bounding box to 10 marker points at leaf edge. Means of five first-fully-expanded leaves from different individual plants within columns followed by the same letters are not significantly different at  $p < 0.01$  by Duncan's new multiple range test (Duncan, 1955). m3 to m6 are significantly different at  $p < 0.05$  tested by oneway ANOSIM, calculated with the software package PAST (Hammer *et al.*, 2001). 30 individual leaves from 10 plants were used for this analysis.



Hiermit erkläre ich, dass ich die vorliegende Dissertation, abgesehen von der Benutzung der angegebenen Hilfsmittel, selbstständig verfasst habe.

Alle Stellen, die gemäß Wortlaut oder Inhalt aus anderen Arbeiten entnommen sind, wurden durch Angabe der Quelle als Entlehnungen kenntlich gemacht.

Diese Dissertation liegt in gleicher oder ähnlicher Form keiner anderen Prüfungsbehörde vor.

Karlsruhe, im Juni 2013

A handwritten signature in black ink, appearing to read 'Xin Guan', written in a cursive style.

(Xin Guan)

## Curriculum Vitae

### PERSONAL DATA

**Name:** Xin Guan

**Sex:** Female

**Nationality:** P.R. China

**Date of Birth:** December 31, 1984

**Place of Birth:** Jinan City, Shandong Province, P. R. China

**Email:** xin.guan@partner.kit.edu; xinguan.cnde@googlemail.com

### EDUCATION

- 2010.09 – 2013.07 Ph. D. Sc. student, Molecular Cell Biology, Botanical Institute, Chemistry and Biosciences, Karlsruhe Institute of Technology, Germany.

**Main research:** Functional Analysis of Cytoskeletal Signalling in the Defence Response of Grapevine

- 2007.09 – 2010.06 M. Agri., College of Horticulture, Northwest A&F University, P. R. China.

**Thesis:** A Study of the Genetic Transformation of Susceptible Grapes with a Novel Glyoxal Oxidase Related Gene from Chinese Wild *Vitis pseudoreticulata*

- 2003.09 – 2007.06 B. Agri., College of Horticulture, Qingdao Agriculture University, P. R. China.

**Thesis:** Growth Development and Observation of Ultrastructure on 'Hongdeng' Sweet Cherry. Review of a Study on Influences on Fruit under the Microenvironment of Bagging

- 2000.09 – 2003.06 Senior middle school, Shandong Experimental High School, China.
- 1997.09 – 2000.06 Junior middle school, Junior middle school attached to Jinan Fertilizer Plant Co., Ltd. China.
- 1991.09 – 1997.06 Primary school, Primary school attached to Jinan Fertilizer Plant Co., Ltd. China.

### PUBLICATIONS

**Xin Guan**, Heqing Zhao, Yan Xu, Yuejin Wang. **2011**. Transient expression of glyoxal oxidase from the Chinese wild grape *Vitis pseudoreticulata* can suppress Powdery Mildew in a susceptible genotype. *Protoplasma*, **248**: 415-423

Mingyang He, Yan Xu, Jiangling Cao, Ziguo Zhu, Yuntong Jiao, Yuejin Wang, **Xin Guan**, Yazhou Yang, Weirong Xu and Zhenfang Fu. **2012**. Subcellular localization and functional analyses of a PR10 protein gene from *Vitis pseudoreticulata* in response to *Plasmopara viticola* infection. *Protoplasma*, **250**: 129-140

Heqing Zhao, **Xin Guan** (contribution equally), Yan Xu, Yuejin Wang. **2012**. Characterization of novel gene expression related to glyoxal oxidase by agro-infiltration of the leaves of *accession* Baihe-35-1 of *Vitis pseudoreticulata* involved in production of H<sub>2</sub>O<sub>2</sub> for resistance to *Erysiphe necator*. *Protoplasma*, **250**: 765-777

**Xin Guan**, Günther Buchholz, Peter Nick. **2013**. The cytoskeleton is disrupted by the bacterial effector HrpZ, but not by the bacterial PAMP flg22 in tobacco BY-2 cells. *Journal of Experimental Botany*, **64**: 1805-1816

**Xin Guan**, Heqing Zhao, Yan Xu, Yuejin Wang. **2013**. Studies on genetic transformation of grape shoot apical meristems by *Agrobacterium*-mediated transformation. *Vitis* accepted

**Xin Guan**, Günther Buchholz, Peter Nick. **2013**. Actin marker lines in grapevine reveal a gatekeeper function of guard cells. shortly before submitting

**Xin Guan**, Günther Buchholz, Peter Nick. **2013**. Roles of microtubule of grapevine responses to biotic and abiotic challenge. shortly before submitting

**Xin Guan**, Günther Buchholz, Peter Nick. **2013**. A staining technique for *in vivo* imaging of *Plasmopara viticola* in grapevine leaves during Down Mildew infection. Preparing